personal buildup for

Force Motors Ltd.

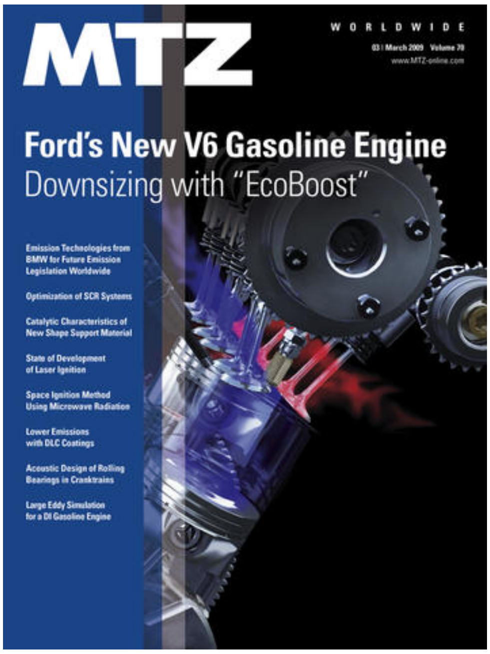

MTZ worldwide 3/2009, as epaper released on 12.02.2009
http://www.mtz-worldwide.com

content:

MTZ

WORLDWIDE

03 | March 2009 Volume 70

www.MTZ-online.com

Ford's New V6 Gasoline Engine
Downsizing with "EcoBoost"

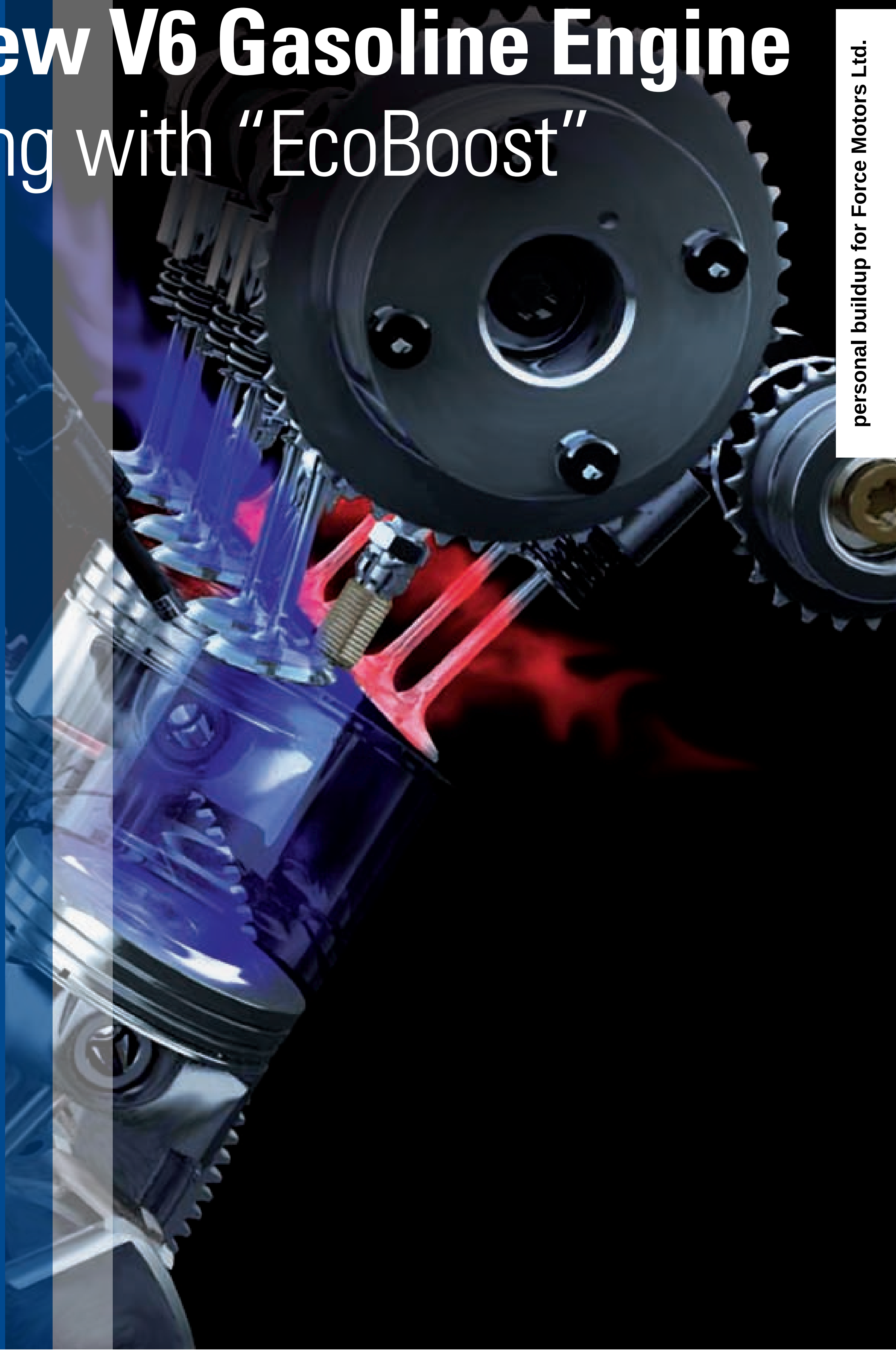

For more information visit:
www.MTZ-online.com

COVER STORY

Ford's New V6 Gasoline Engine
Downsizing with "EcoBoost"

4
Ford banded a new motor technology as "EcoBoost". It applies direct fuel injection and turbocharging to gasoline engines. The first Ford engine with this technology is the **3.5 l V6 "EcoBoost"** in the 2010 Lincoln MKS luxury sedan.

Reading Helps

Dear Reader,

For a year now, we have been publishing the English-language version of ATZ as an e-magazine. We have been very pleased with the positive response and grateful for your loyalty and for any suggestions on how we can make the magazine even better for you.

I often find that top managers say that they have hardly any time to read. As understandable as this may be in times of crisis, I would maintain that now, of all times, it is more important than ever to take some time out to read. Speed is essential for putting out fires, but it is less helpful for developing a strategy to reduce the risk of a fire. On the contrary, many fires are caused by carelessness, almost always a side-effect of hastiness.

There are, however, also areas in which printed paper has significant disadvantages compared to electronic media – especially when you are in a hurry and need to look up a reference quickly. Today, ATZonline.com already offers you a much better service – free of charge – than we are able to provide with the printed version.

You can find the very latest, constantly updated business news and, as a new service, a greatly expanded calendar of events. For example, you can research events on individual topics, view the complete programme via the links and even register online.

Johannes Winterhagen
Wiesbaden, 26 January 2009

Johannes Winterhagen
Editor-in-Chief

MTZ WORLDWIDE
03I2009

Founded 1939 by
Prof. Dr.-Ing. E. h. Heinrich Buschmann and
Dr.-Ing. E. h. Prosper L'Orange

Organ of the Fachverband Motoren und Systeme im VDMA, Verband Deutscher Maschinen- und Anlagenbau e. V., Frankfurt/Main, for the areas combustion engines and gas turbines

Organ of the Forschungsvereinigung Verbrennungskraftmaschinen e. V. (FVV)

Organ of the Wissenschaftliche Gesellschaft für Kraftfahrzeug- und Motorentechnik e. V. (WKM)

Organ of the Österreichischer Verein für Kraftfahrzeugtechnik (ÖVK)

Cooperation with the STG, Schiffbautechnische Gesellschaft e. V., Hamburg, in the area of ship drives by combustion engines

Ford's New 3.5 l V6 Gasoline Engine
Downsizing with "EcoBoost"

Ford banded a new motor technology as "EcoBoost". It applies direct fuel injection and turbocharging to gasoline engines and provides a major improvement in fuel economy via engine downsizing, combined with improved performance. The first Ford engine with this technology is the 3.5 l V6 EcoBoost in the 2010 Lincoln MKS luxury sedan. Combustion, fuel, boost, and power conversion systems are discussed in detail with emphasis on the efficiency and value of these systems. Engine level fuel economy and performance are discussed, and compared to conventional gasoline engines.

1 Introduction

In 2006 Ford introduced the 3.5 l V6 Duratec engine, and applied it across a wide range of makes and models. The engine has received excellent reviews from both consumers and media. Subsequent introductions from this family included the 3.7 l V6 Duratec in 2008, and most recently the 3.5 l V6 EcoBoost for 2009.

Common design elements of the engine family are a 60 degree bank angle with 106 mm bore spacing, aluminum cylinder head and block castings, and double overhead cams with variable intake cam timing, **Table**. In order to optimize the functional attributes of the EcoBoost engine, adjustments were made in compression ratio, cam timing, fuel type, and maximum engine speed. In addition, design changes were made in virtually all primary and secondary engine systems, including combustion, fuel, intake, exhaust, power conversion, cooling, lubrication, positive crankcase ventilation, sealing, and valvetrain. These changes resulted in approximately 75 new or redesigned components, **Figure 1**.

Common functional objectives of all versions include:

- 10 year / 150,000 mile durability
- Best in class acoustics
- PZEV emissions capability.

Whereas the 3.5 l and 3.7 l engines are port fuel injected and naturally aspirated and rated at 198 and 206 kW respectively, the new Motor is direct fuel injected and twin turbocharged and rated at 265 kW and 350 lb-ft of torque. This article describes the engine developments made to provide the great customer driving experience of a larger engine, while preserving the fuel economy of a smaller architecture.

2 Effects on Fuel Economy and Performance

Earlier research [1, 2] has identified that the combined use of turbocharging, direct fuel injection, and variable cam timing is particularly advantageous:

- significantly improved power and torque relative to naturally-aspirated, port fuel injected engines
- improved low speed steady state and transient torque relative to turbocharged, port fuel injected engines; this is due to improved volumetric efficiency, improved residual scavenging
- consistent real-world fuel economy benefit, regardless of drive cycle relative to turbocharged, port fuel injected engines; this is due to improved knock resistance enabling higher compression ratio, and a wider $\lambda = 1$ operating range
- stop/start capability due to improved transient fuel control with direct injection.

Table: Specification of EcoBoost versus Duratec engine

Specification	3.5L V6 EcoBoost	3.5L V6 Duratec
Bore (mm)	92.5	92.5
Stroke (mm)	86.7	86.7
Bank Angle (deg)	60	60
Bore Spacing (mm)	106	106
Compression Ratio	10.0:1	10.3:1
Intake Duration (deg)	236	248
Intake Valve Opening (deg BTDC)	40 (full adv)	40 (full adv)
Intake Valve Closing (deg ABDC)	16 (full adv)	28 (full adv)
Exhaust Duration (deg)	236	248
Exhaust Valve Opening (deg BBDC)	46	58
Exhaust Valve Closing (deg ATDC)	10	10
Fuel Recommendation (RON)	95	91
Maximum Engine Speed (RPM)	6300	6700
Maximum Cylinder Pressure (bar)	100 (3 sigma)	93 (3 sigma)

The Authors


Dr. Gerhard Schmidt
is Vice President, Research & Advanced Deveolopment, at Ford Motor Company, in Dearborn, Michigan (USA).


Mr. Daniel Kapp
is Director, Research & Advanced Powertrain, at Ford Motor Company, in Dearborn, Michigan (USA).


Dr. Andreas Schamel
is Chief Engineer, Research & Advanced Powertrain at Ford Motor Company, in Dearborn, Michigan (USA).


Brett Hinds
is Advanced Gasoline Engine at Ford Motor Company, in Dearborn, Michigan (USA).


Dr. Corey Weaver
is Technical Expert, Advanced Gasoline Engine, at Ford Motor Company, in Dearborn, Michigan (USA).

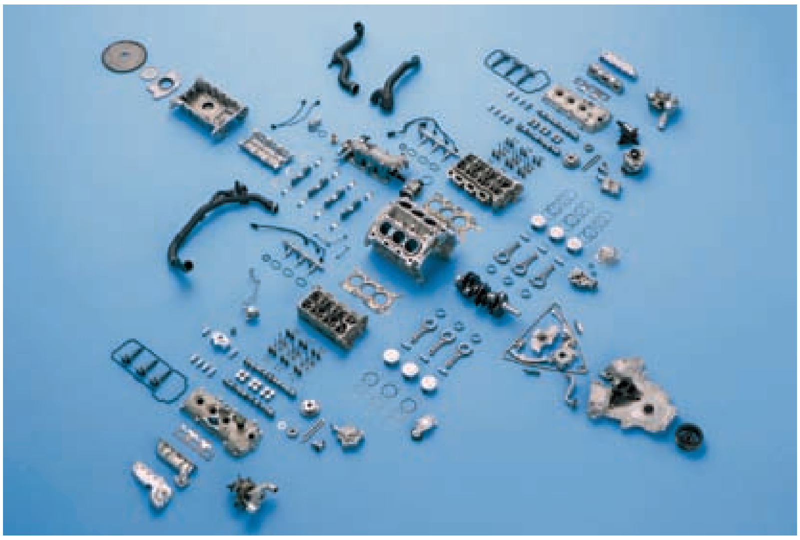

Figure 1: Complete 3.5 l V6 EcoBoost engine assembly

In combination, these advantages enable significant engine downsizing with a resulting improvement of fuel economy by up to 20 %.

3 Engine Attributes

The previously noted functional advantages of turbocharged, direct fuel injected engines led to the following top level program objectives:

- power of 254 kW at 5650 rpm, competitive with premium V8's
- torque of 340 lb-ft from 2000 to 4000 rpm, better than premium V8's
- fuel consumption equal to the 3.5 l V6 Duratec, and much better than premium V8's regardless of drive cycle.

The 3.5 l V6 EcoBoost engine achieves 265 kW from 5250 to 5650 rpm, **Figure 2**, and 350 lb-ft from 1500 rpm to 5250 rpm; this represents an 88 % increase at 2000 rpm and 40 % increase at 4500 rpm relative to the 3.5 l V6 Duratec engine. The broad, flat torque curve of the EcoBoost is torque limited in this application; future applications could offer higher output. The new engine also has a larger stoichiometric operating range than the Duratec engine, ensuring consistent real-world fuel economy benefit.

The part-load fuel consumption of the turbo engine, **Figure 3**, is equivalent to the Duratec naturally aspirated engine. The 7 speed/load points shown are the most heavily weighted points in typical customer drive cycles. The engine with EcoBoost technique delivers slightly improved fuel consumption at some points, and slightly degraded at the other points; these differences are largely related to changed dilution tolerance and resultant cam timing at each point. Relative to competitive and aspirational vehicles with V8 engines, **Figure 4**, the EcoBoost delivers superior fuel economy and competitive performance.

4 Combustion System

The combustion system consists of the intake and exhaust ports, combustion chamber surface, piston dome surface, and fuel injector spray specification, **Figure 5** and **Figure 6**. The design and development of the combustion system utilized a three-level methodology successfully demonstrated on prior turbocharged, direct fuel injected engine research programs within Ford:

- Ford's Multi-dimensional Engine Simulation (MESIM) CFD code, incorporating industry-leading fuel spray, mixing, and combustion models
- a single-cylinder optical engine laboratory
- a single / multi-cylinder thermodynamic engine laboratory.

This three-level methodology allowed early, rapid, and cost-effective combustion system design and development, thereby supporting high confidence multi-cylinder engine builds early in the program for further engine systems and vehicle systems development.

To address the significant challenges associated with turbocharged direct fuel injected combustion [3, 4], the following objectives were adopted:

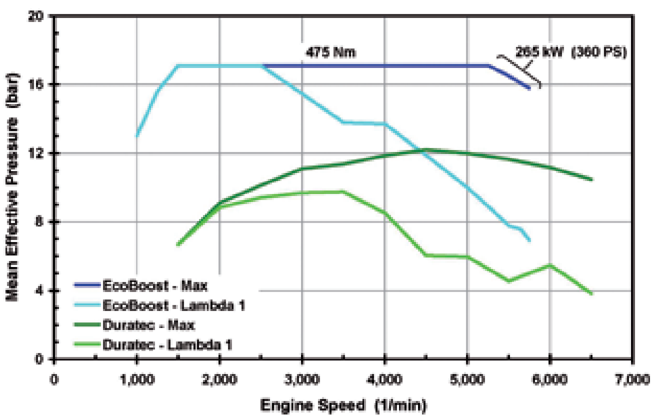

Figure 2: EcoBoost and Duratec: full-load output and air/fuel ratio

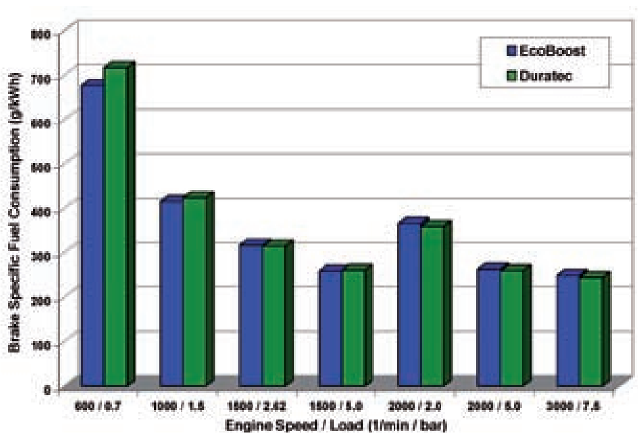

Figure 3: EcoBoost and Duratec part-load fuel consumption

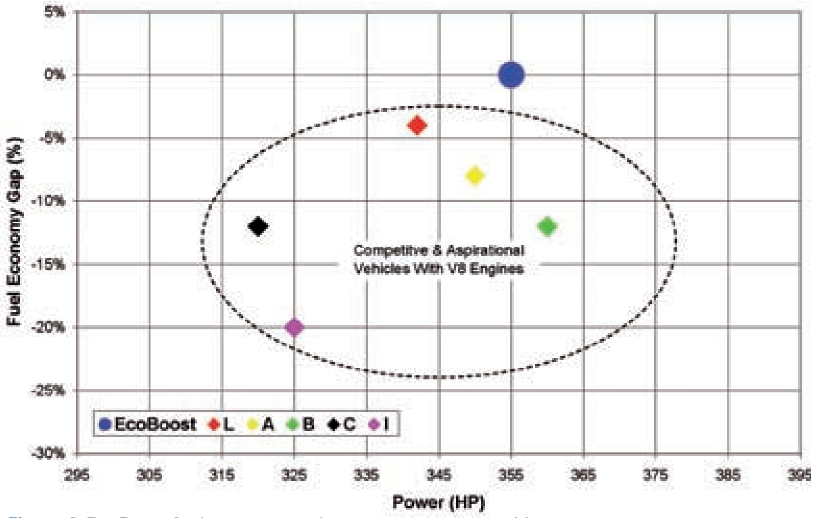

Figure 4: EcoBoost fuel economy and power versus competition

- stable operation, high exhaust heat flux, and minimum emissions under split injection, cold start operating conditions
- complete air/fuel mixing under early injection, cold start operating conditions
- complete air/fuel mixing under early injection, low speed, full load operating conditions
- fast burn rate under early injection, full load operating conditions (thus enabling maximum compression ratio and minimum fuel enrichment)
- minimum fuel/cylinder impingement and fuel/oil dilution under all operating conditions

In order to deliver the most cost-effective combustion system, these objectives were to be achieved without additional charge motion, fuel system, or air system assist devices.

Given the above objectives and within the architectural confines of the 3.5 l V6 Duratec engine family, the 3.5 l V6 EcoBoost combustion system was optimized through approximately 50 "MESIM" CFD iterations of the intake and exhaust ports, combustion chamber surface, piston dome surface, and fuel injector spray specification. High confidence outputs from the MESIM CFD were translated to less than 10 single-cylinder engine iterations, and finally less than 5 multi-cylinder engine iterations over the duration of the program.

Through this methodology, the combustion system achieved the program objectives:

- under split injection, cold start operating conditions, IMEP fluctuations of 0.32 bar, heat flux of 7200 W/L, and 0-20 s feedgas emissions supporting PZEV emissions
- under early injection, cold start and also under early injection, low speed, full load operating conditions, air/fuel mixing comparable to PFI engines (0.2 % O_2 emissions)
- under early injection, full load operating conditions, burn rate sufficient to enable a 10.0:1 compression ratio and to avoid low speed fuel enrichment
- under all operating conditions, undetectable fuel/cylinder impingement and fuel/oil dilution comparable to other direct fuel injected engines (approximately 5 % dilution).

5 Fuel System

The fuel system consists of the high pressure fuel pump and mounting pedestal, high pressure fuel line assembly, fuel rails, and fuel injectors, **Figure 7**. The high pressure fuel pump is a stainless steel, single piston, demand delivery design. The pump is secured to the cylinder head through the left-hand cam cover by a die cast aluminium mounting pedestal, re-

Figure 5: Combustion system

Figure 6: Combustion system with fuel injection spray

Figure 7: Fuel system

placing two conventional cam caps from the base engine. The pump is actuated by the left-hand intake camshaft via a 4.4 mm lift / four lobe cam and associated roller follower; the follower is oil pressure fed through the pedestal. The above fuel pump and drive configuration yields 1.125 cc fuel delivery per cam revolution, sufficient to support engine full rated output. The high pressure fuel line assembly is an extruded stainless steel, robotically formed and brazed design which connects the high pressure fuel pump to the fuel rails. The assembly is secured to the respective fuel system components by compression fittings and to the left-hand cylinder head by a stamped bracket. The fuel rails are also an extruded stainless steel, robotically brazed design; the left-hand rail includes an integrated pressure sensor which supports the high pressure fuel pump demand delivery function. The rails are secured to the cylinder heads by six stamped brackets per rail, and capture the respective injectors by three stamped injector cups per rail.

The fuel injectors are a stainless steel, six hole, solenoid actuated design. The injectors are mechanically oriented and preloaded to the respective cylinder heads to ensure consistent spray orientation. The injectors are sealed by a low temperature capable, Silicone o-ring to the fuel rail and a high temperature capable Teflon compression ring to the cylinder head. The above configuration yields 22.5 cc fuel delivery per injector per second, sufficient to support engine full rated output.

In addition to the spray specification, CAE methods were employed throughout the design process to ensure component and system durability at engine full rated output; these included hydraulic system simulation to ensure minimum pressure pulsation, maximum frequency separation, and minimum fuel vaporization (under hot soak conditions). Additionally, experimental measurements were made to ensure acceptability of other critical characteristics, including injector deposit resistance and pumping/vibration force fatigue resistance.

6 Boost System

The boost system consists of the intake manifold, exhaust manifolds, twin parallel turbochargers, low and high pressure air systems, and air-to-air intercooler. The intake manifold is a cast aluminium, single plenum design with an integrated coolant crossover, coolant outlet, and coolant inlet / thermostat housing assembly. The intake manifold features a 65 mm electronic throttle body, TMAP sensor, boost control solenoid, and spigots for vapour purge, heater core, crankcase ventilation, and brake vacuum. The integrated functional elements and high feature density enabled the intake manifold to be used across all EcoBoost applications as a singular design, thereby representing a cost-effective solution to a traditionally application specific component.

The exhaust manifolds are a stamped stainless steel, air-gapped dual wall, robotically welded design. The inner wall material is a 309 stainless steel / 1.5 mm wall thickness, while the outer wall material is a 441 stainless steel (18 CrCb) / 2.0 mm wall thickness; the inner and outer walls are separated by a 3.4 mm air-gap. The 309 stainless steel inner was selected to match the 950 deg C maximum exhaust gas temperature, while the 441 stainless steel outer was selected to match to the approximately 100 deg C air-gap reduction, to minimize the system thermal expansion, and to minimize the system cost (i.e. less than 1 % Ni content). The exhaust manifold flange at the cylinder head is a 1008 low carbon steel (300 deg C max material temp), while the flange at the turbocharger is a 439 wrought stainless steel (750 deg C max material temp); the 439 stainless was also selected for good weldability.

CAE methods were employed throughout the design process to ensure component and system durability at engine full rated output; these included thermal / mechanical fatigue simulation of the complete exhaust system (cylinder head interface, exhaust manifold, turbocharger, catalyst, support brackets, and gaskets). Measurements verified other critical characteristics, including material temperatures and thermal expansion vectors. Although the development of an air-gap dual wall design was more complex than a cast design, it was found to be more cost effective. Likewise, although the right and left-hand exhaust manifolds were unique, they shared four of six inner wall stampings, **Figure 8**.

The twin parallel turbochargers, **Figure 9**, are of conventional design. Although the right and left-hand turbochargers have unique castings, the rotating assemblies are identical. The compressor wheel is a TiAl alloy, 49 mm diameter, and the turbine wheel is an Inconel alloy, 41 mm diameter. The maximum speed of the rotating assembly is 205,000 rpm. CAE methods were employed to select the thermodynamic match to ensure maximum low speed boost response and minimum high speed backpressure. The turbine housing casting is a D5-S Ni-Resist cast iron alloy, which was selected to match the 950 deg C maximum exhaust gas temperature at minimum system cost. Normal boost control is via an electronic solenoid valve which modulates the wastegate actuators, while over-boost control is via a pair of electronic anti-surge valves connecting the low and high pressure air systems.

Figure 8: Left-hand exhaust manifold and turbocharger

Figure 9: Right-hand turbocharger (sectioned)

7 Power Conversion System

The power conversion system consists of the crankshaft, pistons, connecting rods, and cylinder block. The crankshaft is a forged steel, fully counterweighted design. The material is a high tensile strength, micro-alloy forged steel for enhanced durability. The connecting rod pin journal diameters are 56.0 mm in diameter and 22.0 mm in width, while the main bearing journal diameters are 67.5 mm in diameter and 26.0 mm in width. The crankshaft design was revised from the base engine to include optimized geometry for improved fatigue strength and optimized counterweighting for improved balance capability. Additionally, the pin journal fillet rolling loads were revised from the base engine to variable rolling, and also increased in magnitude to improve the fatigue strength.

The pistons are gravity fed, permanent mold aluminium castings, **Figure 10**. The material is a hypereutectic AlSi alloy for enhanced durability. The piston design was revised from the base engine to include:

Figure 10: EcoBoost piston

- a fully machined dome with direct injection bowl and valve clearance pockets, thereby requiring unique right and left bank pistons
- an anodized top ring groove
- a revised pin boss, the latter two for enhanced durability. The piston pin was revised to a full floating configuration with increased wall thickness. The pistons have a mass of 377 grams, while the piston pins have a mass of 127 grams; these reciprocating masses are tightly controlled to eliminate the pin end weight pad on the connecting rod. The upper compression ring was revised to include a slightly increased tension and a revised face coating for enhanced durability, while the lower compression ring and oil control assembly are carry-over from the base engine.

The cylinder block is a die cast, deep skirt, open deck design. The material is a proprietary Al alloy for enhanced durability. The cylinder block design was revised to include:

- bulkhead style piston cooling squirt jet machining
- deleted crankcase breather windows for improved fatigue strength
- additional bosses for turbocharger support and oil return. Finite Element Analysis was employed throughout the design process to ensure component and system durability at engine full rated output, complemented by experimental measurements of other critical characteristics, such as bore distortion, bore wear, and metal temperatures.

8 Summary

Ford Motor Company has developed Turbo DI gasoline engines, branded as EcoBoost, to deliver improved fuel consumption with fun-to-drive. In this article, fundamentals of this technique for fuel economy and deployment plans are reviewed. The specifications, performance, and fuel economy of the 3.5 l V6 EcoBoost engine are summarized. Finally, objectives and design choices for the combustion system, fuel system, boost system, and power conversion system are discussed.

Ford anticipates widespread demand for, and therefore widespread impact of the new engine technique. Ford is therefore actively researching technologies that will further enhance EcoBoost.

References

[1] Kapp, D.; Schamel, A.; Hinds, B.; Weaver, C.: 3.5L V6 EcoBoost – Democratization of Sustainable Engine Technology Aachener Kolloquium Fahrzeug- und Motorentechnik, Aachen 2008

[2] Borrmann, D.; Brinkmann, F.; Walder, K.; Pingen, B.; Wojahn, J.; Behrends, P.: Benzindirekteinspritzung mit Turboaufladung – ein interessantes Downsizingkonzept Aachener Kolloquium Fahrzeug- und Motorentechnik, Aachen 2002

[3] Wirth, M.; Mayerhofer, U.; Piock, W.; Fraidl, G.: Turbocharging the DI Gasoline Engine SAE International, Detroit, USA, 2000

[4] Han, A.; Weaver, C.; Wooldridge, S.; Alger, T.; Hilditch, J.; McGee, J.; Westrate, B.; Xu, Z, Yi, J.; Chen, X.; Trigui, N.; Davis, G.: Development of a New Light Stratified-Charge DISI Combustion System for a Family of Engines With Upfront CFD Coupling With Thermal and Optical Engine Experiments SAE International, Detroit, USA, 2004

Emission Technologies from BMW for Future Emission Legislation Worldwide

Exhaust emission legislation is being tightened worldwide, with the added complication of different regulations in Europe, the USA and Japan, demanding not only the continuing development of existing technologies, but also the use of new systems, especially in the area of exhaust gas treatment for diesel engines. To meet the various boundary conditions, therefore, the engine development department of the BMW Group has developed different emission technologies that are best able to resolve this conflict of aims. With the maintenance-free particle filter system, NO_x storage catalyst and the SCR system, BMW has developed a modular emission system which not only retains the virtues of the BMW diesel drivetrains, but also permits the successful deployment of these diesel engines in the USA and Canada.

1 Introduction

Over recent years, the diesel engine has been able to build on its leading position as a powertrain for cars, especially in the mid and upper range segments. Excellent performance combined with low fuel consumption and associated long range have resulted in this sustained trend towards diesel in Europe. In combination with the „EfficientDynamics" measures [1], this development has led to a significant reduction of CO_2 emissions in the vehicle fleet. In addition to the continuous improvements to these important customer-relevant properties, harmful emissions have been drastically reduced at the same time. Thanks to the universal implementation of maintenance-free particle filter, for example, it has been possible to cut particle emissions by 99 %.

The development of the emission limits in Europe and the USA is represented in **Figure 1**, which shows the step by step reduction of the particle and NO_x emissions. Even more stringent NO_x limit values now represent the main challenge. Apart from the different limit values in use around the world, there are also major differences in the quality of available fuel which have a considerable influence on the technical solutions. Designers therefore face the challenge of designing a customized solution for each respective market which, apart from the functional aspects, also takes into account the various boundary conditions in these markets. In addition, the systems must be adaptable across a broad range of vehicles, extending in the case of BMW Group from the Models Mini to the X5. Consequently, the obvious task is to develop a technology kit, from which the ideal solution for the car and market can be created to suit the respective requirements.

2 Internal Modifications in the Engine

In order to comply with the quoted emission limit value stages, internal modifications remain an important factor in the overall reduction of emissions. The key modification measures are described below.

2.1 Optimizations of the Air System

The optimization of the air system is an essential prerequisite for reducing the raw emissions, while at the same time meeting the typical demands for BMW with regard to dynamic performance and comfort. The exhaust gas recirculation (EGR) and the boost pressure are the key variables here. The modifications to the air sys-

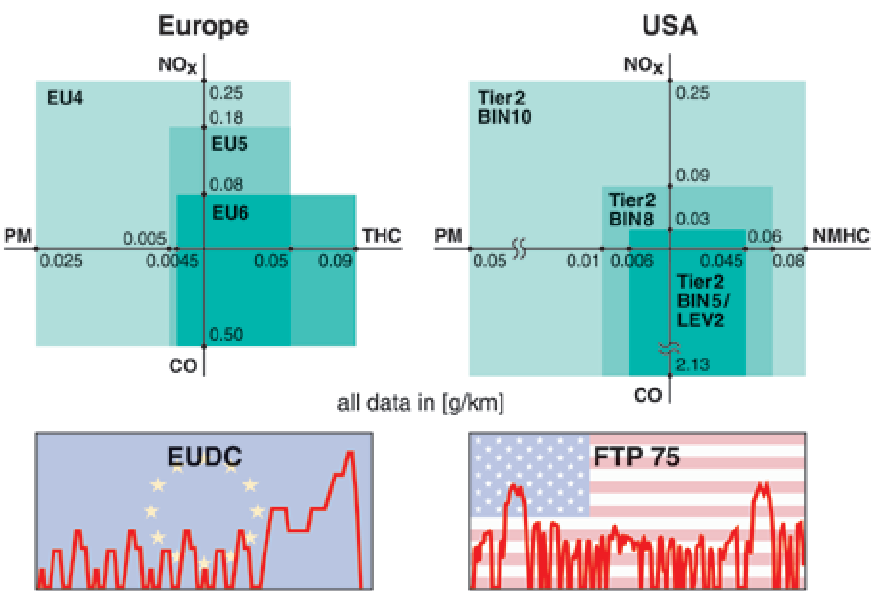

Figure 1: Emissions limit overview in the EU and USA

The Authors

Dipl.-Ing.
Hans-Jürgen Brüne
is head of test department for emission concepts in the diesel engine development department in the BMW Group in Steyr (Austria).

Dipl.-Ing.
Josef Honeder
is head of the test department for fuel-mixture generation and exhaust treatment for special engines in the diesel engine development department in the BMW Group in Steyr (Austria).

Dipl.-Ing.
Peter Raschl
is a specialist in the test department for fuel-mixture generation and combustion for 6-cylinder diesel engines in the BMW Group in Steyr (Austria).

Dr.-Ing.
Michael Schinnerl
is head of the test department for fuel-mixture generation and combustion of 4-cylinder diesel engines in the BMW Group in Steyr (Austria).

Dr. Dipl.-Ing.
Rüdiger Tangemann
is responsible for emission components in the design section of the diesel engine development department in the BMW Group in Steyr (Austria).

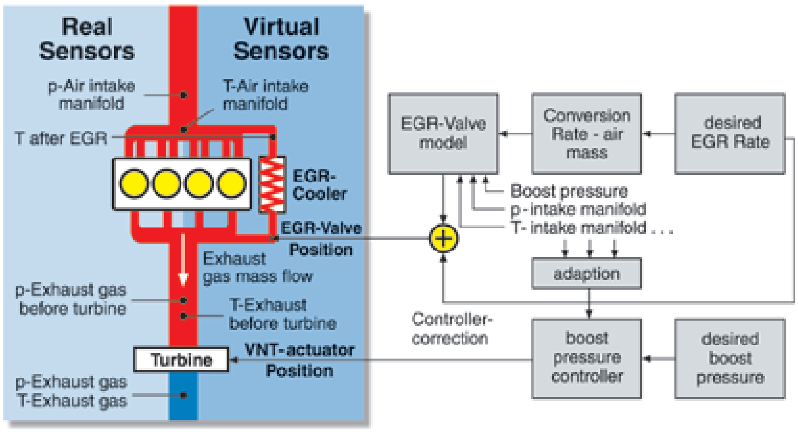

Figure 2: Air system and control structure in the engine control unit

tem are aimed at reducing the average level of emissions and the dispersion of the individual exhaust gas components.

The following components were modified with the introduction of EU5:

- electrical EGR valve
- pressure sensor in the exhaust manifold
- temperature sensor after the EGR valve
- enlarged EGR cooler for heavy vehicles.

Due to the additional sensors and improved actuators, the dynamic behaviour of the air system can be recorded more precisely, while closed-loop control operations are possible with a higher level of quality. These properties are the basis for a series of motor control functions for improving the behaviour of the air system. By way of example, two of these functions are considered in detail below.

2.1.1 EGR Rate Regulation

With the implementation of the EU5 exhaust standard, the reference variable of the EGR control of the air mass was converted to the ratio of exhaust mass flow to fresh air mass, which is also termed the EGR rate. This made it possible to reduce the influence of the distribution of sensors or components – such as the air mass meter, the volumetric efficiency or the boost pressure sensor – on the NO_x emissions. Furthermore, a special controller structure in the engine control unit enabled high EGR rates to be set in steady-state points, yet without falling below the minimum air mass values in the case of transient load states. This means that it is possible to accelerate with moderate particulate emissions, high dynamics and low NO_x emissions.

2.1.2 Learning Function for Boost Pressure Control

With the aid of the rate regulation, the ratio of the fresh-air/exhaust-air mixture reaching the engine can be preset. If dispersions now occur when it comes to charging the engine, then the oxygen volume per operating cycle in the cylinder can be significantly increased or reduced at a constant AGR rate. This modified quantity of oxygen can result in unwanted effects such as increased emissions or ignition delay.

The charging of the engine is influenced essentially by the available boost pressure. For this reason, a procedure was developed on the introduction of the EU5 exhaust gas stage which minimizes the distribution of the boost pressure and thus also minimizes the charging.

This means it is also possible to restrict considerably the effects of different exhaust gas turbocharger settings, geometric distributions in the field of the air intake and changes over the life-span of the engine.

Figure 2 shows a schematic arrangement of the sensors and actuators as well as the control functions implemented in the engine control. By physically modelling the air system it is possible, in addition to the values recorded directly by sensors, to calculate other variables relevant to the open- and closed-loop control and for monitoring [2].

The default values for the air system are the EGR rate and the boost pressure. With the aid of the physical model of the engine, the EGR rate is converted into a setpoint fresh-air mass. With the aid of the modelled charging air mass, conclusions can be drawn about any necessary EGR air mass. Using a model of the EGR valve, this is converted into a forward control of the electrical EGR valve. Errors in the forward control are additionally compensated by a higher-level EGR rate regulator.

The boost pressure is now specified independently of the AGR rate. With the aid of a model, the required boost pressure can be used to determine an actuator position of the turbocharger with variable geometry. This model was determined and verified on individual design engines on the test bench and in cars. It may deviate from the actual conditions in the vehicle due to distribution of components or life-cycle effects. For this rea-

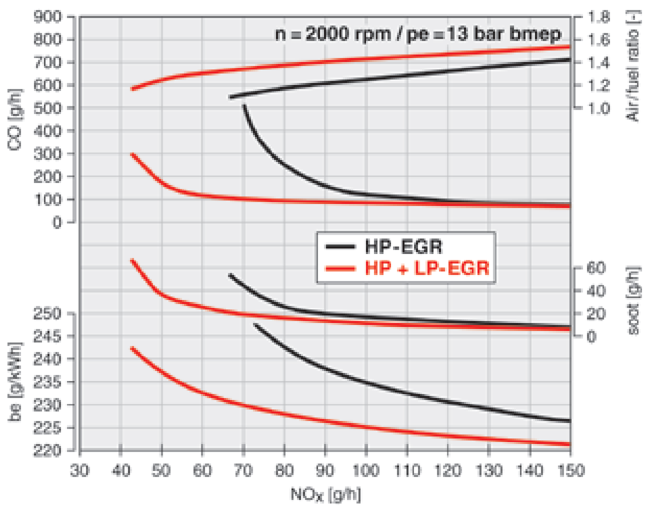

Figure 3: Effect of high-pressure and low-pressure EGR

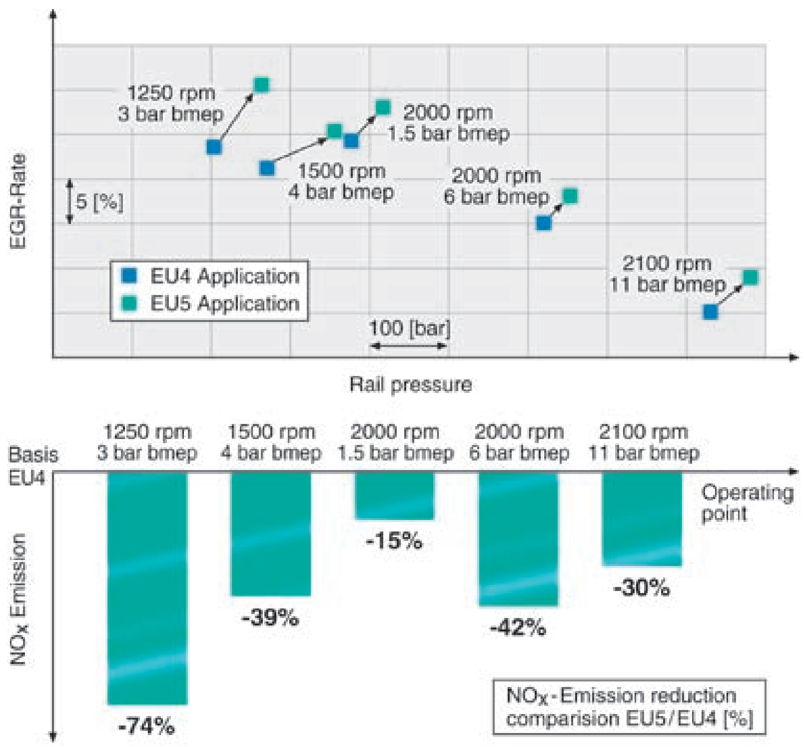

Figure 4: Comparison of EGR-rates EU4 / EU5

son, a learning function is superimposed on the forward control. Compared to the closed loop control of the boost pressure also used in sub-areas, this has the advantage that, even in dynamic processes, a suitable correction of the forward control value can be performed.

The learning function is activated in constant operating points depending on various parameters such as engine speed, fuel injection rate, coolant temperature and EGR rate. When the learning function is active, the control deviation of the boost pressure is determined and entered in a learning characteristic map by means of an evaluation filter. The evaluation filter changes its properties depending on the age of the engine. In a new engine, the error in the boost pressure is quickly learned in order to record deviations due to component distributions and turbochargers with different settings. During the life of the engine, switches are then made to slower evaluation filters. This enables changes to the system to be compensated over the lifespan, while on the other hand the system is robustly protected against transient disturbances that would otherwise corrupt the learning result.

2.1.3 Low-pressure Exhaust Gas Recirculation

In addition to the measures mentioned above, a further improvement of EGR system performance is necessary for the emission control of heavier vehicles according to Tier 2 Bin5, in order to cut the NO_x raw emission level accordingly. To do this, a low-pressure EGR system was also investigated, in which the exhaust gas is not extracted until after particle filter and fed into the fresh-air before the compressor. This version delivered the greatest potential for reducing nitrogen oxide, especially in the case of high-load operating points, **Figure 3**. The positive effect on the fuel consumption is due, on the one hand, to the operating point offset of the exhaust gas turbocharger and, on the other hand, to the lack of throttling, which would be necessary in order to achieve the scavenging gradient because of the use of fixed geometry chargers in multi-stage turbocharging in the X5 xDrive35d.

2.2 Optimization of Combustion

The essential challenge in attaining the EU5 exhaust gas standard is the reliable compliance with the NO_x limit values using internal engine modifications. As a result of the optimizations in the air system described in the section above, it was possible to raise the EGR rate significantly. The resulting increase in the particulate mass was compensated on the one hand by the use of new injection nozzles, optimized in terms of carbon-particular emissions, and on the other hand by increasing the injection pressure. Due to the increased injection pressure, it is possible to achieve an improved jet preparation and thus demonstrate improved EGR compatibility. In addition, the combustion peak is moved to the late position, which also results in a reduction of the NO_x emissions and of the combustion noise. At the top of **Figure 4** the EGR rates and the injection pressures of the EU4 and EU5 application of the four-cylinder engine are compared for some fixed points. Using the modifications described, it was possible to reduce the NO_x emission by the values shown at the bottom of Figure 4 compared to the EU4 application at the same degree of combustion efficiency.

3 Exhaust Gas Treatment

Apart from the internal engine modifications, further development of the existing exhaust gas treatment technology is essential, in order to comply with the US and EU6 limits, in particular for the NO_x exhaust gas component. The technologies used for this – the NO_x storage catalyst (NSC) and the Selective Catalytic Reduction (SCR) – are described below.

3.1 Mode of Operation of the NO_x Storage Catalyst

The nitrogen oxides generated during lean operation are stored as nitrates in the storage catalyst. As a part exists in the form of NO, this must first be oxidized to NO_2. In cyclic rich operation phases (Lambda < 1), in which sufficient reduction agent (H_2, CO and HC) is made available for a low oxygen concentration (< 1 %), this is reduced. The stored nitrates and the reduction agent react to form N_2, H_2O and CO_2. The typical operating range of an NSC is between 150 °C and 500 °C and thus covers a wide engine-map range of a diesel engine almost all the way to full load [3].

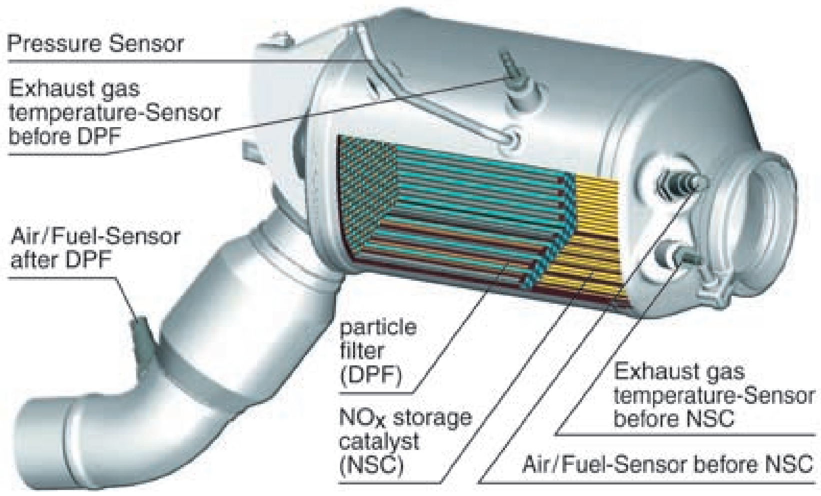

Figure 5: Engine-level NSC and DPF

3.1.1 Close-coupled NSC System

In the development of the NSC system the following objectives had to be ensured:

– modular solution to a basic model [4] with specified package and ready-to-use application
– same customer properties as the basic model with regard to driving performance and comfort
– low system complexity
– fast readiness of system after engine start
– low exhaust gas counter-pressure.

Under the above specifications a engine-level concept was implemented. The oxidation catalyst of the basic application is replaced here by an NO_x storage catalyst of the same size. In addition to storing the NO_x this also performs the catalytic tasks of HC and CO reduction. The NSC volume is just under 2 l, the diesel particle filter (DPF) is dimensioned at almost 4 l as in the basic application. As additional sensors, a second lambda probe is required after the particle filter and a temperature sensor after the NSC. The Lambda probe, the exhaust gas pressure sensor and the temperature sensor ahead of the NSC are already present in the basic model, **Figure 5**. An additional temperature sensor is required after the high-pressure EGR cooler in order to meet the more stringent requirements of the EGR measurement in rich operation. A combined fresh-air mass and exhaust gas recirculation rate control by means of high-pressure EGR valve and throttle valve is applied.

3.1.2 Switching Between Lean/Rich Operating Modes

A challenge for the application of an NSC in the diesel engine is represented by the rich operation mode (Lambda < 1) for the regular regeneration of the NSC ($DeNO_x$ phase). To achieve this, the fresh air mass is severely throttled and the exhaust gas enriched accordingly by further injection of fuel. The periodic switchovers should take place regardless of the engine speed and without being acoustically noticeable. This should not cause any appreciable rise in fuel consumption. For a successful $DeNO_x$ phase, the exhaust gas components and the oxygen concentration are to be strictly observed. This is ensured by means of a Lambda controller integrated into the engine electronics. The rich operating range extends across a window of engine speeds from 900 to 3000 rpm which are frequently used by diesel engines and a torque range up to just below full power. The necessity of a $DeNO_x$ phase is determined with the aid of a raw NO_x model and an NSC loading model, which are stored in the engine control unit. By means of an operating mode coordinator the engine changes from lean to rich mode and is operated under-stoichiometrically until a termination condition occurs. Such a condition could be the departure from the approved operating range described above, the existence of excessive NSC component temperatures, for which thermal blowout of NO_2 or in extreme cases, thermal damage of the NSC can occur or, on the other hand, a complete discharge of the NSC. The latter is recognized by the "rich breakthrough" after the NSC (Lambda switches from 1 to less than 1) by means of the additional Lambda probe after the particle filter. It is therefore completely normal for the complete discharge of the NSC to require several short rich phases with a duration of a few, but no more than 10 s. In the NEDC this results in one, two or three rich phases, in order to achieve the EU6 NO_x limit of 0.08 g/km at an EU5 raw emission level, **Figure 6**. The two lambda probes can additionally be used for NSC component diagnosis. The area that is enclosed between the two lambda signals in the rich mode correlates to the degree of efficiency of the component. By continuously observing

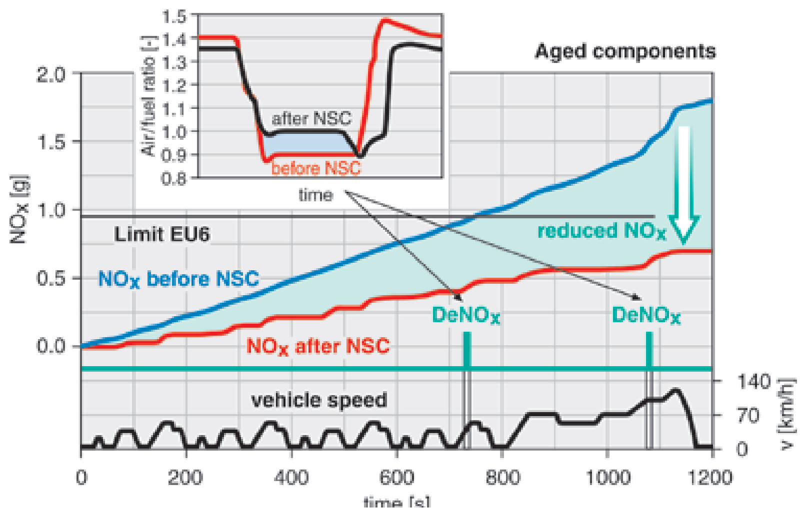

Figure 6: NSC results in the European driving cycle

this property over the entire engine lifespan, any damage to the component can be detected, so that no NO_x sensor is required for diagnostic purposes.

3.1.3 Desulphurization of the NSC

Over the life-span of the vehicle, the sulphur contained in diesel fuel results in sulphur contamination of the NSC. The sulphur is stored as barium sulphate in the NSC, but at the temperatures normally used in lean operation, however, can no longer be removed by means of rich phases. A discharge of the sulphur is only possible at temperatures in excess of 580 °C. As a loss of efficiency is essentially only detectable after the engine has covered several thousand kilometers, it is sufficient to combine a desulphurization with the cyclically occurring particle filter regeneration. The duration of the rich pulse is set in such a way that the desulphurzation process does not produce the foul smelling H_2S, nor will the temperature in the component during and after the rich phase result in thermal aging or damage. In the engine control unit therefore, a sulphur charging and discharging model is implemented on the one hand and a predicted temperature calculation model is implemented on the other. Thanks to the low desulphurization temperature in comparison with earlier NSC coatings and to more highly developed engine control software, it has been possible to significantly improve the aging of the NSC, thus enabling it to be used over the entire life of the vehicle.

3.2 Method of Operation of the SCR System

In comparison with the storage catalyst, the SCR system is a continuously operating $DeNO_x$ system, in which a urea aqueous solution is injected directly into the exhaust flow as a reduction agent. By means of thermolysis and hydrolysis, this creates the actual reduction agent ammonia (NH_3). The NH_3 and NO_x react in the SCR catalyst, finally producing nitrogen and water. The SCR dosing module is positioned as close as possible to the diesel particle filter, as there are higher temperatures here than under the floorpan, which facilitate vaporization of the injected aqueous urea solution. Due to the relatively short mixing path between the injection and the SCR catalyst, the use of a mixer is necessary. The function of the mixer is of crucial importance to the even distribution of NH_3 ahead of the SCR catalyst and thus has a direct influence on the achievable degree of efficiency. **Figure 7** shows how this has been significantly improved through the optimization of the mixer design. When designing the mixer, special effort was taken to ensure that all drops of spray hit the mixer structure. The drops of spray hit the inclined blades and are broken up so that they can vaporize more easily. By conduction of heat in the large blade surfaces, the local cooling of the mixer is reduced and this also aids vaporization of the reduction agent. Small blades are fitted to the back of the mixer to ensure additional turbulent kinetic energy, thereby improving mixing efficiency. This design prevents wisps of NH_3 in the exhaust gas and rules out false measurements of the NO_x sensor located downstream.

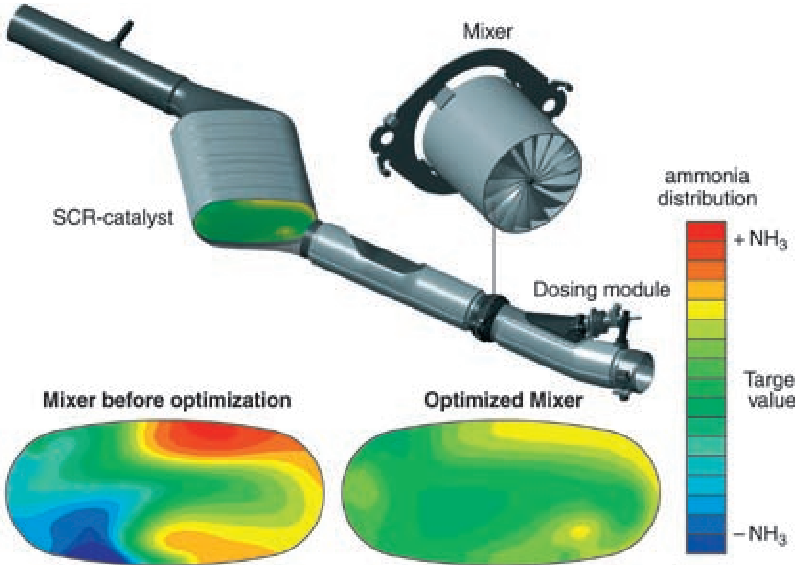

Figure 7: Ammonia distribution ahead of SCR catalytic converter

3.3 Influence of NO_2/NO_x Ratio

The reduction of the nitrogen oxide in the SCR catalyst depends essentially on the temperature, space velocity and the NO_2/NO_x ratio. The working range of maximum conversion is between 200 °C and 300 °C exhaust and catalyst temperature. **Figure 8** shows the degrees of efficiency of

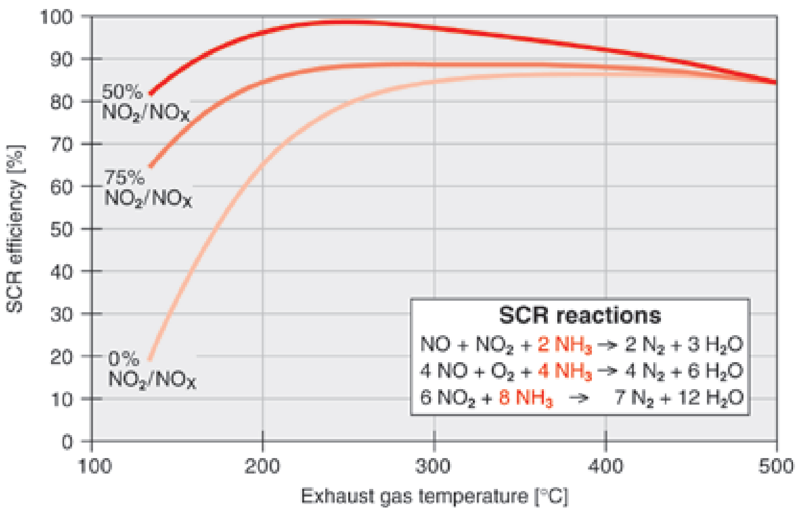

Figure 8: NO_2/NO_x-ratio effect on SCR efficiency

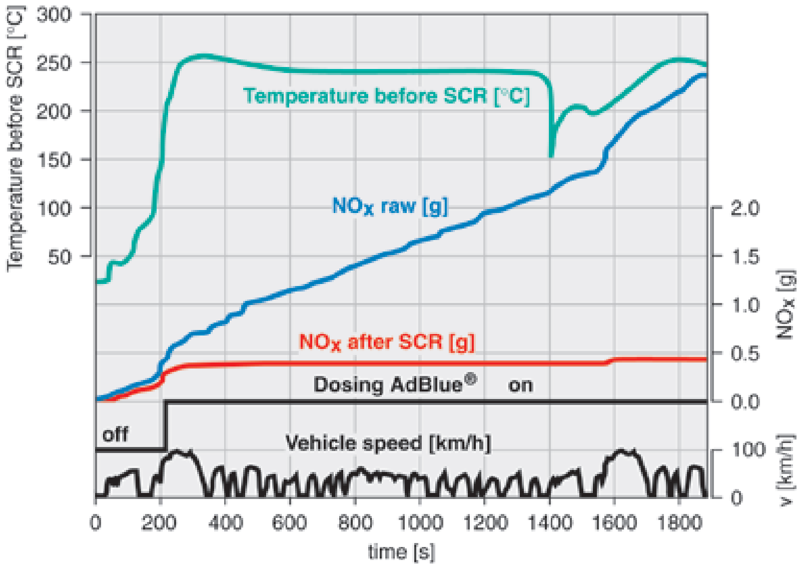

Figure 9: SCR system results in the FTP75

the nitrogen oxide reduction dependent on temperature and NO_2 quota. In addition, the three reactions in the SCR catalyst are listed, which are classified by their speed into very fast, fast and slow SCR reactions. The reaction of the nitrogen oxide to form nitrogen and water is at its fastest with an NO_2/NO_x ratio of 50 %, and at its slowest with an exclusive reduction of NO_2. At the same time, consumption of the reduction agent rises with NO_2 ratios of more than 50 %. Accordingly, the coating selected for the oxidation catalyst and particle filter is of key importance. These oxidizers connected in series must ensure good oxidation of the hydrocarbons and the carbon monoxide and should ideally set a NO_2/NO_x ratio before the SCR catalyst of 50 %. In order to keep below the very demanding NO_x limit values according to Tier 2 Bin5, a coating that is very resistant to aging is accordingly required. In addition, a fast light-off of all catalysts as well as exhaust gas free from hydrocarbons – in order that these do not accumulate in the zeoliths of the SCR catalyst – are necessary for the operation of the SCR system with optimum efficiency.

3.4 Application and Results of the FTP75 Test

Figure 9 shows the results of the application in the FTP75. As this test starts at room temperature, fast heating of the entire exhaust treatment system is decisive. For this reason, a fast heating strategy is used at the start, which is mapped in the control unit. As soon as the SCR catalyst temperature has reached 200 °C, the dosing of AdBlue commences. The degree of efficiency of the $DeNO_x$ system is over 90 % in the test unit, whereas in the second phase it reaches almost 100 %.

4 Implementation of the Emission Concepts in the Car

Depending on the vehicle weight, engine and not least the target market, the technologies described above can now be used in different combinations. **Figure 10** shows three examples for Euro 5 and 6 and US Tier 2 Bin5.

To meet the EU5 limit value stage, the described internal engine modifications are implemented. These can be implemented step by step, depending on the

Figure 10: BMW emission technology kit

	Technical data	Internal engine techniques	Exhaust gas aftertreatment
EU5  118d	power: 105 kW torque: 300 Nm fuel consumption: 4,5 l/100 km	+ Improved high pressure EGR cooling + EGR Rate regulation + learning functions	DOC DPF
EU6  330d	power: 180 kW torque: 520 Nm fuel consumption: 5,7 l/100 km	+ Improved high pressure EGR cooling + EGR Rate regulation + learning functions	NSC DPF
US Tier2Bin5  X5 xDrive35d	power: 200 kW torque: 580 Nm fuel consumption: 29 mpg	+ Improved high pressure EGR cooling + low-pressure EGR + EGR Rate regulation + learning functions	DOC DPF SCR

vehicle weight, or are scalable as in the case of the EGR cooling. The example of the 118d shows that the performance data of the engine as well as the fuel consumption remain unchanged compared to the EU4 version despite the reduced emissions.

The 330d is the first diesel car to meet the EU6 limit value stage. In this concept, not only the internal engine measures, but also the described NO_x storage catalysts are used. It was possible to compensate for the low additional consumption required as a matter of principle due to additional measures, so that here too the fuel consumption remains unchanged compared to the EU5 version also offered.

Compliance with the US Tier 2 Bin5 limit value stage demands the use of an SCR system as well as internal measures in the engine, especially in heavier vehicles. The X5 xDrive35d and the 335d equipped with this solution permits the entry of BMW diesel cars into the US market.

5 Summary

Due to the continuing development of existing technologies in combination with new developments in exhaust gas treatment, BMW has already managed to comply with the demanding EU6 and Tier 2 Bin5 limit value stages. Using the modular conception presented here, optimum adaptation of the technology used to the various requirements, in terms of both the legislation and the vehicle is possible. With the introduction of the SCR technology, the foundation has been laid for the market entry in all 50 states of the USA and in Canada, and thus the way prepared for a further expansion of diesel drivetrains. In combination with the „EfficientDynamics“ measures to reduce fuel consumption the new emission technology assure the future of diesel engines as sustainable drivetrain.

References

[1] Borgmann, K.; Klüting, M.: Efficient dynamics – the ultimate target for BMW powertrains. In: MTZ Extra Drivetrains with a future (2006)

[2] Ertl, C.; Honeder, J.; Schinnerl, M.: Engine control system for the new 4-cylinder engine in the BMW 1 Series. 6th Symposium on Control Systems for Vehicle Drivetrains, 2007

[3] Rohr, F.; Sundararajan, A.; Müller, W.; Heiml, O.; Dornoff, J.: New Efficient NO_x Storage Catalysts Systems for the EU 6 Launch of the BMW 330d. 17th Aachen Colloquium on Vehicle and Engine Technology 2008

[4] Dworschak, J.; Neuhauser, W.; Rechberger, E.; Stastny, H.: The new BMW 6-Cylinder Diesel Engine. In: MTZ 2009 Nr. 1

IMPRINT

MTZ WORLDWIDE

www.MTZ-online.com

03|2009 · March 2009 · Volume 70

Springer Automotive Media | GWV Fachverlage GmbH
P.O. Box 15 46 · 65173 Wiesbaden · Germany
Abraham-Lincoln-Straße 46 · 65189 Wiesbaden · Germany

Managing Directors Dr. Ralf Birkelbach, Albrecht Schirmacher
Advertising Director Thomas Werner
Production Director Ingo Eichel
Sales Director Gabriel Göttlinger

EDITORS-IN-CHARGE

Dr.-Ing. E. h. Richard van Basshuysen
Wolfgang Siebenpfeiffer

EDITORIAL STAFF

Editor-in-Chief
Johannes Winterhagen (win)
Phone +49 611 7878-342 · Fax +49 611 7878-462
E-Mail: johannes.winterhagen@springer.com

Vice-Editor-in-Chief
Dipl.-Ing. Michael Reichenbach (rei)
Phone +49 611 7878-341 · Fax +49 611 7878-462
E-Mail: michael.reichenbach@springer.com

Chief-on-Duty
Kirsten Beckmann M. A. (kb)
Phone +49 611 7878-343 · Fax +49 611 7878-462
E-Mail: kirsten.beckmann@springer.com

Sections

Electrics, Electronics
Markus Schöttle (scho)
Phone +49 611 7878-257 · Fax +49 611 7878-462
E-Mail: markus.schoettle@springer.com

Engine
Dipl.-Ing. (FH) Richard Backhaus (rb)
Phone +49 611 5045-982 · Fax +49 611 5045-983
E-Mail: richard.backhaus@rb-communications.de

Heavy Duty Techniques
Ruben Danisch (rd)
Phone +49 611 7878-393 · Fax +49 611 7878-462
E-Mail: ruben.danisch@springer.com

Online
Dipl.-Ing. (FH) Caterina Schröder (cs)
Phone +49 611 78 78-190 · Fax +49 611 7878-462
E-Mail: caterina.schroeder@springer.com

Production, Materials
Stefan Schlott (hlo)
Phone +49 8191 70845 · Fax +49 8191 66002
E-Mail: Redaktion_Schlott@gmx.net

Service, Event Calendar
Martina Schraad
Phone +49 212 64 235 16
E-Mail: martina.schraad@springer.com

Transmission, Research
Dipl.-Ing. Michael Reichenbach (rei)
Phone +49 611 7878-341 · Fax +49 611 7878-462
E-Mail: michael.reichenbach@springer.com

English Language Consultant
Paul Willin (pw)

Permanent Contributors
Christian Bartsch (cb), Prof. Dr.-Ing. Peter Boy (bo), Prof. Dr.-Ing. Stefan Breuer (sb), Jörg Christoffel (jc), Jürgen Grandel (gl), Erich Hoepke (ho), Ulrich Knorra (kno), Prof. Dr.-Ing. Fred Schäfer (fs), Roland Schedel (rs), Bettina Seehawer (bs)

Address
P.O. Box 15 46, 65173 Wiesbaden, Germany
E-Mail: redaktion@ATZonline.de

MARKETING | OFFPRINTS

Product Management Automotive Media
Sabrina Brokopp
Phone +49 611 7878-192 · Fax +49 611 7878-407
E-Mail: sabrina.brokopp@springer.com

Offprints
Martin Leopold
Phone +49 2642 9075-96 · Fax +49 2642 9075-97
E-Mail: leopold@medien-kontor.de

ADVERTISING | GWV MEDIA

Key Account Manager
Elisabeth Maßfeller
Phone +49 611 7878-399 · Fax +49 611 7878-140
E-Mail: elisabeth.massfeller@gwv-media.de

Ad Sales
Frank Nagel
Phone +49 611 7878-395 · Fax +49 611 7878-140
E-Mail: frank.nagel@gwv-media.de

Display Ad Manager
Susanne Bretschneider
Phone +49 611 7878-153 · Fax +49 611 7878-443
E-Mail: susanne.bretschneider@gwv-media.de

Ad Prices
Price List No. 52

SUBSCRIPTIONS

VVA-Zeitschriftenservice, Abt. D6 F6, MTZ
P. O. Box 77 77, 33310 Gütersloh, Germany
Renate Vies
Phone +49 5241 80-1692 · Fax +49 5241 80-9620
E-Mail: SpringerAutomotive@abo-service.info

SUBSCRIPTION CONDITIONS

The emagazine appears 11 times a year at an annual subscription rate of 269 €. Special rate for students on proof of status in the form of current registration certificate 124 €. Special rate for VDI/ÖVK/VKS members on proof of status in the form of current member certificate 208 €. Special rate for studying VDI members on proof of status in the form of current registration and member certificate 89 €. The subscribtion can be cancelled in written form at any time with effect from the next available issue.

PRODUCTION | LAYOUT

Heiko Köllner
Phone +49 611 7878-177 · Fax +49 611 7878-464
E-Mail: heiko.koellner@gwv-fachverlage.de

HINTS FOR AUTHORS

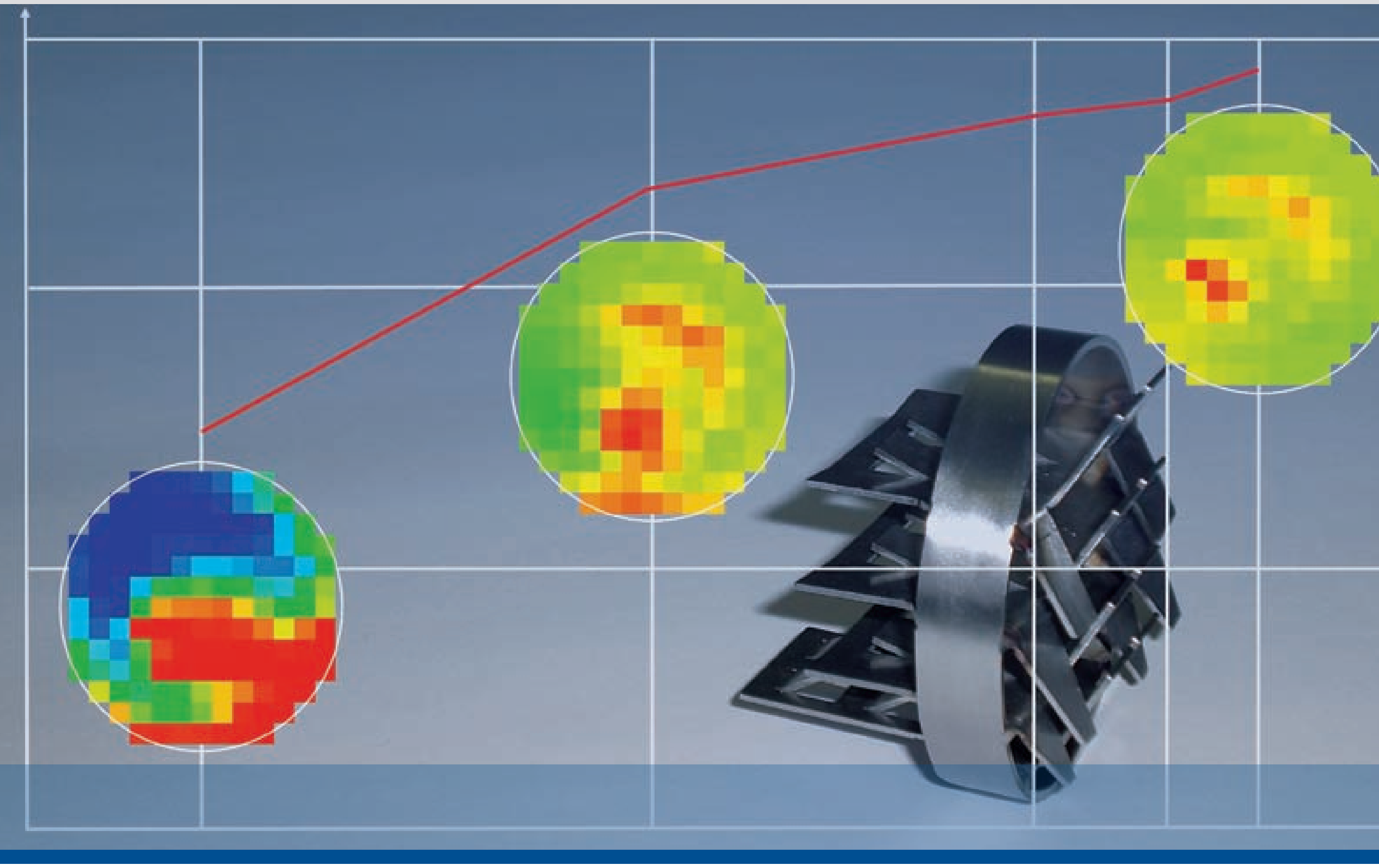

personal buildup for Force Motors Ltd.

Optimization of SCR Systems by Integration of Mixture Elements

Efficient SCR systems require an optimal reductant conditioning and a uniform NH_3 distribution. This can only be achieved by the choice and the optimization of the appropriate mixing device. A novel, at Tenneco developed two-stage mixer provides a very good mixing performance at a comparatively low pressure loss. For a rapid and cost efficient system optimization, Tenneco uses the CFD simulation in combination with a high resolution measuring procedure for the determination of the local NH_3 concentration.

1 Introduction

Future vehicle emission limits such as EU6 and Tier 2 Bin5 require again a significant reduction of pollutant emissions, especially for nitrogen oxides (NO_x). At the same time, a decrease in fuel consumption and thereby CO_2 emission is required. Current engines offer high power in combination with low fuel consumption and consequently low CO_2 emissions. However this in combination with increased nitrogen oxide emissions. Thus, the demanding NO_x limitations are not achievable only by the improvements to the engine, they require an additional exhaust gas aftertreatment, the most promising is the SCR technology.

2 SCR Technology

NO_x reduction via the SCR principle is achieved using ammonia or ammonia constituent substances. Known since the end of the seventies, this technique is successfully adapted for power station applications, in which pure ammonia is used as reductant. Ammonia though is dangerous and inappropriate for mobile applications. In the automotive sector the Selective Catalytic Reduction with 32.5 % hydrous urea is used. In this case, the aqueous urea solution is injected into the exhaust gas system, vaporized and converted to ammonia through thermolysis and hydrolysis, Eq. (1a) to (1c). In the SCR catalyst this ammonia reduces selectively the nitrogen oxides into nitrogen and water, Eq. (2a) to (2c). The fastest reaction is in accordance with Eq. (2b), where NO and NO_2 exist in equal parts. Conversion rates up to 100 % can be reached with an optimal layout of the SCR system. Even at temperatures down to 250 °C conversion rates of over 85 % can be achieved.

Table 1: Parameters for the SCR system development

Engine
– Exhaust gas massflow – Exhaust gas temperature – NO_x-emission
Exhaust system
– catalyst volume & space velocity – Inlet geometry & flow distribution – mixing length & -geometry (e. g. bendings, dents) – NO/NO_2-ratio (depending on DOC)
Dosing system & -valve
– Position and orientation in the exhaust system – spray angle – droplet size & size distribution

The big advantage of this technology is the high efficiency over a wide temperature range and the high selectivity. The disadvantage is the need to carry a second fluid, which increases weight and package requirements. Furthermore the additional efforts for the injection, conditioning and distribution of the urea have to be taken into consideration.

The injection and conditioning of the reductant is essential for the SCR converter, the main parameters are:

- position and orientation of the injector have an impact to the droplet transportation and distribution in the gas flow and therefore on the accumulation of deposits
- the spray angle influences the distribution in the pipe
- droplet size and droplet diameter distribution: the smaller the droplets are, the shorter the required vaporization time the better the distribution in the flow
- mixing pipe and geometry
- decomposition of urea to ammonia, Eq. (1a) to (1c)
- uniform distribution of ammonia on the SCR catalyst.

A complete vaporization should be achieved ahead of the SCR catalyst itself, otherwise this process will happen in the converter and precious catalyst volume can be lost for the proper SCR reaction itself and the system efficiency decreases. Furthermore a non-uniform distribution and NH_3 slip can occur. Ammonia slip must be avoided, due its toxic and acid nature. Moreover, even small concentrations can lead to an unpleasant smell.

Another important criterion is the avoidance of deposits of urea and urea secondary products such as Biuret, Cyanuric Acid and Cyamelid:

- deposits can influence the flow conditions inside the whole mixing length and therefore also the urea conditioning
- settled urea is not available for the SCR reaction, thus decreasing the conversion rate
- the removal of deposits requires higher temperatures and leads to the release of ammonia.

Table 1 gives an overview of the key parameters. Due to these influences the development requires an analytical approach and the appropriate development tools.

3 Tools for SCR System Development

Measuring the average values behind the SCR catalyst on an engine bench gives only an answer, whether a certain emission target will be fulfilled or not.

For a detailed evaluation and the optimization of the system, the measurement of the local NH_3 concentration is required. Therefore a procedure and a testrig were developed, that allows the characterization of the SCR system under real conditions. In parallel, the CFD modeling was developed further.

The Authors

Dipl.-Ing. (FH), M.Sc. Joachim Gehrlein is supervisor product development in the department exhaust gas aftertreatment at Tenneco-Gillet in Edenkoben (Germany).

Dipl.-Ing. Andreas Lang is supervisor simulation in the exhaust gas aftertreatment department at Tenneco-Gillet in Edenkoben (Germany).

Dr. Günter Palmer is advanced engineer in the department exhaust gas aftertreatment at Tenneco-Gillet in Edenkoben (Germany).

3.1 CFD Modeling

The commercial software suite „STAR-CD" is used to describe and predict the behaviour of injected reactant droplets. Fully coupled Euler-Lagrange Two-Phase flow calculations are conducted with interphase momentum-heat and mass transfer. The result is the interaction of the spray with the flow as well as the trajectories of the evaporating droplets and information on the temperature and concentration distribution.

For these types of applications the reacting surface is an important measure. Therefore special care has to be taken in modeling the characteristics of the nozzle. Due to the fact that small droplets behave differently in the gas flow than bigger droplets, the Tenneco approach is to divide the measured droplet size spectrum in many numerical classes, whilst maintaining the Sauter Mean Diameter. The characteristic of the nozzle is modeled accurately in respect to number, configuration and shape of the spray. This is done by user-defined subroutines, which enables a rapid transfer to different projects without any errors.

Due to the multitude of possible phenomena, droplet-wall interaction is a challenge, as under certain circumstances deposits may occur which might considerably disturb the proper function of the system.

3.2 Procedure for Urea Distribution Measurement

For the determination of the local reductant concentration, a testrig with Roots Compressors and electrical heaters is available to reproduce the real conditions of an engine. For heavy duty applications with higher mass flows a gas burner will be used. A gas dosing unit is installed for the adjustment of the exact concentration of the nitrogen oxide. For the local concentration measurement, an X-Y table allows the fully automated scanning of the complete cross section behind the SCR catalyst. Based on the measured local values, the test bench software will create a concentration distribution profile. The sampling will take place directly behind the catalyst outlet face via a sampling pipe and heated hoses to the CLD. The determination of the local NH_3 concentration is based on the measurement of the local NO_x conversion, which requires two separate measurements, one without and one with urea injection, **Figure 1**. Based on Eq. (3) and Eq. (2a) to (2c) the local ammonia concentration can be determined.

As assessment criterion for the reductant distribution the NH_3 uniformity index (NH_3 UI) is used, the definition is analog to the flow uniformity index introduced by Tenneco in 1993. The smaller the total deviation of the measured local concentration is in relation to the average value, the better is the reductant uniformity. The maximum achievable value is 1.0, Eq. (4).

Figure 1 shows the experimental test setup in the flow lab and the result from a measurement in comparison with the CFD calculation. Both distributions show good agreement with respect to homogeneity and the location of maxima and minima.

The advantages of flow lab measurement are:

- measurements under real conditions possible (mass flow, temperature, NO_x concentration)
- lower testing time and costs in comparison with the engine bench test
- quick measurement and rapid results: approximately 45 min for one operating point (based on a resolution of 150 measuring segments behind the catalyst)
- a high resolution shows local minima and maxima, e.g. ammonia slip; with a low resolution measurement & interpolation, local peaks could be overlooked
- good repeatability due to an exact adjustment of the parameters, on an engine bench fluctuations caused by external circumstances are possible.

Figure 1: Test rig and NO_x concentration measurement w/o and with urea injection, NH_3 distribution in comparison with the CFD calculation

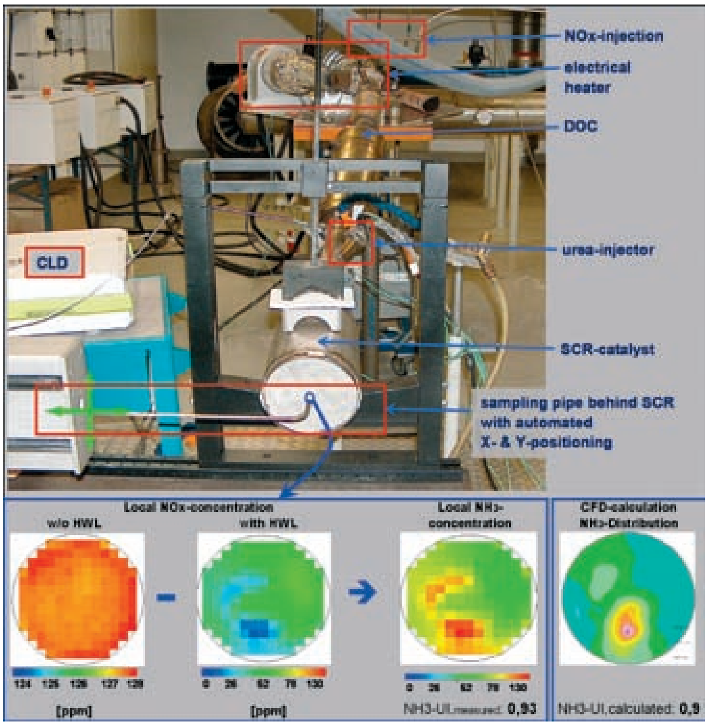

Equations

Decomposition of urea:

$(NH_2)_2CO$	⇔	$NH_3 + HNCO$	Eq. (1a)
$HNCO + H_2O$	⇔	$NH_3 + CO_2$	Eq. (1b)
$(NH_2)_2CO + H_2O$	⇔	$2\,NH_3 + CO_2$	Eq. (1c)

SCR-reaction:

$4\,NH_3 + 4\,NO + O_2$	⇔	$4\,N_2 + 6\,H_2O$	Eq. (2a)
$2\,NH_3 + NO + NO_2$	⇔	$2\,N_2 + 3\,H_2O$	Eq. (2b)
$4\,NH_3 + 2\,NO_2 + O_2$	⇔	$3\,N_2 + 6\,H_2O$	Eq. (2c)

Determination of the local NH_3-concentration

$$c_{NH_3} = \Delta c_{NOx} = c_{NOx,ohneHWL} - c_{NOx,mitHWL} \qquad \text{Eq. (3)}$$

NH_3-Uniformity-Index:

$$\gamma = 1 - \frac{\sum_{i=1}^{n} A_i * \sqrt{\left(c_{NH3,i} - \overline{c_{NH3}}\right)^2}}{2 * \sum_{i=1}^{n} A_i * \overline{c_{NH3}}} \qquad \text{Eq. (4)}$$

Table 2: Requirements of a mixing element

– Atomization
– Evaporation
– Mixing
– No deposits or clogging
– Low pressure loss
– Simple manufacturability & integration in the system
– Low costs
– Durability (thermomechanics & vibration)
– No / low acoustic impact

4 Mixer Development

In most passenger car applications the package boundaries for SCR system integration are difficult, an adequate mixing length or the ideal injector position cannot be realized.

These circumstances require the use of a mixing device which has to be adjusted and optimized to the specific application. Furthermore, it has to fulfill various requirements, **Table 2**.

Main functions of the mixer are:

- atomization: The mixer is acting as a collision surface, the droplet break up on impact. Smaller droplets will evaporate quicker due to the better surface to volume ratio
- evaporation: The hot mixer surface helps to evaporate and decompose the reductant
- mixing: An even reductant distribution requires macroscopic mixing.

Different mixing devices were tested in the flow lab. An abstract is shown in **Figure 2**. Without mixer the distribution is inadequate, with the wire mesh mixer the results improve but there is no macroscopic mixing. The blade mixer “sym B6” causes a macroscopic mixing and shows a better distribution. Due to the small surface of the blades, the conditioning of the urea is not optimal. The results of the baseline and the swirl mixers show an increased homogeneity of ammonia. The best results can be obtained with a two stage reductant conditioning.

An additional fact which has to be considered is, that the spray position of the injector valve and therefore the mixer impingement can vary depending on the mass flow and temperature, **Figure 3**. To avoid the jet shooting through the mixer at some operating points, it is necessary to design a mixer with a dense structure, e.g. through increasing the mixer blade angle. The disadvantage of this modification is the associated increase in pressure loss.

Tenneco has developed a novel two-stage mixing device, which compensates the mass flow depending spray position by a pre-mixing zone and ensures an excellent conditioning and an equal distribution. At low load operation points, the injected reductant is hitting the mixer in the bottom area, **Figure 4** center left. The lower surface will deflect a part of the exhaust gas and reductant to the middle.

In the shown example this effect will be enhanced by the main mixer. At high loads the urea spray will hit the pre-mixer in the upper area. Figure 4 center right. The blades of the pre-mixer deflect the urea into the center. The macroscopic mixing is performed by the main mixing device. The choice of the main mixing element and principle is related to the specific application. CFD calculations, Figure 3, and the results of the measurements, Figure 4, show a homogeneous distribution of the ammonia independent of the exhaust gas mass flow.

The pre-mixing device leads to a minimal additional pressure drop, on the other hand, the deflection surface angle of the main mixer can be flattened and in total the pressure value is lower.

The individual adjustment of the mixer to the boundary conditions can be realized by the optimization of the parameters such as the blade angle, the orientation or the distance between injector and mixer as shown in **Figure 5**. A length reduction leads to a better homogeneity in all three operating points.

Finally **Figure 6** shows the achieved NH_3 homogeneity plotted against the pressure loss of different mixing devices. Compared to the other mixing elements tested, the two-stage mixer shows with

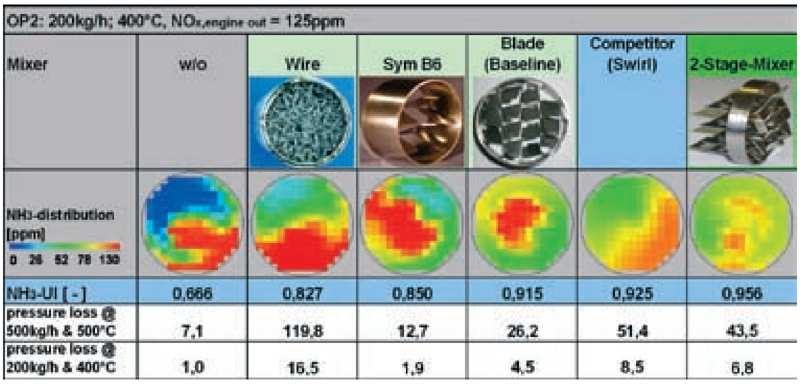

Figure 2: NH_3 uniformity measurement for different mixers

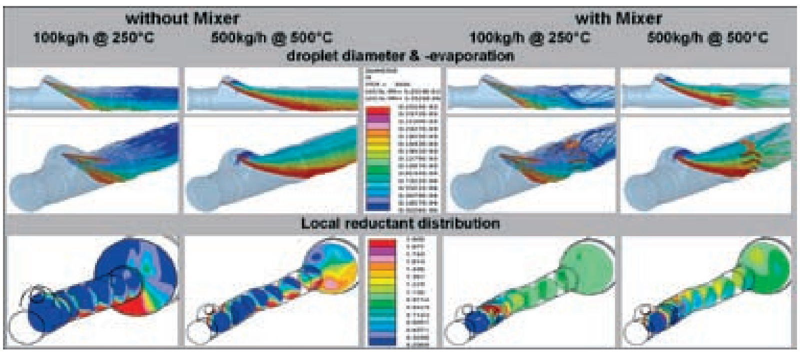

Figure 3: CFD simulation of droplet injection, evaporation and reductant distribution

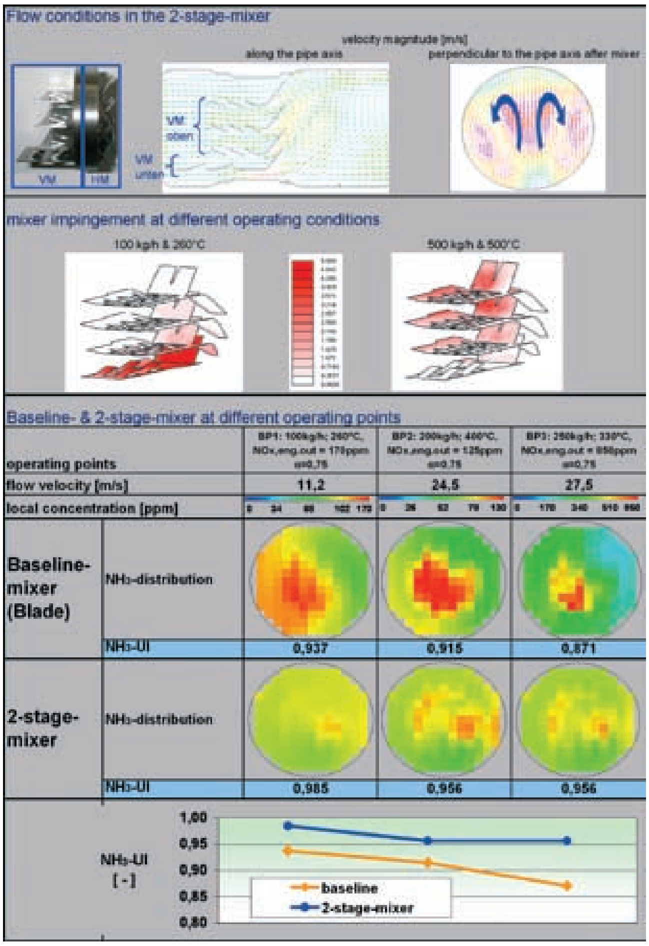

Figure 4: Function of two-stage mixer and comparison to the baseline mixer in different operating points

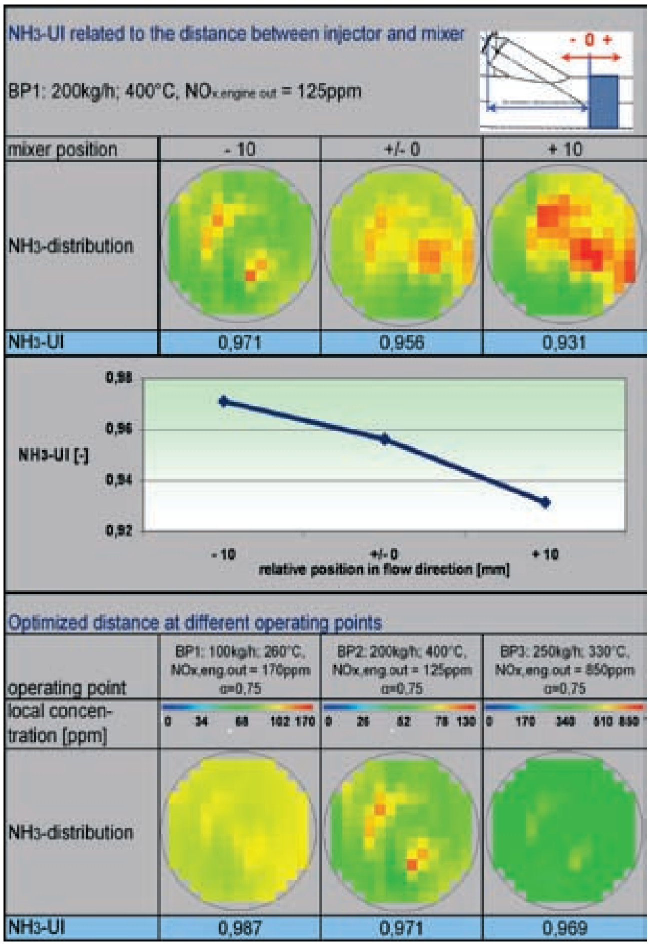

Figure 5: NH_3 distribution related to the distance between injector and mixer

an uniformity index of over 0.95 a very high performance. With smaller blade angles the ammonia distribution declines a little bit but the pressure loss decreases significantly.

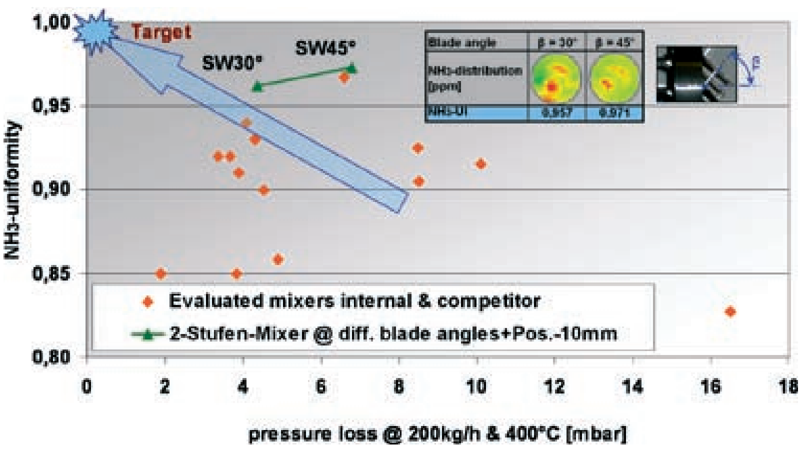

Figure 6: NH_3 uniformity versus the pressure loss for different mixing elements

5 Conclusion

Effective SCR systems require an optimal reductant conditioning and distribution as well as prevention of deposits and ammonia slip. Together with CFD Simulation, the high resolution measurement of the local concentration under laboratory conditions is a fast, competitive and reproducible method for the optimization of a SCR system.

With the Integration of a two-stage mixing element an optimal NH_3 distribution with the lowest possible increase of back pressure can be accomplished.

Especially for passenger car applications with tight package constraints, short mixing length and complex pipe geometries, mass flow and temperature related spray behaviour, the two-stage mixer concept demonstrated a high performance.

The development tools presented in this paper and the two-stage mixer are important elements for SCR system optimization, which can also be applied to different tasks, for example HC injection for active filter regeneration. ■


ATZ
Cockpit Development
Improving Processes
and Ergonomics
iBook

Mazda's LNT

Catalytic Characteristics of the New Shape Support Material

The new shape ceria-based support material for a lean Nitrogen oxide (NO_x) trap catalyst (LNT) was developed by Mazda. It has a unique shape that each fine particle of raw material is formed into hollow sphere. Samples of platinum loaded powder catalysts were obtained with either the hollow sphere ceria-based material or two kinds of the conventional shape one and their catalytic activities were evaluated with the synthetic gas. The characterisation results indicate that the hollow sphere ceria-based material had high thermal stability [1].

1 Introduction

For the reduction of NO_x emissions from a diesel engine, it is effective to apply a lean NO_x trap (LNT) catalyst to the after-treatment system [2, 3]. In order to comply with the emission regulation becoming stricter worldwide, it is required to improve the performance and the durability of LNT catalysts [4]. In the LNT catalyst, NO_x is adsorbed as the nitrates of NO_x storage materials (for example, alkaline earth oxide) during the lean air/fuel (A/F) operation. Then the adsorbed NO_x is released and reduced to Nitrogen (N_2) and Oxygen (O_2) by the reductant agents such as Carbon monoxide (CO), Hydrogen (H_2) and Hydrocarbon (HC) during the periodic rich A/F operation. It is important to reduce NO_x during not only lean but also rich A/F condition. To promote efficiently the NO_x reductive reaction is contributing to the reduction of NO_x emissions during the rich operation [4]. It is one of the keys promoting this reaction to improve the thermal stability of the support materials, on which the precious metals and NO_x storage materials are loaded in the formulation of the LNT catalyst. It was reported to be effective for the improvement of LNT's performances to load a certain amount of ceria material as one of the support materials [5].

In this study, as one approach to improve the thermal stability of ceria material, the new shape ceria-based material has been developed and its catalytic characteristics were studied. The feature of this new ceria-based material is that each fine particle of raw material is formed into hollow sphere, **Figure 1**. The catalytic activity of the hollow sphere ceria-based material was evaluated on a powder model catalyst and its characteristics were investigated by Transmission Electron Microscope (TEM), X-Ray diffraction (XRD) and BET.

2 Experimental

2.1 Specimen Preparation

Three kinds of the ceria-based mixed oxide powder with the same composition ($Ce0.19Zr0.81O_2$) are prepared. One is the hollow sphere material, and the others are the conventional shape materials. They are listed in the **Table**, which refers to the sample labelling, the shape of the materials, and the preparation method, respectively. Two samples with conventional shape were prepared by either the co-precipitation method or the spray pyrolysis. Although the hollow sphere particle was also basically prepared using the same spray pyrolysis apparatus, its specific preparation condition was controlled to form hollow sphere shape.

Powder catalysts were prepared by wet impregnation of the ceria-based mixed oxide powders with a platinum (Pt) aqueous solution. The impregnated powders were dried at 150 °C and then calcined in air at 500 °C for 2 h. The Pt loading amount of the powder catalysts was 1 wt%.

The fresh powder catalysts were aged in air at 750 °C for 24 h, referred to as the oxidation pre-treatment. The aged catalysts were then loaded in a quartz reactor, and reduced in 2.2 % CO balanced with helium gas at 600 °C for 10 min and cooled to room temperature, referred to as the reduction pre-treatment.

2.2 Characterisation

The catalytic studies can be characterised as follows:

- Powder shapes: The powder shape was observed with TEM. The voltage was 300 keV.
- Crystal structure: Crystal structural information of the powder was obtained from the XRD tests. The X-ray diffractometer was operated by using

Table: List of the powders

Sample label	Shape	Preparation method
Conventional particle	Conventional	Co-precipitation
Fine particle	Conventional	Spray pyrolysis
Hollow sphere particle	Hollow sphere	Spray pyrolysis

The Authors


Dr. Akihide Takami
is Senior Researcher, Catalyst and material research, Technical Research Center at Mazda Motor Corporation in Hiroshima (Japan).


Dr. Yoshinori Tsushio
is Senior Technical Specialist, Material research, Technical Research Center at Mazda Motor Corporation in Hiroshima (Japan).


Kouichiro Harada
works at the Technical Research Center, Catalyst research at Mazda Motor Corporation in Hiroshima (Japan).


Dr. Hiroshi Yamada
is Senior Technical Specialist, Catalyst research, Technical Research Center at Mazda Motor Corporation in Hiroshima (Japan).


Seiji Miyoshi
is Senior Specialist, Catalyst system design, Powertrain Development Division at Mazda Motor Corporation in Hiroshima (Japan).


Dr. Hideharu Iwakuni
is Senior Technical Specialist, Catalyst Research, Technical Research Center at Mazda Motor Corporation in Hiroshima (Japan).

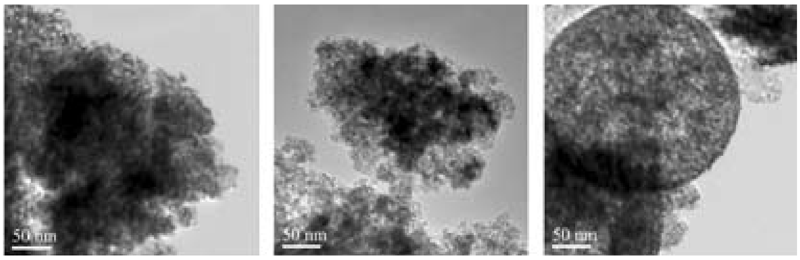

Figure 1: Left: TEM image of the fresh conventional particle; middle: TEM image of the fresh fine particle; right: TEM image of the fresh hollow sphere particle

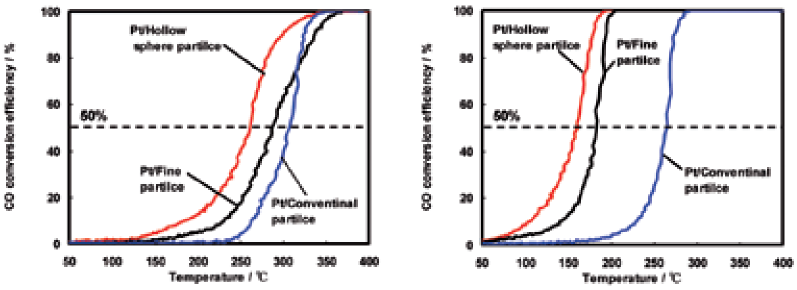

Figure 2: Left: CO conversion profiles of the aged powder catalysts during the CO oxidation performance test after the oxidation pre-treatment; right: CO conversion profiles of the aged powder catalysts during the CO oxidation performances test after the reduction pre-treatment

Cu-Kα radiation accelerating voltage of 50 kV with the current of 240 mA.

- Specific surface area: The surface area of the powder catalysts was measured by BET surface analysis procedure with nitrogen adsorption.
- Micropore distribution: The micropore distribution data of the powder catalysts was collected by the volumetric gas adsorption method using nitrogen gas.

2.3 Catalytic Activity

2.3.1 Catalytic Performance

CO oxidation performance of the powder catalysts are evaluated with a fixed bed reactor. The powder catalyst was heated at a rate of 20 °C/min in 1 % CO and 0.5 % O_2 balanced with helium gas; the CO conversion efficiency was measured. The temperature at which the conversion efficiency of CO reached to 50 % was measured and called as CO_T50 (°C).

2.3.2 Oxygen Release Characteristics

The oxygen release characteristic was evaluated with the temperature programmed reduction (TPR). The powder catalyst was loaded in a quartz reactor. It was heated from room temperature to 600 °C at 20 °C/min under flowing 2.2 % CO balanced with helium gas. The flow rate was 100 ml/min. The generated Carbon dioxide (CO_2) was measured by the mass spectroscopy.

3 Results and Discussion

3.1 Properties of the Mixed Oxide Materials

Figure 1 shows the TEM images of the as-prepared powders. As for the conventional particle and fine particle, **Figure 2** left and middle, each primary particle is aggregating shape. By contrast, in the TEM image of the hollow sphere particle, Figure 2 right, there is the sphere particle with the diameter of approximately 500 nm. It was made up of a lot of primary particles. The shell thickness of this hollow sphere particle is thought to be about 20 nm.

The primary particle diameter of the conventional particle was about 10 nm to 15 nm, Figure 2 left. In case of the fine particle and the hollow sphere particle, it was about 5 nm to 10 nm, Figure 2 middle and right. The two powders prepared by the spray pyrolysis had smaller primary particle size than the powder prepared by co-precipitation method.

3.2 Investigation of Catalytic Performances of the Powder Catalysts

A LNT catalyst is exposed to both oxidation and reduction atmosphere in the exhaust system. Therefore, the three powder catalysts were evaluated after both reduction and oxidation pre-treatment. First, CO conversion performance tests of the powder catalysts, which are aged in air at 750 °C for 24 h, were performed after the oxidation pre-treatment. Figure 2 left shows the CO conversion efficiency as a function of temperature. CO_T50, the temperature at which the CO conversion reached to 50 %, was lower in the order of Pt/hollow sphere particle, Pt/fine particle, Pt/conventional particle.

The aged catalysts were also evaluated after the reduction pre-treatment, and the results are displayed in Figure 2 right. The order of CO_T50 was the same as that after the oxidation pre-treatment. Thus, the Pt/hollow sphere parti-

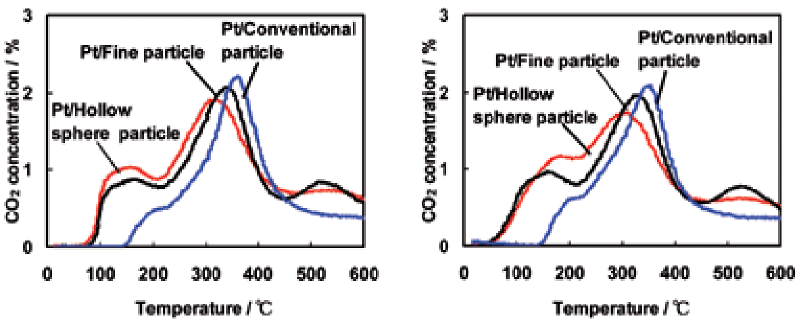

Figure 3: Left: Temperature programmed reduction profiles of the aged powder catalysts after the oxidation pre-treatment; right: Temperature programmed reduction profiles of the aged powder catalysts after the reduction pre-treatment

cle had the lowest CO_T50 indicating the highest CO oxidation performance at the temperatures of 300 °C or lower after both the oxidation and the reduction pre-treatment.

All powders were the ceria-based material, so they have the oxygen storage capacity (OSC), that ceria adsorb excess oxygen under lean A/F conditions and release the stored oxygen under rich conditions. To access the oxygen release characteristics, CO-TPR was carried out after either oxidation or reduction pre-treatment. **Figure 3** shows respectively the TPR profiles of the aged catalysts after each pre-treatment as a function of temperature. At both pre-conditions, Pt/hollow sphere particle highest oxygen capacity below 300 °C among the catalysts. It was thought that more released oxygen contributed to promote CO oxidation reaction at the temperatures of 300 °C or lower after both the oxidation and the reduction pre-treatment.

3.3 Characterisation of the Powder Catalysts

Figure 4 shows TEM images of the each powder catalyst after aging treatment in air at 750 °C for 24 h. The primary particle diameter of Pt/conventional particle, Pt/fine particle, and Pt/hollow sphere particle is approximately 20 nm to 30 nm, 10 nm to 20 nm and 10 nm to 15 nm, respectively. While Pt/conventional particle and Pt/fine particle became much larger after the aging treatment, Pt/hollow sphere particle was maintained to be the smallest among the catalysts.

Figure 5 left shows the BET surface area of the powder catalysts before and after aging. At the fresh condition, the all catalysts had almost the similar surface area. On the contrary, the surface area after the aging was higher in the order of Pt/hollow sphere particle, Pt/fine particle, Pt/conventional particle. It also means that the decreasing rate of Pt/hollow sphere particle was smallest among the catalysts. Additionally, it was found the order of the surface area was same as that of CO_T50 after both the pre-treatment, which was described above.

Figure 5 right shows the micropore distribution of the aged catalysts. The pore diameter for Pt/hollow sphere particle ranged from 2 nm to 130 nm. This distribution range was the widest among the catalysts.

Particularly, its pore volume at the diameter ranging from 2 nm to 20 nm was the highest among the catalyst. From the TEM results, it was thought that these were due to the clearance between the primary particles. It was assumed that the sintering of the primary particle in Pt/hollow sphere particle was reduced compared with the others.

These results suggested that Pt/hollow sphere particle had the highest thermal stability among the catalysts. It is thought that its higher thermal stability was one of the reasons contributing to the better CO oxidation performance.

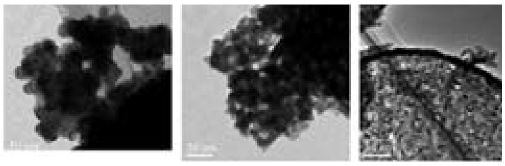

Figure 4: Left: TEM image of the aged conventional particle; middle: TEM image of the aged fine particle; right: TEM image of the aged hollow sphere particle

4 Conclusion

The new ceria-based hollow sphere material had been developed, and its catalytic performances had been investigated as Pt supported catalyst. The following results were obtained.

- Pt/ceria-based hollow sphere material had higher CO oxidation performance and oxygen storage capacity at the temperatures of 300 °C or lower than Pt/conventional shape ceria-based materials.
- The primary particles for the Pt/ceria-based hollow sphere were maintained approximately 5 nm to 10 nm in diameter, and its surface area was higher than the Pt/conventional shape ceria-based materials after aging treatment in air at 750 °C for 24 h.
- Pt/ceria-based hollow sphere material had the pores ranging from 2 nm to 130 nm, which was the wider range distribution compared with Pt/conventional shape ceria-based materials.

References

[1] Reprinted with permission from SAE Paper # 2007-01-3732 © 2007 SAE International

[2] Miyoshi, Naoto; Matsumoto, S.; Katoh, K.; Tanaka, T.; Harada, J.; Takahashi, N.; Yokota, K.; Sgiura, M.; Kasahara, K.: Development of New Concept Three-Way Catalyst for Automotive Lean-Burn Engines, SAE Paper no. 950809

[3] Hepburn, Jeffery S.; Thanasiu, Eva; Dobson, Douglas A.; Watkins, William L.: Experimental and Modeling Investigation of NO_x Trap Performance, SAE 962051

[4] Brogan, M.; Clark, A.; Brisley, R.: Recent Progress in NO_x Trap Technology, SAE Paper no. 980933

[5] Theis, J.; Ura, J.; Li, J.; Surnilla, G.; Roth, J.; Goralski Jr. C.: NO_x Release Characteristics of Lean NO_x Traps during Rich Purges, SAE Paper No.2003-01-1159

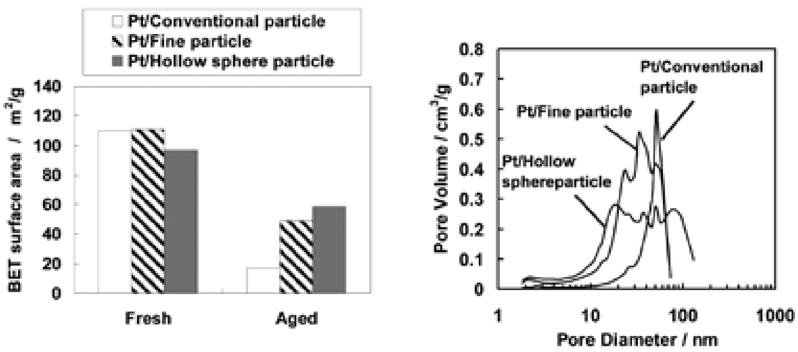

Figure 5: Left: Specific surface are of the fresh and aged powder catalysts; right: Micropore distributions of the aged catalysts

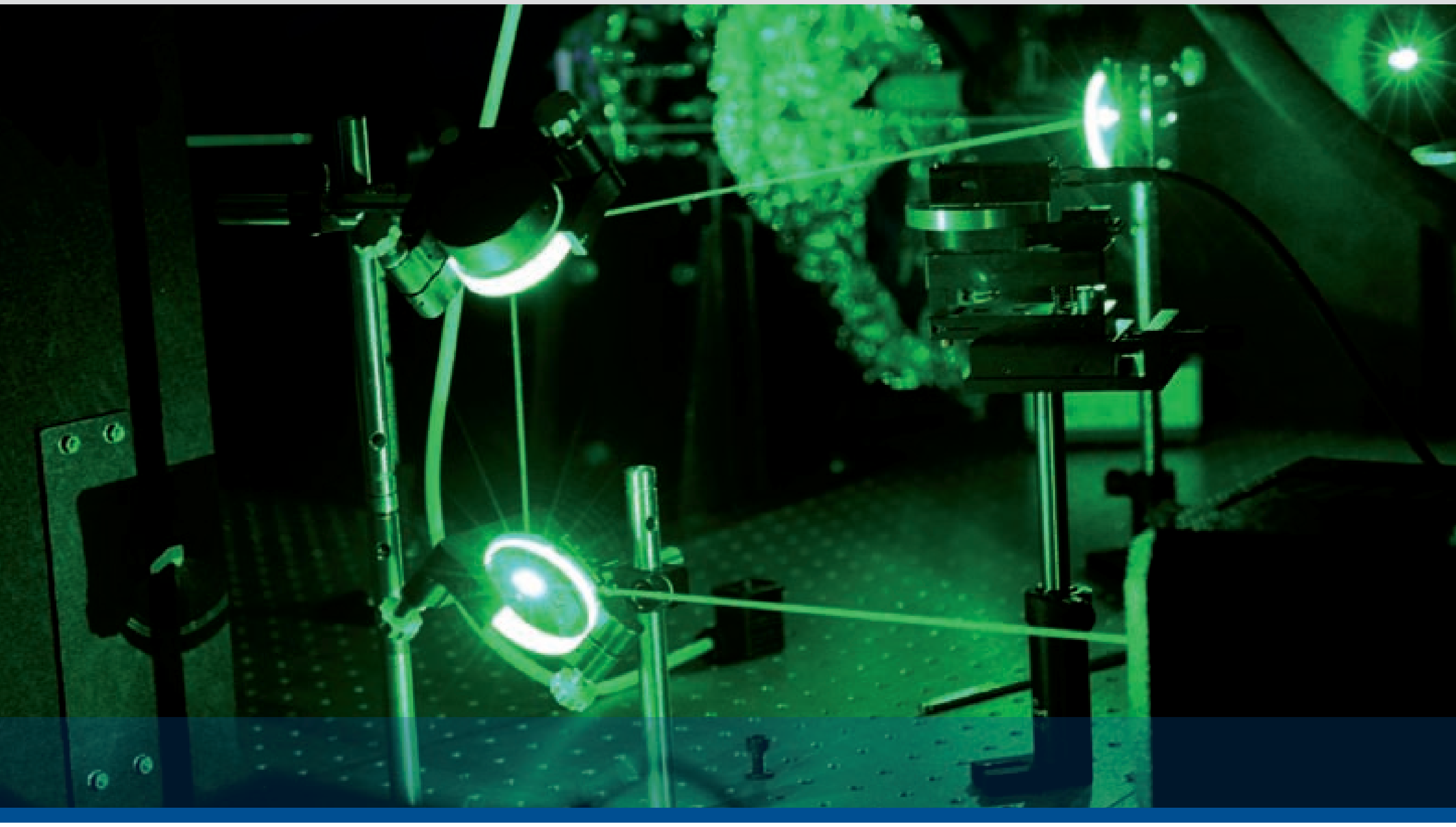

personal buildup for Force Motors Ltd.

State of Development of Laser Ignition

A holistic optimization of combustion engines with the aim of conserving resources has to include an improvement of the ignition mechanism as well. In the field of spark-ignition combustion engines the development of laser-induced ignition systems is advanced worldwide. This article of the Bayreuth Engine Research Center (BERC) gives an overview of the current development status and future trends in the field of laser ignition.

1 Introduction

No matter whether the motivation for the reduction of fuel consumption and the emission lies in the restricted resources, human health or the conservation of the environment it is without doubt that both issues are the main goals in the traffic sector. In this context the optimization and control of the combustion itself is one main step to reach that goal.

A promising option to influence the burning rates offers laser-induced ignition. A laser beam is focused at a point of the combustion chamber leading to a so-called optical breakdown. As a result of multiphoton-ionisation a luminous and very hot plasma is generated where highly reactive radicals are formed and extremely high temperatures and pressures prevail. For such a breakdown photon densities in the range of approximately 10^{29}/cm²s are needed. This corresponds to a laser output of about 100 GW/cm². Starting from this plasma kernel, in which temperatures of 10^5 to 10^6 K prevail, a pressurewave propagates through the mixture at supersonic speed and heats it. It also may cause a weak ionization of the molecules. In combination with the effects of the pressurewave, heat conduction and convection from the plasma kernel and diffusion of the radicals finally trigger the ignition of the mixture around the plasma kernel [1]. The advantages of this type of ignition are manifold. Ignition due to a laser enables a completely free choice of the place of ignition. This is a decisive advantage particularly with modern concepts of SI engine combustion [2]. Due to the opportunity of an ignition away from the cylinder walls, energy loss and wear can be reduced. Moreover, laser-induced ignition is able to ignite leaner mixtures compared to a conventional spark plug. Particularly aspect that makes laser ignition attractive for the application in stationary gas engines in terms of fuel saving.

2 Fundamental Studies on Laser Ignition

The principle of laser ignition described here is known for a long time and thus many contributions of various groups of researchers can be found in literature, the basic research still represents a crucial part in this area. Whereas earlier studies focused on feasibility studies, the determination of the minimum ignition energies of various fuels, and the necessary qualities of the laser beam, recent studies go a step further [3, 4]. In a project a department of the Bayreuth Engine Research Center (BERC), for example, investigates the controlled influence of spatially or temporally separated multipoint ignitions on the combustion process [5]. In this context fundamental research is made in homogeneous hydrogen/air and methane/air mixtures to study the potential of this further degree of freedom for ignition.

Figure 1 shows a principle sketch of a spatial dual ignition. Data of the employed laser is outlined in the **Table**. The detected combustion time of different compositions of mixtures of methane and air is compared in **Figure 2**. It can be seen that by means of laser ignition using multiple points the combustion time can be further reduced.

For the potential of laser ignition in basic is promising, one main goal is to develop laser systems with sufficient power densities and acceptable size and price. The laser plug of the company CTR developed in cooperation with AVL List-GmbH is now disposable in a second-generation and was designed for use in internal combustion engines [6].

3 Status of Laser Ignition for Engine Applications

Based on the above mentioned basic research in stationary combustion chambers, the first laser-fired single-cylinder engine was already put into operation about five years ago. It was a collaboration between the University of Vienna and the company AVL. The results of these initial investigations confirmed the expectations that had been set in the potential of laser ignition. It was actually possible to ignite very lean mixtures and, consequently, realize higher exhaust gas recirculation rates [2]. The laser ignition also showed little interference due to high flow speed and turbulence that may lead to flame quenching in conventional ignition systems. Moreover, there were advantages concerning fuel consumption and the HC emissions. Meanwhile numerous research groups around the globe deal with this issue. They apply laser ignition to both gasoline engines and stationary gas engines.

In the field of stationary gas engines, for example, investigations carried out by the Argonne National Laboratory showed that the flame propagation speed in the combustion chamber increases for all stages of combustion initiated by laser ignition [7]. The increased combustion speed leads to a faster and more intense conversion of the fuel mixture and entails a significant reduction of the consumption in conjunction with a leaner mixture. In addition very low cycle-to-cycle fluctuations could be achieved. This group gave an account of reduction of NO_x emissions by 70 % at constant efficiency respectively an efficiency gain of 3 % at constant NO_x emissions. Similar results were obtained by a project of the company GE Jenbacher and the Institute for Photonics at the Technical University of Vienna [8]. The application of laser-induced ignition in gasoline engines mainly takes place in direct injection engines. However, there are still inves-

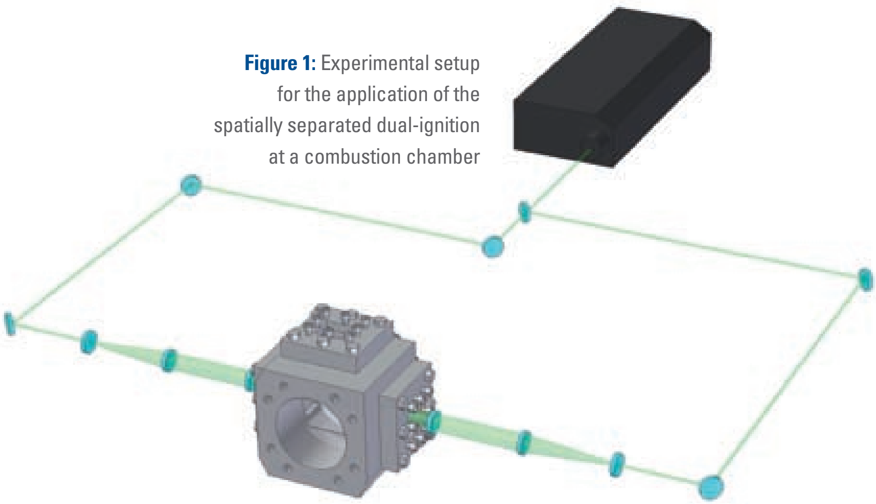

Figure 1: Experimental setup for the application of the spatially separated dual-ignition at a combustion chamber

The Authors

Prof. Dr.-Ing. Dieter Brüggeman holds the Chair of Engineering Thermodynamics and Transport Processes (LTTT) at University of Bayreuth and is spokesman of the Bayreuth Engine Research Center (BERC) in Bayreuth (Germany).

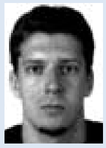

Dipl.-Ing. Christian Hüttl is researching assistant at LTTT and works on engine related projects within BERC in Bayreuth (Germany).

Table: Technical data of the laser

Property	Value	Unit
Type	Nd:YAG solid state laser	
Pumping	Flashlamp	
Manufacturer	New Wave Research	
Model	Solo PIV	
Wavelength	532	nm
Maximum pulse energy	100	mJ
Pulse length	6	ns
Beam diameter	5	mm

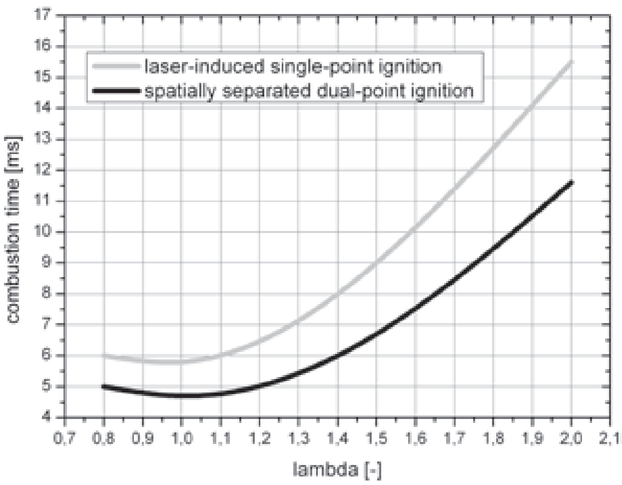

Figure 2: Combustion time of various mixtures of methane and air for laser-induced single and dual-point-ignition

tigations studying homogeneous operations. Mullet et al. published results concerning the influence of beam energy, quality and focal dimensions on the ignition control in internal combustion engines in homogeneous operation [9]. This work was focussed on the effects of different beam qualities and thus focal diameters and lengths on flame propagation and stability of combustion. It showed that the influence of the intensity distribution over the laser cross section and focus properties is relatively low compared to the actual beam size and the intensity fluctuations between individual pulses. Furthermore it could be shown that the laser ignition entails much lower cycle fluctuations than the conventional spark ignition. In the field of direct injection engines recent studies of a group of BMW AG confirm these results [10]. In these studies, laser ignition was applied both in homogeneous and in stratified operation of a spray-guided combustion concept. It was shown again, that the ignition speed increases when using a laser as a source of ignition compared to an inductive spark plug. However, there were problems with misfire in stratified operation which occurred due to the short life time of the laser-induced plasma in comparison to the spark of a conventional plug. Similar studies on direct-injection gasoline engines were also made by the TU Vienna and its cooperation partners [2].

Despite the existing problems of pollution of the optics by combustion chamber deposits and the still high costs of laser ignition systems, during the last years a number of patents has appeared who either deal with laser ignition systems or with strategies of ignition. This large number of patents and the successful application of laser ignition on close-to-production engines clearly show the potential of this technique. Series technology, however, can only be realized if the laser ignition consistently goes on with the development of new laser systems regarding higher robustness and last but not least low costs.

4 Summary

Due to the promising potential for consumption and emission reduction that results from the laser ignition, there is great interest in developing this technology. The large number of patents in this area and the activity of numerous research groups in this area demonstrates this very clearly. Meanwhile this technology is advanced so far, that first laser ignition systems for the engine sector are commercially available. Such systems have been successfully implemented in stationary gas engines as well as in smaller gasoline engines. Especially in the field of new combustion processes, such as the direct-injection gasoline concepts, the various prospects of laser ignition are obvious. If the costs for the applied laser systems can be further reduced, laser ignition might become a real alternative to conventional spark ignition for some applications.

References

[1] Phuoc, T. X.: Review: Laser-induced spark ignition fundamental and applications. In: Optics and Lasers in Engineering 44 (2006), S. 351-397

[2] Geringer, B. et al.: Laserzündung – Ein neuer Weg für den Ottomotor. In: MTZ 65 (2004), Nr. 3, S. 214 - 219

[3] Morsy, M. H. et al.: Laser-induced Two-point Ignition of Premixture with a Single-Shot Laser. In: Combustion an Flame 125 (2001), S. 724-727

[4] Kopecek, H. et al.: Laser ignition of methan-air mixtures at high pressures and diagnostics. In: Journal of Engineering for Gas Turbines and Power 127 (2005), S. 213 - 219

[5] Mönch, M.; Hüttl, C.; Brüggemann, D.: Einfluss der laserinduzierten Mehrfachzündung auf die Flammenausbreitung in homogenen Gemischen. In: 23. Deutscher Flammentag – Verbrennung und Feuerung, VDI-Berichte 1988 (2007), S. 271 – 276

[6] Carinthian Tech Research, URL: http://www.ctr.at/carinthian_tech_research_deutsch/; Stand 05.12.2008

[7] Bihari, B. et al.: Development for Advanced Laser Ignition System for Stationary Natural Gas reciprocating engines. In: ICEF2005-1325, ASME-ICE 2005 Fall Technical Conference, Ottawa, Canada

[8] URL: http://www.wtz.de/4DGMK/Laserzuendung_fuer_Gasmotoren_6_Jahre_Erfahrungen.htm; Stand: 05.12.2008

[9] Mullet, J. D. et al.: The influence of beam energy, mode and focal length on the control of laser ignition in an internal combustion engine. In: Journal of Physics D: Applied Physics 40 (2007), S. 4730 - 4739

[10] Feßler, M. et al.: Ermittlung von thermodynamischen Potenzialen alternativer Zündsysteme an einem strahlgeführten Brennverfahren. In: AVL (Hrsg.): 8. Internationales Symposium für Verbrennungsdiagnostik – Beiträge ISBN 978-3-00-022057-9 (2008), S. 515 – 530

Brands of the Century –

from Aspirin to Zeiss

Florian Langenscheidt (Ed.)
German Standards – Brands of the Century
German champions in products and services from Aspirin to Zeiss
2004. 400 pp. Hardc.
EUR 62,00
ISBN 978-3-409-12659-5

The 14th fully revised edition of „Marken des Jahrhunderts“ from the Deutsche Standards EDITIONEN GmbH in association with Gabler publishing house presents a fine selection of the best German brands in first-class quality.

Conceived as an encyclopaedia of German brands, the project in editor Dr. Florian Langenscheidt's eyes emphatically pays tribute to Germany as an attractive business and investment location while also serving as a positive signal and encouraging recommendation to call to mind the country's solid economic foundation.

In response to the resounding international interest in the original, an English edition, „Brands of the Century“, has been published containing a selection of the most prominent German brands on the global market.

The Author

Florian Langenscheidt *is proprietor of the Langenscheidt Publishing Group, he serves on several supervisory boards, assists start-up companies with funding and advice, and he is chairman of the board of the Atlantikbrücke. He is member of the board of trustees of the WWF, chairman of the board of CHILDREN, as well as a founding member of the BRAND CLUB.*

Please send me

Fax +49(0)611. 7878 - 420

____ Copies:
German Standards - Brands of the Century
ISBN 978-3-409-12659-5
EUR 62,00
+ shipping and handling

Last Name, First Name	Company Address
Company | University | Institute | Organization	Department | Position
Branch | Number of employees within the company	Street (no postbox, please)
City | ZIP-Code	Country
Date | Signature	e-mail

32108055

Subject to change.
Available in bookshops or at the publisher.
Status 6 | 2008

Gabler Verlag | GWV Fachverlage GmbH
Abraham-Lincoln-Str. 46
65189 Wiesbaden | Germany
Managing Directors: Dr. Ralf Birkelbach,
Albrecht F. Schirmacher,
AG Wiesbaden HRB 9754

KOMPETENZ IN SACHEN WIRTSCHAFT

GABLER

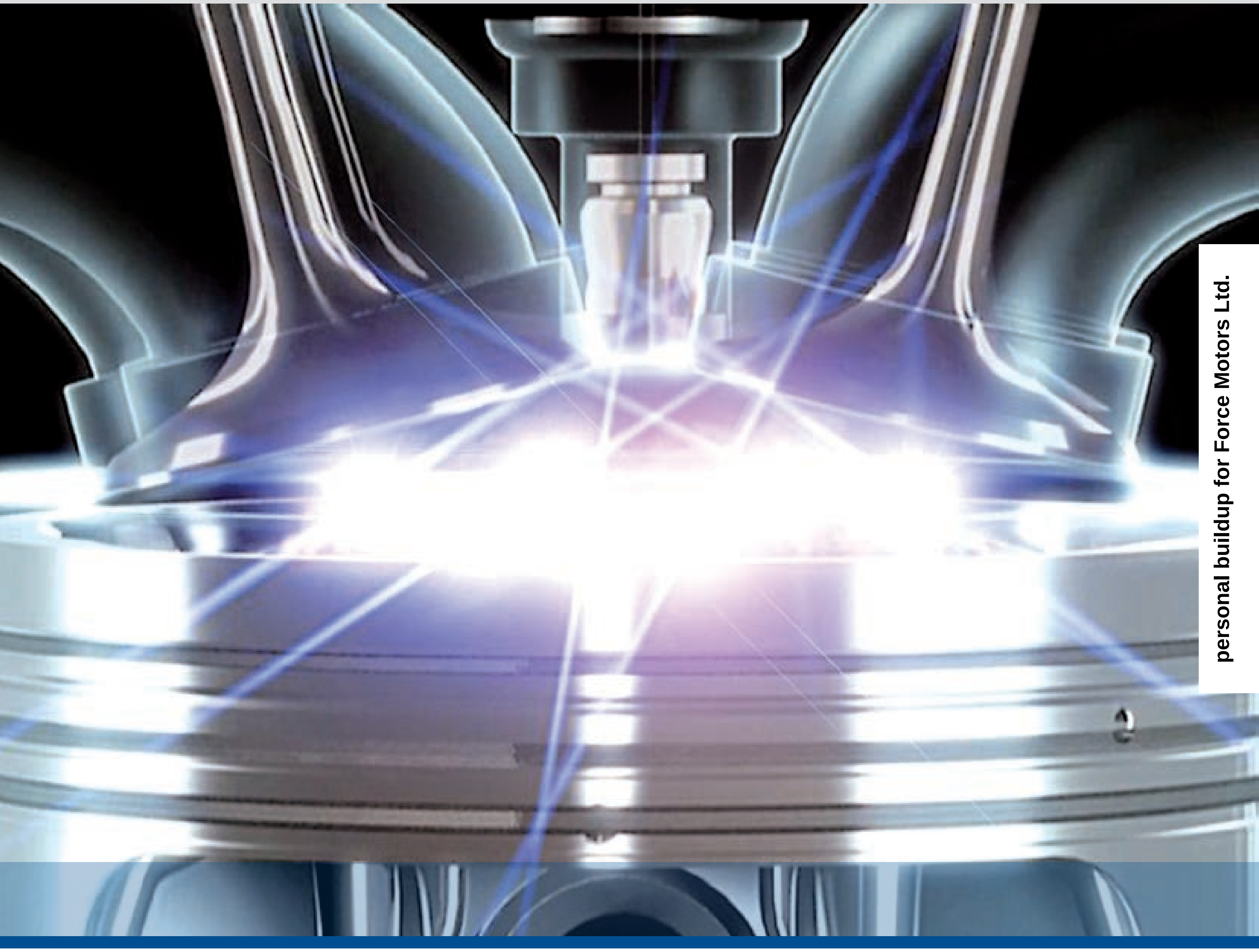

Space Ignition Method Using Microwave Radiation

Highest efficiency in fuel consumption – a target the Micro Wave Ignition AG faced by developing its new microwave ignition of combustion engines. This space ignition method can be utilised to save up to 30 % fuel consumption and prevents up to 80 % of pollutant emissions.

1 Introduction

For over 100 years now, the spark plug has been the centrepiece of conventional ignition technologies for gasoline engines as it generates a spark that triggers combustion from a compressed air/fuel mix. Thus far, many sources of this energy potential have remained untapped. Engineers at Micro Wave Ignition (MWI) AG have developed a technology that has picked up on the idle energy potential and, in doing so, is now able to replace the previous standard ignition methods in the long term. This innovation relies on a system where microwave radiation is used for the ignition of combustion engines, **Figure 1**. The space ignition method can be utilised to save up to 30 % fuel consumption and prevents up to 80 % of pollutant emissions. With this process, engines can operate on an extremely lean mix (Lambda = 1.5 to 3). The technology can be applied in all classic gasoline engines and diesel engines if required. In addition to conventional fluels, heavy oils such as rape oil, palm oil, jatropah oil, soya oil and other oil types from renewable raw materials can be ignited.

2 Prevention of the Laminar Combustion Phase by Implementing the Space Ignition Method

The combustion process in engines incorporating conventional ignition technology starts directly after ignition has taken place with an initial, very incomplete and therefore inefficient laminar combustion phase, in which a flame front forms and then spreads very slowly in all directions. The flame front reaches a dispersion speed of 20 cm/s during this phase. This initial flame development phase produces, on the one hand, the majority of pollutants and, on the other hand, unnecessary lost heat. This part of fuel energy, however, cannot be used for mechanical operation; the efficient, turbulent combustion phase only starts to act at a later point in time. Flame turbulences seen today develop much more quickly and spread at a flame speed of between 200 m/s and 300 m/s.

These well-known technical processes led to the basic consideration to engineer the combustion process such that the laminar phase is reduced or even eliminated completely. Based on the works of

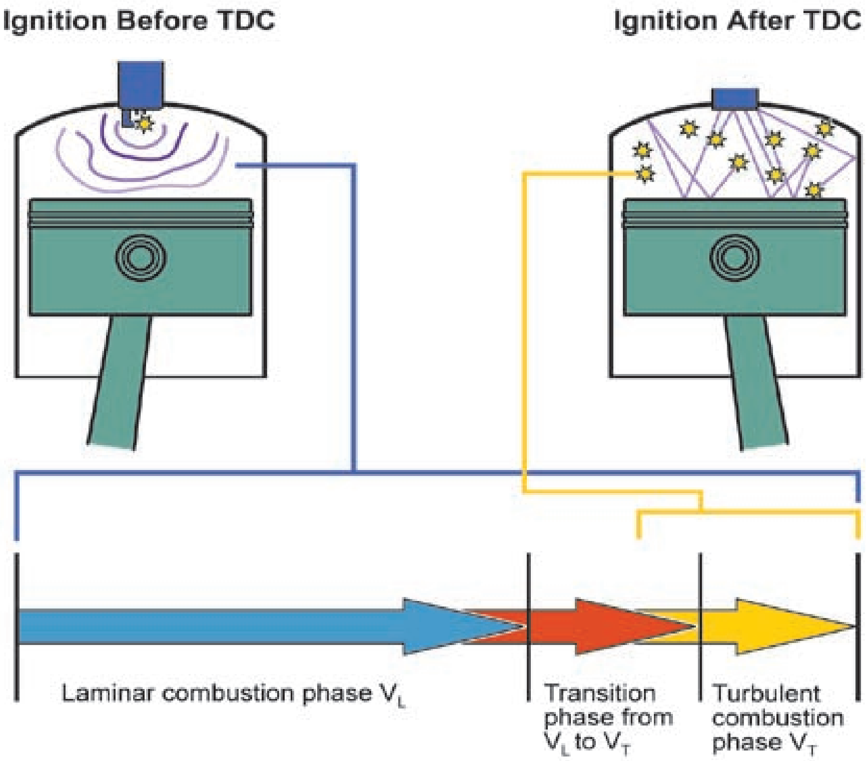

Figure 1: The microwave ignition provides a real ground-breaking space ignition method in opposition to conventional ignition technologies

The Authors

Professor Dr. rer. nat. Nikita Hirsch is member of the Managing Board of the MWI Micro Wave Ignition AG in Empfingen (Germany).

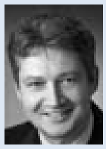

Dipl.-Ing. Armin Gallatz is Chief Operating Officer of the MWI Micro Wave Ignition AG in Empfingen (Germany).

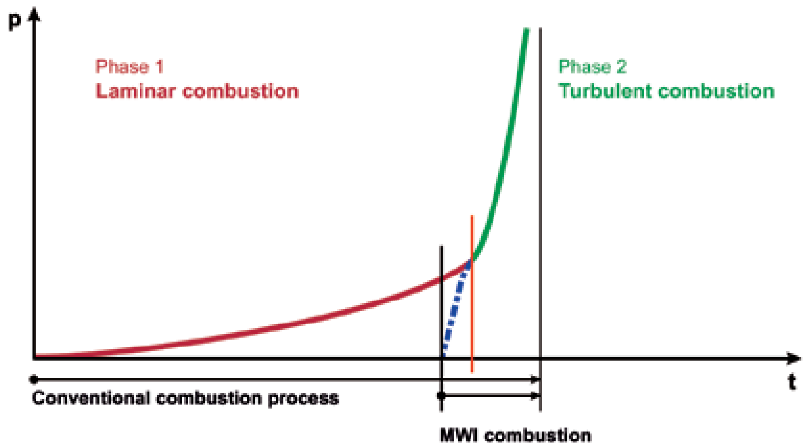

Figure 2: The inefficient laminar combustion phase can be nearly eliminated by MWI technology

Borghi, it can now be envisaged that, in the entire combustion chamber, only those processes are allowed to take place which are already known in the burning process development with conventional ignition during the turbulent phase [1]. This is made possible by virtue of a pulsed, space-specific supply of microwave energy, which now gives us a concept for the first genuine space ignition method, **Figure 2**.

3 Faster and Complete Combustion

The applied space ignition method allows a considerably more effective fuel application by omitting the inefficient laminar combustion phase. This means fuel consumption can be drastically reduced. The homogeneous distribution of several ignition spots in the entire combustion chamber can be used to make combustion considerably faster than is possible with conventional spark plug ignition, which is started with detailed control, **Figure 3**. With the MWI method, the absorbing capacity of certain hydrocarbons is utilised. These hydrocarbons are split or cracked and trigger a radical chain reaction. Its high efficiency allows this type of space ignition method, which works using the pulsed entry of microwave energy, to use considerably leaner fuel mixtures. Whilst classic spark ignition already attains the absolute upper limit when a value of Lambda = 1.35 is reached, the MWI method can be used to successfully ignite fuel mixtures in the Lambda = 1.5 to 1.8 range. As a consequence, the combustion process is more complete by virtue of the leaner air/fuel mixtures utilised, and this is accompanied by a clear reduction in the residues containing pollutants.

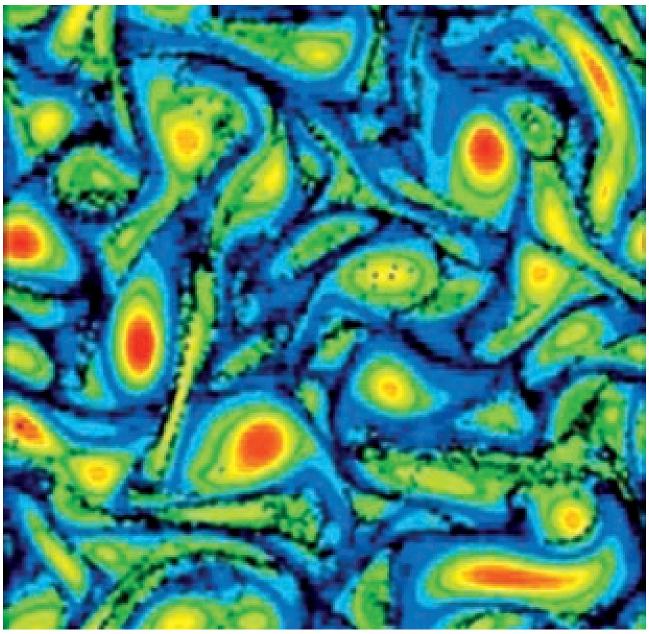

Figure 3: Homogeneous distribution of several ignition spots in the entire combustion chamber

4 Theoretical Principles of Microwave Ignition

Initial theoretical considerations on the acting mechanisms in MWI technology are taken into account further below. The description explains the initiation of electromagnetic radiation through the generation of self-supporting oscillations in a system through the influence of external electromagnetic radiation. The possible impacts of an externally-acting electromagnetic field upon an atomic or molecular system can generally be limited to the two following cases:

- stimulated emission or absorption of the electromagnetic radiation
- induction of electric and magnetic moments.

Stimulated emission or absorption of electromagnetic radiation occurs if the frequency ω of the electromagnetic radiation corresponds with the splitting of the atomic or molecular energy level, so that the equation $\hbar\omega = \Delta E$ is fulfilled. The reaction of an electron or a group of electrons to an electromagnetic field causes a magnetic moment. Although, when looked at separately, individual electrons generate a magnetic field by spinning and by their rotation around the core, two electrons in the outer shell can generate a resulting magnetic moment of zero with the presence of counter spin. At the same time, chemical compounds generated by atoms by virtue of electron sharing do not show a magnetic moment for the same (split) electrons. As a result, electrons that initiate chemical bonds (under normal conditions) do not display any mutual reaction to electromagnetic fields (EMF), since the resulting magnetic moment is zero – as can be verified in an electron spin resonance (ESR) experiment. A population inversion can be utilised to generate stimulated electromagnetic radiation. The anisotropic electromagnetic parameters are the relative permittivity, conduction capacity or thermal EMF.

While electromagnetic stimulation of unpaired electrons is a widely known phenomenon and the basis for methods such as the previously mentioned ESR experiment, the stimulation of chemical bonds can be viewed as the basis for MWI technology, because MWI technology represents an instrument for influencing chemical bonds using an electromagnetic field or an electromagnetic wave with vector potential Ā and for cracking bonds in hydrocarbons. Electromagnetic fields or waves with a suitable vector potential Ā can be generated with distributed parameters using a self-supporting oscillation system which works within a superposition of mode conditions. Under these conditions, electric and magnetic moments are induced into the chemical bonding electrons and the symmetry of the resulting wave function of these chemical bonds is changed. An effect of this type leads to the stimulation of the chemical bondings.

Above a certain energy level, the chemical bonds are broken up by fuel constituents, thus setting off the radical chain reaction. An extensive theory on the quantum-mechanical processes that describes the ignition process extensively has not yet been developed in full. However, technical procedures on the acceleration of chemical processes – with surprisingly low excitation energy in the classic sense – are known as a result of practical experiments on the interaction of electromagnetic radiation and hydrocarbons [2]. The excitation of certain hydrocarbons with certain frequencies and pulse trains is therefore beneficial, because the excited polar-like molecules show characteristic resonant frequencies. This enables these frequencies to crack the selected hydrocarbons using particularly low excitation levels. After a cold "ignition" of the air/fuel mix through pulsed microwave radiation in the entire combustion chamber, certain processes are run through that are already known from the burning process development using conventional ignition (turbulent phase). Chemical combustion reactions are processed in multi-layered, complex forms. An example of this is the reaction between methane (CH_4) and oxygen (O_2), which is normally explained by the following (very) much simplified reaction equation:

$$CH_4 + 2O_2 \Rightarrow CO_2 + 2H_2O$$

In actual fact, however, the combustion process is like a chain of individual reactions:

$$CH_4 + O \Rightarrow CH_3 + OH$$

$$CH_4 + H \Rightarrow CH_3 + H_2$$

$$CH_4 + OH \Rightarrow CH_3 + H_2O...$$

It is important to make sure that the thermal release of energy caused by chemical reactions is in excess of the heat dissipation, and the resulting heat continues to accelerate the exothermal reactions. The timing of the "cold natural ignition" can be influenced by controlling the pulsed microwave energy supply. With MWI technology, it is not the entire fuel mix that is ignited, but rather approx. three percent of the fuel quantity – depending on the fuel composition – is cracked per firing stroke for ignition purposes. Frequency selection can be used to concentrate the entry of energy onto selected hydrocarbons. Faster combustion can be expected as a result of the low fuel quantity during ignition, but this combustion process is not explosive.

5 Benefits of the MWI Technology

MWI technology utilises the energy potential that was practically thrown away in previous ignition methods. This gives the innovative technology considerable advantages compared to conventional ignition methods – especially when one considers the current demands on the engine industry and, above all, the car industry in terms of reducing consumption and emissions:

- the option of being able to reliably ignite lean mixtures using MWI technology has rendered enriching the (spark-plug friendly) air/fuel levels for igniting the combustion as no longer necessary
- MWI combustion is, in contrast to conventional combustion, much less dependent upon the burning rate in the form of diffusion flames, as it is a space ignition method
- this space ignition method allows faster and therefore colder combustion, which increases efficiency while simultaneously reducing the fuel consumption and the concentration levels of poisonous combustion residue
- the microwave ignition system is maintenance-free and resistant to wear
- the operating costs for cooling systems, catalytic converters and soot filters are considerably reduced.

6 Summary and Perspectives

From previously calculated and measured performance parameters it is safe to say that the following results can be achieved when MWI technology is implemented successfully:

- up to 30 % lower fuel consumption for the same engine performance
- up to 30 % fewer CO_2 emissions
- up to 80 % fewer poisonous combustion residues such as CO, SO_x, NO_x, HC.

Thus, an important step has been taken in achieving the development of a low-emission engine. A prototype for the large-size engine sector is currently being developed in collaboration with Neuen Maschinenbau, Halberstadt, which means the previous series of practical tests for MWI technology has been continued. In the long term, it is intended that this technology become established in the large-size engine, car engine and aeroplane engine markets. Its introduction on to the market will take approximately 10 years due to the high requirements to be met particularly by series production in the automobile sector. It should then be possible to not only install MWI technology in new engines, but to also introduce it in old engines.

References

[1] Schäfer, F.; van Basshuysen, R.: Handbuch Verbrennungsmotor. Wiesbaden: Vieweg, 2005
[2] FhG Karlsruhe: Ignition of explosive substances, Research Centre Karlsruhe. Acceleration of polymerization

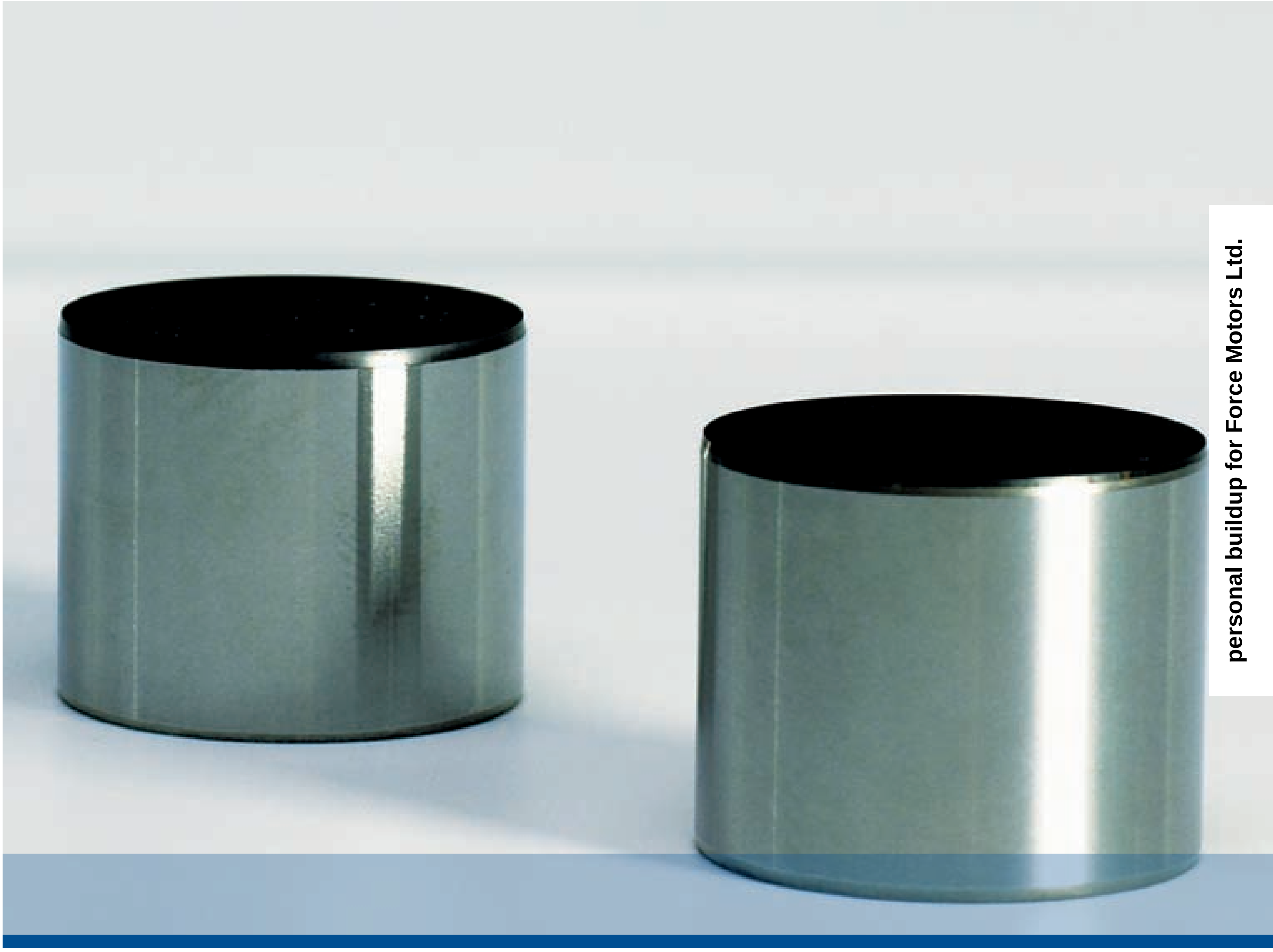

Lower Emissions with DLC Coatings

Frictional Behaviour within Valve Train

With vehicle production growing annually and pressure on manufacturers to reduce vehicle emissions, innovative methods will have to be found to make engines more efficient. The PSA Group has set up with Bekaert a cooperative test programme to measure the impact of Diamond-like Carbon (DLC) coatings on the frictional behaviour of certain components within the valve train of a production engine.

1 Introduction

The European Union is the largest vehicle producing region in the world, accounting for more than 17 million passenger cars in 2007, or 32 % of the global passenger car market. With the increase in the world's population, the number of cars on the road is set to increase year-on-year until a suitable, alternative mode of transport can be found. As that development is still many years away, the demand for conventional internal combustion-engined passenger vehicles can be expected to continue to grow.

Faced with this inevitability, the European Commission (EC) has developed a programme of Carbon dioxide (CO_2) vehicle emission reduction which motor manufacturers must adhere to, and failure to meet these emission limits will attract financial penalties in the future. In order therefore to avoid the possibility of incurring such fines, manufacturers are working feverishly towards making their vehicles ever-more fuel efficient.

In 2007, global passenger car sales in the Peugeot Citroën (PSA) Group rose to 2.99 million units, of which the European market accounted for almost half, and projected sales for 2008 are expected to rise by a further 5 %. Although global production of motor vehicles is soft right now, the annual production is still expected to exceed 3 % every year up to 2013. PSA global vehicle sales in 2010 are expected to top 4.0 million units, failing to meet the EC's strict CO_2 emissions targets is not an option, as the financial penalties would be substantial. These penalties would be progressive and although it is proposed that they would not come into effect before 2015, emissions targets of 130 g/km already agreed come into effect in 2012. However, as from 2015 the penalties for emissions exceeding these agreed levels would amount to 95 euros per gram per vehicle (European Commission proposal on reducing CO_2 emissions from passenger cars, September 2008).

Besides the potential financial impact for the market, the car-buying public to-

The Author

Mark Boghe
is Product Market Manager Automotive and Racing worldwide at Bekaert in Zulte (Belgium).

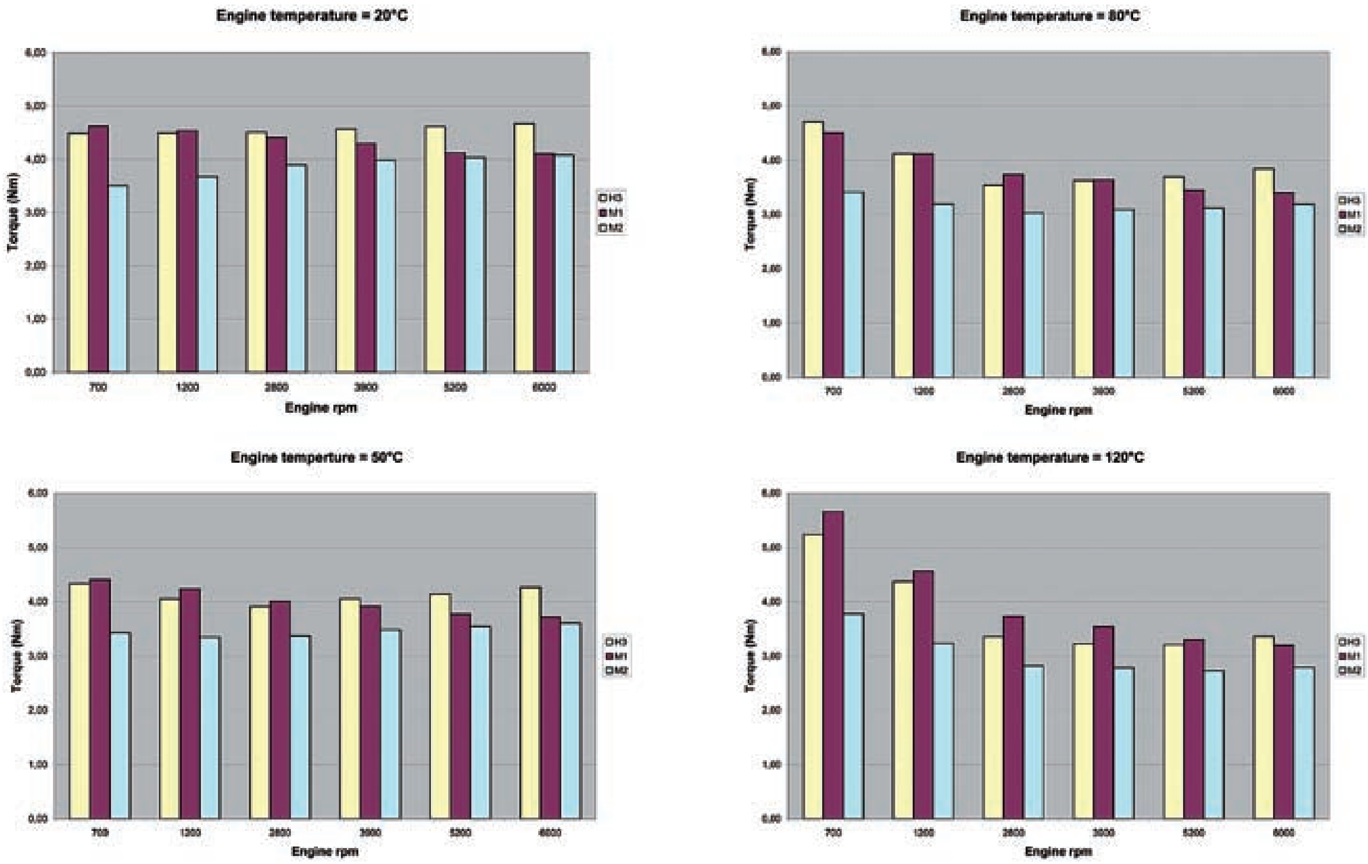

Figure 1: Test results

day is fast becoming a very well informed group and if certain manufacturers are not being seen to meet the buyer's own perceived environmental expectations, that company runs the risk of losing that all-important purchase. However, the PSA Group is well positioned, as for the second year in a row, the Group sold one million vehicles emitting less than 140 g/km CO_2 and with 750,000 emitting less than 130 g/km CO_2. More than 200,000 vehicles were sold which emitted less than 110 g/km CO_2 (essentially made up of Citroën C1 and Peugeot 107 sales), representing 55.7 % of the market for this class of vehicles in Europe.

2 Component Testing

Advances in engine component coatings made by Bekaert, who have been working in the field for many years, attracted the attentions of the PSA Group. Twenty-four months ago, a cooperative test programme was set up between these two companies to measure the impact of DLC coatings on the frictional behaviour of certain components within the valve train of a production engine. For this purpose, certain components within the valve train were coated with Bekaert's "Dylyn Plus", a member of the company's DLC family of coatings. "Dylyn Plus" is specifically aimed at high-volume automotive applications and most of the properties of this product can be precisely tuned to match the customer's needs.

Working with the test engine, a four-cylinder 1.6 l petrol engine from PSA's current engine range, Bekaert prepared certain components within the valve train assembly by coating these with "Dylyn Plus". Run on an electrically driven test rig, the tests were executed over a wide temperature range (20 °C to 120 °C) in order to study the behaviour in different conditions and to quantify these results.

The first test was conducted on an engine using hydraulic tappets, and this was followed in 2008 by a similar test but this time using mechanical tappets. In the tests featuring the engine with hydraulic tappets, H3 refers to those tappets in which the top of the tappet was coated and the camshaft against which it was running was tribo finished.

In the test engine using mechanical tappets, M1 refers to an uncoated tappet used as the reference component, while the M2 tappets were DLC coated on the top and ran against a tribo finished camshaft. All of these tests were performed at different controlled engine temperatures, the results being measured at 20 °C, 50 °C, 80 °C and 120 °C where 20 °C is considered to be a normal start-up engine temperature while 80 °C to 120 °C is the normal working temperature for an engine.

3 Test Analysis and Observation

In **Figure 1**, the red bar (M1) represents a normal mechanical tappet system in a current engine and the blue bar (M2) is where the tappets have been coated. M1 is an uncoated mechanical tappet without modification, M2 is the same mechanical tappets but DLC coated on the top, and running against a tribo finished camshaft.

For instance at 20 °C and 700 rpm (X-axis), the torque needed to drive the valve train (Y-axis) for M1 is 4.63 Nm and for M2 it is 3.5 Nm – which shows a distinct difference between the normal system and the potential system with the coated tappets. At 700 rpm, the reduction in torque required to turn the system falls from 4.6 Nm to 3.5 Nm, a saving of 24 % in engine efficiency, **Figure 2**.

Therefore one can say that in the low rpm range, the energy needed can be reduced (or the friction losses be minimised) by around 24 %, but this impact reduces as the engine revolutions increase at this temperature. This is a pattern that is repeated through all temperatures tested. At lower rpm levels, the tribological system is not yet in a fully hydrodynamic state and therefore friction levels are higher and the impact of the coating is more important. The efficiency saving is therefore greatest in the lower rpm range when the oil film is thicker.

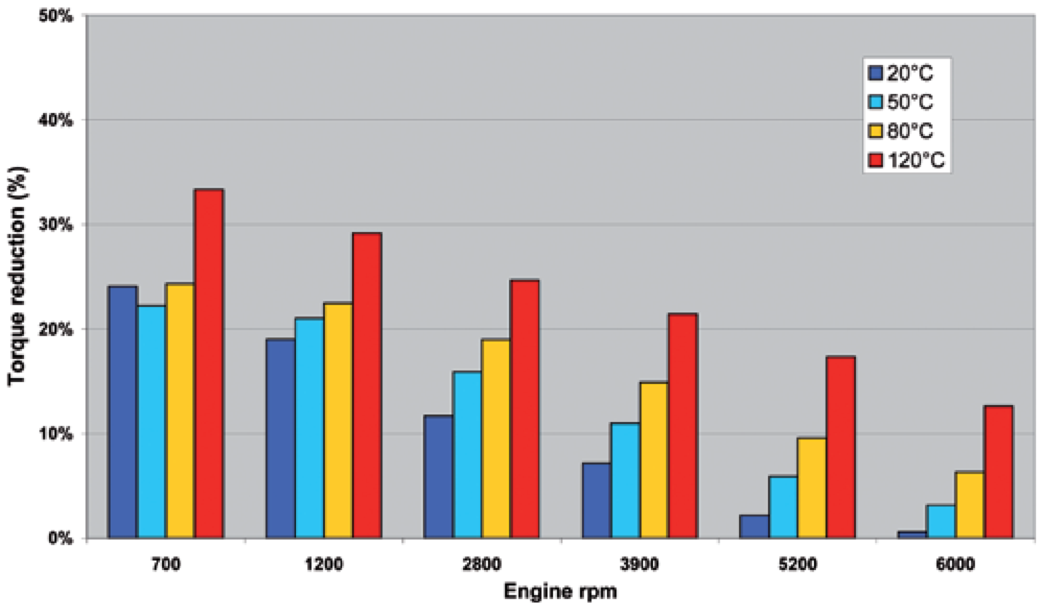

Figure 2: Friction reduction at different temperatures for mechanical tappets

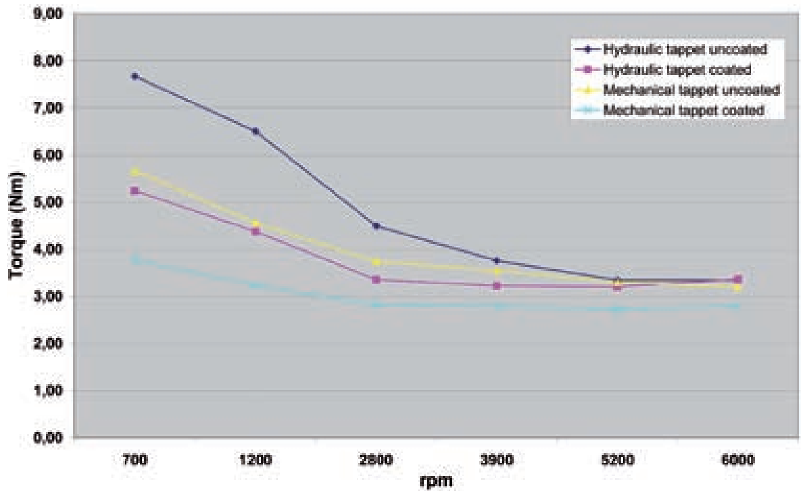

Figure 3: Summarised graph

Observing the results at 700 rpm and at 50 °C and beyond, gives one an idea of how this system would behave in start-up conditions after the engine has already run, which also confirms that there are no negative effects on the valve train under these starting conditions.

In fact the gain is even more pronounced for the higher temperatures and the explanation for this is that at 20 °C, the viscosity of oil is very high, but as the engine heats up, the oil becomes less viscous. At 20 °C the oil has a higher resistance to flow (high viscosity) and this explains why good lubrication is observed throughout the whole rpm range at this temperature. There is an impact on the coating but nevertheless the environment contains rather viscous oil, which ensures presence of the oil film between the parts. But at 120 °C it can be seen that at 700 rpm, the M1 component reading goes from 5.67 Nm down to 3.68 Nm thereby showing a reduction in torque of about 33 % (at normal an engine operating temperature of 120 °C) which compares to only 24 % at low temperature. This difference is essentially due to the oil getting thinner at the higher temperature.

The percentage gains in torque reduction were plotted and the red bar here shows the greatest gains for mechanical tappets at all temperatures tested and at all engine revolution control breaks. Figure 2 takes the reduction in friction and translates it into gain in torque efficiency (or reduction in actual torque required). Therefore, overall at low rpm, the gain is more important or more pronounced than at high rpm.

Also, if one compares the higher temperatures the gains are more important for the engine, but at low rpm at lower temperatures this is not negligible either. As most urban journeys are not very long, most of the driving is done at lower revs and over a shorter distance, during which time engine friction is at its highest. On engine start up, there is an immediate 20 % gain as soon as the engine gets into working temperature at low rpms, which at idle is 700 rpm, and this moves up to over 30 % at normal operating temperatures. This means that in a typical urban cycle, where most drivers do not exceed 3000 rpm (the typical urban range is 700 rpm to 2800 rpm), one can expect a reduction of between 25 % to 35 % in friction losses.

4 Test Summary

Estimates by PSA are that this would translate into a fuel consumption reduction of between 1 % to 2 % in the overall consumption. This might not sound like a lot, but for a small engine it translates into a saving of somewhere between 2 g/km and 3 g/km of CO_2 which is important.

When this saving is multiplied by the number of cars on the road, this brings the justification for the experiment sharply into perspective. Another factor which plays a big role in this equation, are the vehicle emission limits that have been set by the European Commission. By 2015, a penalty of 95 euros is applied for every gram above the limit set by the EC, so that is when every gram starts to count.

In **Figure 3**, it can be seen that for both uncoated mechanical and hydraulic tappets, the level of torque required to turn the camshafts is higher than for the coated equivalents. This graph shows the results of an engine at normal operating temperature (120 °C) and the lower torque levels required in each case, applies across the entire rev range of the test.

5 Conclusion

Indicators in the market show that the benefits of DLC valve train coatings would be felt mostly in smaller petrol engined cars, as in small cars at least, the trend is going to be towards petrol rather than diesel engines. The reason for this swing is due to the particulate filters needed in a diesel system and combined with Nitrogen oxide emissions; this will discourage much more development in smaller engined diesel cars especially as it increases the overall cost of those engines significantly. Several motor manufacturers are even developing three-cylinder petrol engines for their city cars.

As for the Bekaert/PSA project, one could expect to see the DLC coatings applied to the valve train system in production as early as 2011. ■

Peer Review ATZ|MTZ

Peer Review Process for Research Articles in ATZ and MTZ

Steering Committee

Prof. Dr.-Ing. Stefan Gies	RWTH Aachen	Institut für Kraftfahrwesen Aachen
Prof. Dipl.-Des. Wolfgang Kraus	HAW Hamburg	Department Fahrzeugtechnik und Flugzeugbau
Prof. Dr.-Ing. Ferit Küçükay	Technische Universität Braunschweig	Institut für Fahrzeugtechnik
Prof. Dr.-Ing. Stefan Pischinger	RWTH Aachen	Lehrstuhl für Verbrennungskraftmaschinen
Prof. Dr.-Ing. Hans-Christian Reuss	Universität Stuttgart	Institut für Verbrennungsmotoren und Kraftfahrwesen
Prof. Dr.-Ing. Ulrich Spicher	Universität Karlsruhe	Institut für Kolbenmaschinen
Prof. Dr.-Ing. Hans Zellbeck	Technische Universität Dresden	Lehrstuhl für Verbrennungsmotoren

Advisory Board

Prof. Dr.-Ing. Klaus Augsburg	**Dr.-Ing. Markus Lienkamp**
Prof. Dr.-Ing. Bernard Bäker	**Prof. Dr. rer. nat. habil. Ulrich Maas**
Prof. Dr.-Ing. Michael Bargende	**Prof. Dr.-Ing. Martin Meywerk**
Dr.-Ing. Christoph Bollig	**Prof. Dr.-Ing. Werner Mischke**
Prof. Dr. sc. techn. Konstantinos Boulouchos	**Prof. Dr.-Ing. Klaus D. Müller-Glaser**
Prof. Dr.-Ing. Ralph Bruder	**Dr. techn. Reinhard Mundl**
Dr. Gerhard Bruner	**Dr.-Ing. Lothar Patberg**
Prof. Dr. rer. nat. Heiner Bubb	**Prof. Dr.-Ing. Peter Pelz**
Prof. Dr. rer. nat. habil. Olaf Deutschmann	**Prof. Dr. techn. Ernst Pucher**
Dr. techn. Arno Eichberger	**Dr. Jochen Rauh**
Prof. Dr. techn. Helmut Eichlseder	**Prof. Dr.-Ing. Konrad Reif**
Dr.-Ing. Gerald Eifler	**Dr.-Ing. Swen Schaub**
Prof. Dr.-Ing. Wolfgang Eifler	**Prof. Dr. sc. nat. Christoph Schierz**
Prof. Dr. rer. nat. Frank Gauterin	**Prof. Dr. rer.-nat. Christof Schulz**
Prof. Dr. techn. Bernhard Geringer	**Prof. Dr. rer. nat. Andy Schürr**
Prof. Dr.-Ing. Uwe Grebe	**Prof. Dr.-Ing. Ulrich Seiffert**
Prof. Dr.-Ing. Horst Harndorf	**Prof. Dr.-Ing. Hermann J. Stadtfeld**
Prof. Dr. techn. Wolfgang Hirschberg	**Prof. Dr. techn. Hermann Steffan**
Univ.-Doz. Dr. techn. Peter Hofmann	**Dr.-Ing. Wolfgang Steiger**
Prof. Dr.-Ing. Günter Hohenberg	**Prof. Dr.-Ing. Peter Steinberg**
Prof. Dr.-Ing. Bernd-Robert Höhn	**Prof. Dr.-Ing. Christoph Stiller**
Prof. Dr. rer. nat. Peter Holstein	**Dr.-Ing. Peter Stommel**
Prof. Dr.-Ing. habil. Werner Hufenbach	**Prof. Dr.-Ing. Wolfgang Thiemann**
Prof. Dr.- Ing. Roland Kasper	**Prof. Dr.-Ing. Helmut Tschöke**
Prof. Dr.-Ing. Tran Quoc Khanh	**Dr.-Ing. Pim van der Jagt**
Dr. Philip Köhn	**Prof. Dr.-Ing. Georg Wachtmeister**
Prof. Dr.-Ing. Ulrich Konigorski	**Prof. Dr.-Ing. Henning Wallentowitz**
Dr. Oliver Kröcher	**Prof. Dr.-Ing. Jochen Wiedemann**
Dr. Christian Krüger	**Prof. Dr. techn. Andreas Wimmer**
Univ.-Ass. Dr. techn. Thomas Lauer	**Prof Dr. rer. nat. Hermann Winner**
Prof. Dr. rer. nat. Uli Lemmer	**Prof. Dr. med. habil. Hartmut Witte**
Dr. Malte Lewerenz	**Dr. rer. nat. Bodo Wolf**

Seal of Approval – this seal is awarded to articles in ATZ/MTZ that have successfully completed the peer review process

Scientific articles in ATZ Automobiltechnische Zeitschrift and MTZ Motortechnische Zeitschrift are subject to a proofing method, the so-called peer review process. Articles accepted by the editors are reviewed by experts from research and industry before publication. For the reader, the peer review process further enhances the quality of ATZ and MTZ as leading scientific journals in the field of vehicle and engine technology on a national and international level. For authors, it provides a scientifically recognised publication platform.

Therefore, since the second quarter of 2008, ATZ and MTZ have the status of refereed publications. The German association "WKM Wissenschaftliche Gesellschaft für Kraftfahrzeug- und Motorentechnik" supports the magazines in the introduction and execution of the peer review process. The WKM has also applied to the German Research Foundation (DFG) for the magazines to be included in the "Impact Factor" (IF) list.

In the ATZ/MTZ Peer Review Process, once the editorial staff has received an article, it is reviewed by two experts from the Advisory Board. If these experts do not reach a unanimous agreement, a member of the Steering Committee acts as an arbitrator. Following the experts' recommended corrections and subsequent editing by the author, the article is accepted. *rei*

MTZ Peer Review

The Seal of Approval for scientific articles in MTZ.

Reviewed by experts from research and industry.

Received ....

Reviewed ....

Accepted ....

FKFS

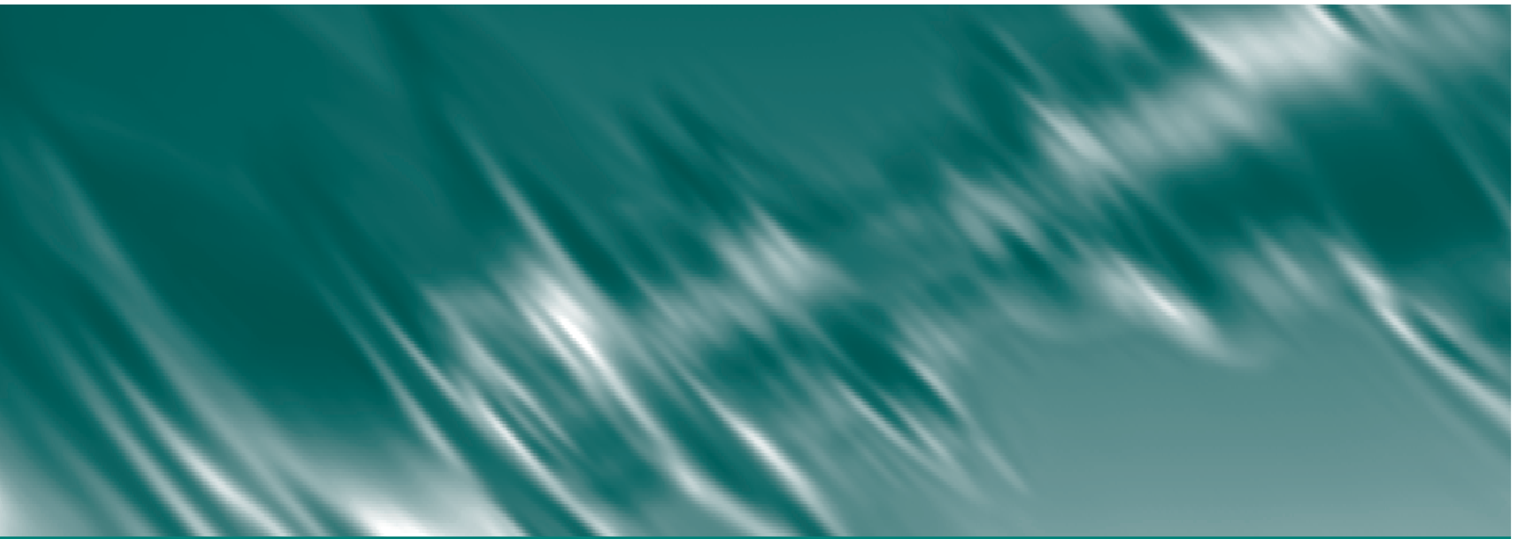

9th Stuttgart International Symposium

Automotive and Engine Technology

Event in cooperation with

ATZ live

___ Yes, I would like to know more! Please send me more detailed Information about the „9th Stuttgart International Symposium“ via e-mail.

First name ______ Family Name ______

Company/Institute ______

Department ______

Street/PO Box ______

Post code/town ______

Phone ______ Fax ______

e-mail ______

ATZlive
Abraham-Lincoln-Straße 46
65189 Wiesbaden | Germany
Phone +49(0)611. 7878-131
www.ATZlive.de

FAX +49(0)611. 7878-452

Acoustic Design of Rolling Bearings in Cranktrains

The fuel consumption of combustion engines is significantly influenced by engine friction as well as the efficiency of the charge cycle and combustion. Substituting the plain bearings, which are normally used as the main crankshaft bearings, with rolling bearings offers a significant potential for friction reduction, but simultaneously poses high requirements for an acoustically optimized design. Within the FVV (German Research Association for Combustion Engines) research project No. 881 "Acoustics of Rolling Bearing Bedded Crankshafts", undertaken by the Institute for Combustion Engines (VKA) at RWTH Aachen University (Germany), the acoustics of rolling bearings used as crankshaft bearings was investigated and a simulation methodology was developed for calculating and analyzing the acoustic behavior of rolling bearing layouts in cranktrains.

1 Introduction

The mechanical losses in combustion engines have a significant influence on fuel consumption. When analyzing these losses, it becomes clear that, in addition to the piston unit, the main and conrod bearings are the biggest individual components contributing to friction losses, **Figure 1**, left. The high losses from the crankshaft assembly result mainly from the normally used plain bearings [1, 2].

Changing the crankshaft main bearings from plain to rolling bearings offers significant potential for friction reduction. In addition to less bearing friction, there are also less friction losses in the oil pump, as the latter can usually be reduced in size because of the lower lubricant requirements of the rolling bearings [1]. The potential for friction reduction is particularly evident at lower temperatures and correspondingly higher lubricant viscosity, Figure 1, right.

In addition to the stated potentials for friction reduction and thus for fuel consumption reduction, there are also challenges inherent in the use of rolling bearings in combustion engines which concern the areas of acoustics, durability, production and assembly in particular. The widespread use of rolling bearings in crankshaft assemblies has until now been prevented not only by durability requirements but also by the acoustic disadvantages. What needs to be taken into account in this respect is not only the often unfavorable acoustic emission transfer behavior, because this is more direct, but also the additional noise generated by the rolling bearing due to the rolling body dynamics. The acoustic risks that arise from the use of rolling bearings must therefore be countered by an appropriate design of the crankshaft assembly and mounting, as well as the neighboring crankcase structures.

In the context of the research project a simulation methodology, based on coupled multi-body simulations (MBS) and finite-element analysis (FEA) simulations and a mapping-based rolling bearing approach, was developed to enable calculation and analysis of the acoustic behavior of rolling bearing layouts in cranktrains and for use in early development phases for acoustically optimized design.

2 Experimental Investigations

Acoustic measurements were implemented on a test engine with a hybrid crankshaft bearing layout to quantify the acoustic influence of rolling bearings in the crankshaft group and to analyze the sensitivities.

2.1 Test Engine

The test engine was an air-cooled direct injection single-cylinder diesel engine from Motorenfabrik Hatz GmbH & Co. KG, where the standard hybrid crankshaft bearings consist of a combination of plain bearing on the front side and a flywheel-sided grooved ball bearing. The conrod bearing is designed as a conventional plain bearing. **Figure 2** shows a cross-section of the test engine with the hybrid crankshaft bearing layout.

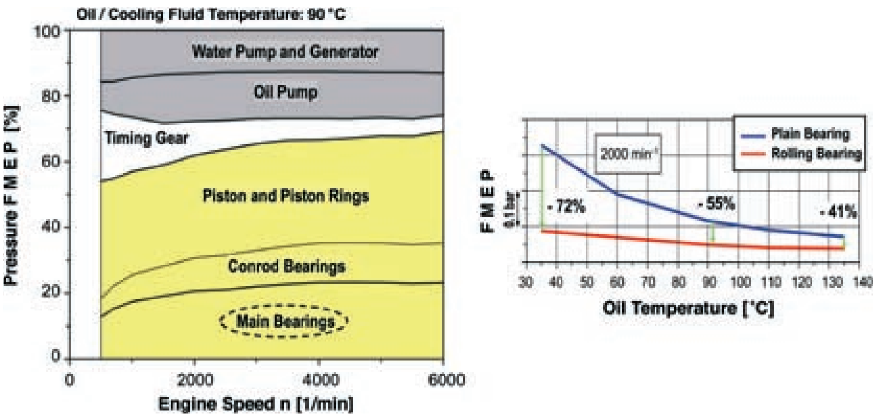

Figure 1: Mechanical losses in petrol engines with plain bearings (left); reduction of friction mean effective pressure when using rolling bearings (right) [1, 2]

The Authors

Prof. Dr.-Ing. Stefan Pischinger is director of the Institute for Combustion Engines (VKA) at RWTH Aachen University in Aachen (Germany).

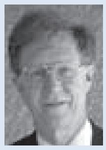

Dr.-Ing. Hans-Alfred Kochanowski was the representative of the FVV 881 project and test department manager of Motorenfabrik Hatz GmbH & Co. KG in Ruhstorf (Germany).

Dr.-Ing. Christoph Steffens is department manager Vehicle Physics/ Acoustics of FEV Motorentechnik GmbH in Aachen (Germany).

Dipl.-Ing. Sebastian Sonnen is scientific assistant at the Institute for Combustion Engines (VKA) at RWTH Aachen University in Aachen (Germany).

Dipl.-Ing. Martin Atzler is scientific assistant at the Institute for Combustion Engines (VKA) at RWTH Aachen University in Aachen (Germany).

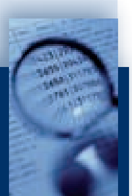

MTZ Peer Review
The Seal of Approval for scientific articles in MTZ.
Reviewed by experts from research and industry.

Received .... October 16, 2008
Reviewed .... November 04, 2008
Accepted .... November 22, 2008

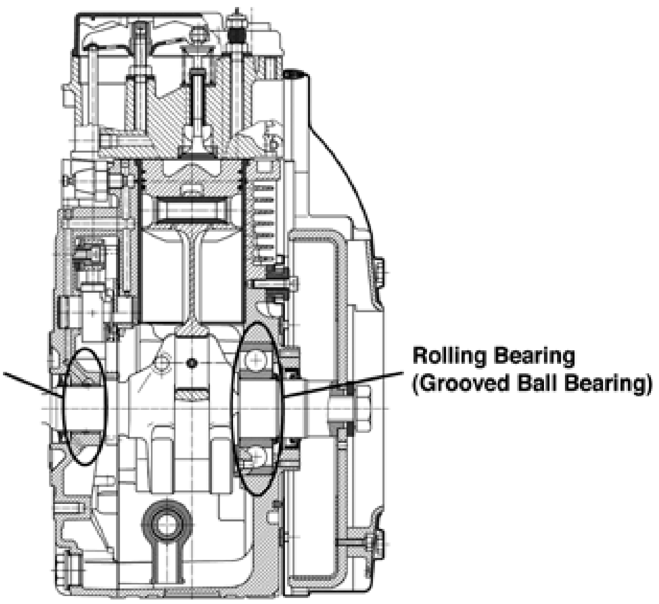

Figure 2: Hybrid crankshaft bearing layout – combination of plain and grooved ball bearing [3]

Table 1: Bearing specifications of the three bearing types grooved ball bearing, swivel ball bearing and needle / angular ball bearing

Type of Rolling Bearing		Grooved Ball Bearing	Swivel Ball Bearing	Needle / Ball Bearing
		6310 C4	1310 TVH	NKIB 5909
Number of Rolling Bodies		8	15 / row	24 / row
Position of Rolling Bodies		single-row	double-row	double-row
Angular Stiffness		medium	no	high
Bearing Clearance measured [µm]	radial	39	26	24
	axial	329.3	160.2	188
Working Clearance calculated [µm] (T = 100 °C)	radial	27.4	15.4	22.1
	axial	276.7	95.3	181.9

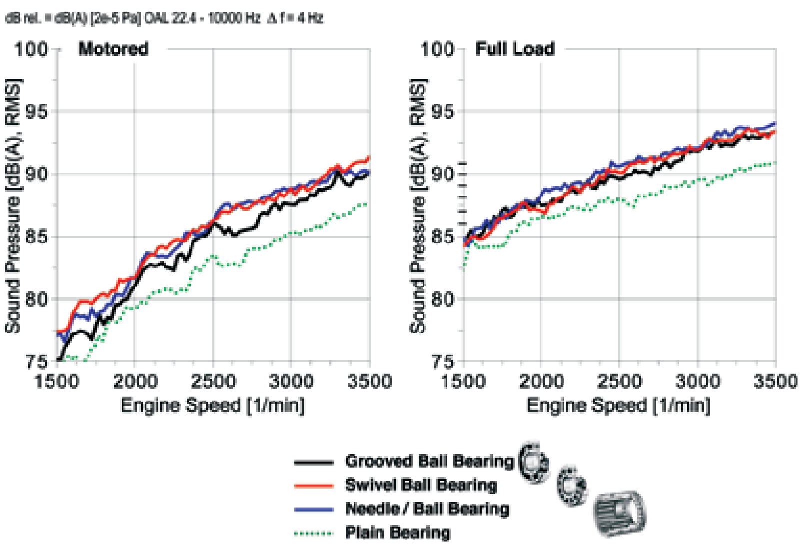

Figure 3: Airborne noise emission for the different bearing types

2.2 Influence of Bearing Configuration

To specify the influence of the crankshaft bearing concept on the acoustics, various bearing configurations were investigated. First of all, the standard hybrid crankshaft bearing layout with the flywheel-sided grooved ball bearing was measured before the grooved ball bearing was consecutively replaced by a swivel ball bearing and then a needle / angular ball bearing. In addition to the hybrid bearing variants, a plain bearing crankshaft setup with a second plain bearing replacing the rolling bearing was also investigated.

In all variants, the plain bearing on the front side remained unchanged. The bearing specifications and the influence of the investigated bearing variants on the airborne noise emission can be seen in **Table 1** and **Figure 3**. The sound pressure in farfield was compared for run-ups from 1500 to 3500 rpm under motored conditions and full load operation.

When comparing the investigated bearing variants, it could be seen that the plain bearing setup had advantages from the acoustic aspect compared to the three hybrid bearing layouts with rolling bearings on one side. The plain bearing configuration clearly evidenced the lowest sound pressure level across the entire speed range both in motored and full load operation. As expected, the greatest level differences were found under motored conditions where mechanical noise dominated. Compared to the loudest hybrid bearing configuration, differences of up to 5 dB(A) were reached. The plain bearing configuration also represented the best variant acoustically with regards to noise characteristics (evaluation of noise irritation).

In comparison to the hybrid bearing variants, the standard configuration with grooved ball bearings was proven to be acoustically advantageous. This applied both to the level of the sound pressure and the noise characteristics. The acoustic advantage of the grooved ball bearing was shown most clearly under motored conditions. Compared to the needle / angular ball bearing, the level reached was up to 1.8 dB(A) lower, while the level compared to the swivel ball bearing was up to 2.2 dB(A) lower.

2.3 Sensitivity Analyses

2.3.1 Influence of Rolling Bearing Clearance

The clearance of the standard grooved ball bearing was varied to quantify the clearance influence. For comparison reasons, an identical grooved ball bearing, differing only in the reduced bearing clearance from the standard bearing was measured (reduction of radial/axial clearance by approximately 70 or 50 %). The bearing specifications and the acoustic improvement potential of the investigated clearance reductions can be seen in **Table 2** and **Figure 4**.

The observed clearance reduction of the rolling bearing had a very positive effect on the acoustics and led in both motored and full load operation to a significant level reduction in sound pressure, which increased even further at higher speeds. Under motored conditions, level differences of up to 3 dB(A) were achieved. Despite this experimentally proven acoustic improvement potential, it must be noted that the acoustic optimization must always be evaluated against the background of durability-relevant requirements. Each application case must therefore be investigated to see whether a clearance reduction can be implemented with regards to bearing durability.

2.3.2 Influence of Rolling Bearing Lubrication Conditions

In addition to the investigation of bearing clearance influence, further sensitivity analyses were carried out, amongst others on the influence of the lubricant viscosity and the lubricant supply of the rolling bearing, **Figure 5**.

During the experimental investigation, it was shown that the observed reduction of oil viscosity from SAE 40 (standard) to SAE 10W (approximately bisection of reduction in viscosity in relevant temperature range) had no significant influence on the emitted airborne noise. In addition, the influence of an external oil supply to the rolling bearing (via an oil bore in the bearing outer race) was investigated together with the standard oil-mist lubrication. While no significant level differences in sound pressure were noted for the grooved ball bearing, the needle / angular ball bearing evi-

Table 2: Bearing specifications of the two variations standard rolling bearing and clearance reduced rolling bearing

Type of Rolling Bearing		Grooved Ball Bearing 6310 C4 (Standard)	Grooved Ball Bearing 6310 CN (Clearance reduced)
Number of Rolling Bodies		8	8
Position of Rolling Bodies		single-row	single-row
Bearing Clearance measured [µm]	radial	39	11.8
	axial	329.3	176.6
Working Clearance calculated [µm] (T = 100 °C)	radial	27.4	- 0.1

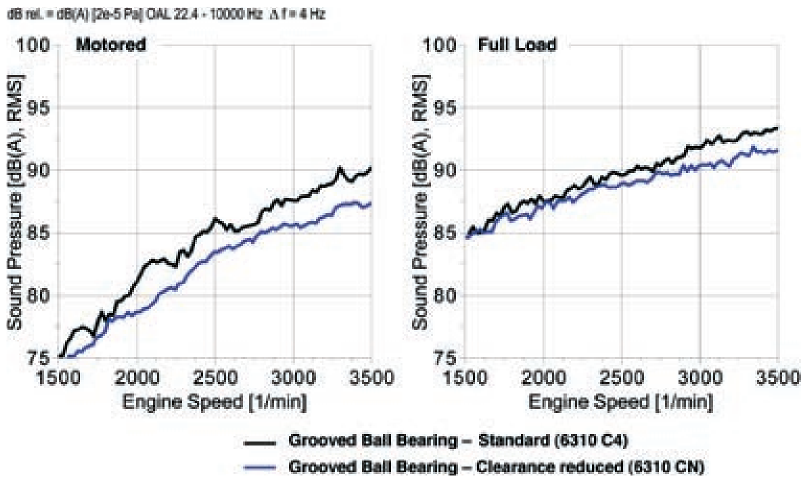

Figure 4: Influence of the clearance reduction on the airborne noise emission

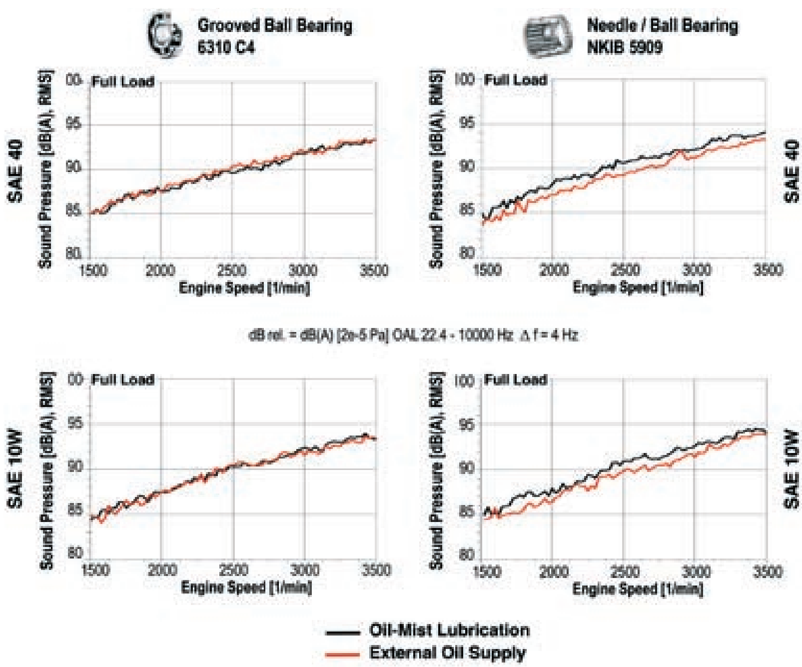

Figure 5: Influence of lubrication conditions on airborne noise emission

denced a marked sensitivity. With the additional oil supply, the sound pressure level could be significantly reduced across the entire speed range for the latter configuration, which indicates that the needle / angular ball bearing was not optimally lubricated in the case of oil-mist lubrication alone.

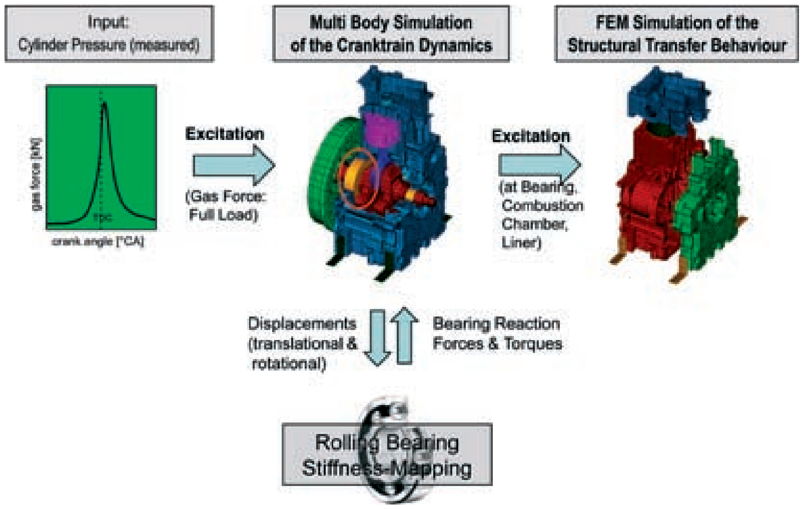

Figure 6: Simulation methodology

3 Simulation

3.1 Simulation Methodology

Coupled MBS and FEA simulations were used for in-depth investigation of the noise generation and transmission path, comprising excitation, structural noise transfer and airborne noise emission. The representation of the rolling bearing transfer behaviour was implemented by means of a mapping-based bearing approach developed and verified within this research project. The simulation methodology is shown in diagrammatic form in **Figure 6**.

3.1.1 Excitation Simulation via MBS

The excitation simulation was based on a MBS model of the cranktrain developed in the commercial software FEV Virtual Engine. Input variables for the simulation were experimentally determined cylinder pressure curves (time signals). The result of the cranktrain simulation were the excitation forces from the cranktrain dynamics, in particular the bearing reaction forces of the crankshaft, which were then used as the basis for the subsequent simulation of the dynamic structural transfer behaviour, Figure 6.

To take into account component elasticity, the crankshaft, cylinder crankcase and fly wheel components were implemented as flexible structures in the model. The quality of the subsequent simulations was highly dependent on the adequate modelling of the crankshaft bearings. A hydrodynamic bearing element from the element library of the MBS program was used for the plain bearing as this element resolved the Reynolds equations for each simulation step on the basis of the bearing dimensions, oil viscosity, temperature and the bearing clearance [4]. As the MBS programs available on the market do not provide any elements for modelling rolling bearings, a mapping-based approach for representing the rolling bearing transfer behaviour within MBS models was developed. Based on a multi-dimensional bearing stiffness mapping (taking into account the axial, radial and angular displacement of the bearing), the bearing reaction forces and torques were determined in relationship to the deflection between the inner and outer races of the bearing and then input back into the model at the position of the bearing, **Figure 7**.

Using the above-mentioned rolling bearing approach, it was therefore possible to model different rolling bearings by implementing appropriate bearing stiffness mappings in the MBS model. The mappings included via a subroutine in the MBS program were kindly provided by Schaeffler KG.

3.1.2 Simulation of the Transfer Behaviour via FEA

The structural response of the engine structure to the previously determined

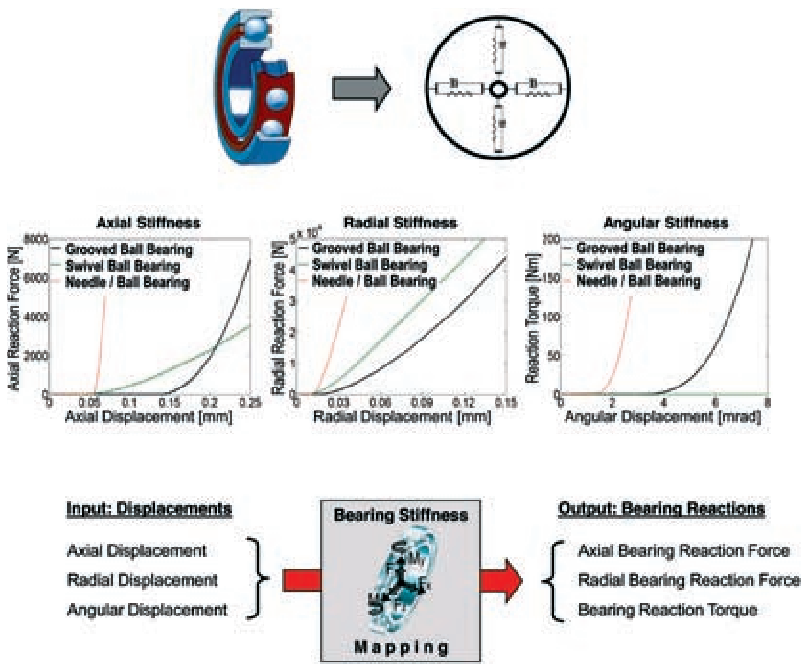

Figure 7: Bearing stiffness mapping of the rolling bearings

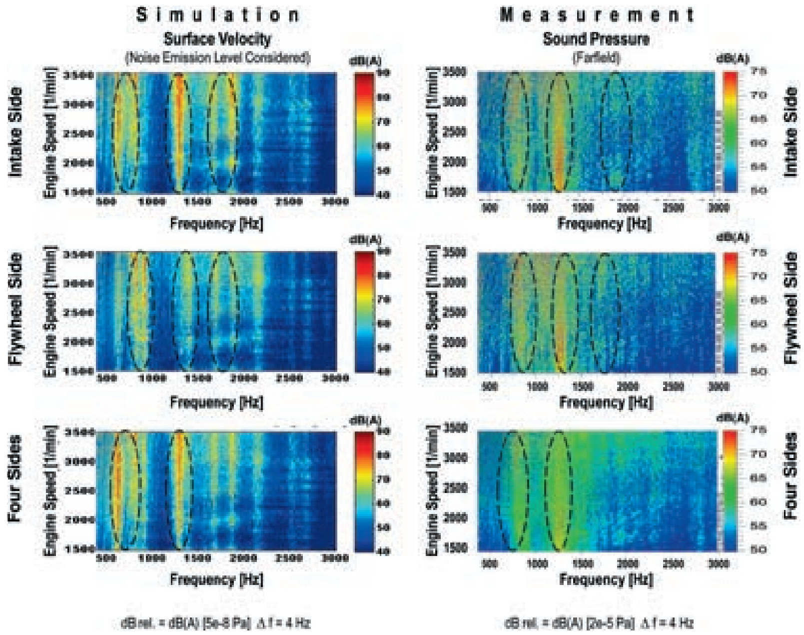

Figure 8: Comparison of simulation vs. measurement results

excitation forces was determined in a FEA simulation. A modal analysis was carried out in the first step of the simulation in order to calculate the eigenmodes of the engine structure up to a limit frequency of 3.5 kHz and verify them using reference measurements (impact tests). In the second step, the excitation forces derived from the MBS cranktrain simulation (main bearing reaction forces, piston liner forces and gas forces) were input at the corresponding points of the FEA model of the engine in the correct phase and direction. The result of this "forced response" simulation carried out in the time domain was the structural response, which could be converted into the corresponding airborne noise emission (sound field intensity), taking into account the noise emission level.

3.2 Simulation Results

The acoustic behaviour of the test engine was calculated experimentally, using the above-described simulation methodology, with a basic configuration and the two hybrid bearing variations described above. Speed run-ups were also evaluated under full load analogous to the measurements. **Figure 8** compares the results of simulation and measurements for the basic configuration with a grooved ball bearing on one side.

As can be seen in Figure 8, there is a good correlation between the sound pressure measured in farfield and the calculated airborne noise emission, described by the surface velocity level, taking into account the noise emission level. However, it must be taken into consideration that the simulation only calculated the sound emission of the engine structure alone, without added components, while the measurements recorded the airborne sound emission of the complete aggregate. Despite this limitation, the essential level increases in measured airborne sound were well represented in the simulation. An example of this is the resonance phenomena at approximately 1250 Hz, which is clearly recognizable in the measurements and simulations, and which is due to the lateral bending of the engine as can be seen in the calculated modal analysis of the engine structure.

In addition to the basic variant, the sound emissions of the hybrid bearing variants with swivel ball bearing or needle / angular ball bearing replacing the grooved ball bearing were also calculated. The same trend statements as in the measurements resulted; in the simulation the grooved ball bearing was shown to be the best rolling bearing acoustically, followed by the swivel ball bearing and the needle / angular ball bearing.

3.3 Sensitivity Analyses Calculations

Sensitivity analyses calculations were implemented on the basis of the verified simulation model. The aim followed here was to indicate acoustic improvement potentials with regards to the design of the crankshaft bearing and the neighboring components, crankshaft and cylinder crankcase. **Figure 9** shows an overview of the implemented sensitivity analyses.

Figure 10 shows a selection of the proven calculated improvement potentials. All simulations were based on full load run-ups. As is clear from the calculated sensitivity analyses, the investigated increase in crankshaft stiffness indicates a great potential for acoustic optimization. The surface mobility, used here as a parameter for sound emission, can be significantly reduced across the entire speed

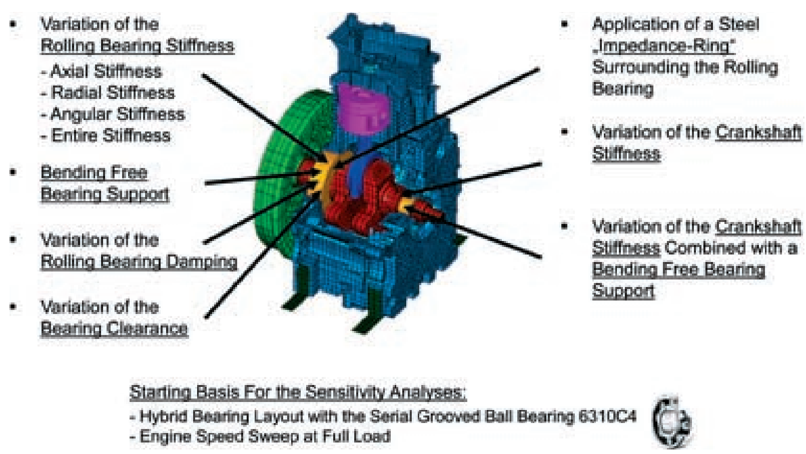

Figure 9: Overview of implemented sensitivity analyses

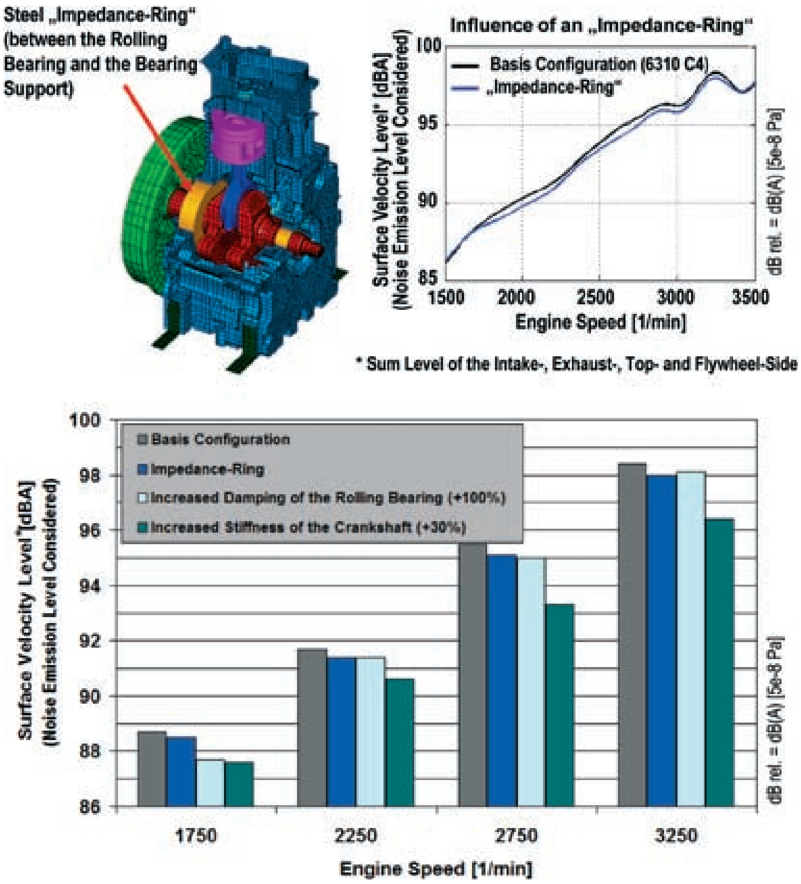

Figure 10: Results of the acoustic sensitivity analyses

range, particularly at higher speeds. Inversely, a reduction in stiffness is correspondingly disadvantageous to the acoustics (not shown here).

Another possibility of acoustic optimization lies in the use of a steel "impedance ring", which is set between the rolling bearing outer race and bearing support, Figure 10, top left. The aim here is to positively influence the input impedance between bearing and crankcase, and therefore to reduce the structure-borne noise transmission into the crankcase. As proven in the simulations, the overall level can be reduced slightly, at approximately constant levels across the whole speed range when the impedance ring is used.

One approach concerning the acoustic optimization of the rolling bearing consists of increasing the internal bearing damping as this improvement potential has been theoretically proven here. A possibility of realizing increased damping lies in increasing the lubricant supply; however this must be evaluated with respect to possible increased bearing friction. In addition, clearance reduction offers another significant improvement potential as was proven by the measurements.

4 Summary

The fuel consumption of combustion engines is influenced to a significant degree by engine friction. Substituting the plain bearings, which are normally used as the main crankshaft bearings, with rolling bearings offers significant potential for friction reduction, but simultaneously poses greater requirements for an acoustically optimized design.

Within the FVV research project No. 881 "Acoustics of Rolling Bearing Bedded Crankshafts", a simulation methodology, based on coupled MBS and FEA simulations and a mapping-based rolling bearing approach, was developed by the Institute for Combustion Engines (VKA) at RWTH Aachen University (Germany), to enable calculation and analysis of the acoustic behavior of rolling bearing layouts in cranktrains. The quality of the simulation method was verified by reference measurements.

Based on calculated sensitivity analyses, acoustic improvement potentials were determined in the area of the rolling bearing, crankshaft and crankcase. The calculation methods presented here for acoustic simulation and analysis are therefore suitable for collecting valuable information about the acoustic balancing of rolling bearings and engines early on in the process of product development and, in this manner, provide an important contribution for acoustically-optimized rolling bearing layouts in cranktrains.

References

[1] Tiemann, C.; Orlowsky, K.; Steffens, C.; Bick, W., K.; Kalenborn, M.: Wälzlagerung im Verbrennungsmotor – ein effektiver Weg zur Verbrauchsreduktion. Tagungsband zum 14. Aachener Kolloquium Fahrzeug- und Motorentechnik, Aachen, 2005

[2] Dohmen, J.: Untersuchungen zum reibungsoptimierten Triebwerk an Pkw-Verbrennungsmotoren. Dissertation, RWTH Aachen, Druck- & Verlagshaus Mainz, Aachen, 2003

[3] Schnittdarstellung Hatz Einzylinderdiesel 1B40. Motorenfabrik Hatz GmbH & Co. KG, Ruhstorf a. d. Rott

[4] Rebbert, M.: Simulation der Kurbelwellendynamik unter Berücksichtigung der hydrodynamischen Lagerung zur Lösung motorakustischer Fragen. Dissertation, RWTH Aachen, 2000

Acknowledgements

This article is the scientific result of a research project assigned by the Forschungsvereinigung Verbrennungskraftmaschinen e. V. (FVV, Frankfurt/Main, Germany) and conducted at the Institute for Combustion Engines (VKA) at Aachen University under the supervision of Professor Stefan Pischinger. The work was funded by FVV resources. The project was supported by an FVV work group under the supervision of Dr. Hans-Alfred Kochanowski. The authors thank this work group for their considerable help. They would also like to thank the companies Motorenfabrik Hatz GmbH & Co. KG and Schaeffler KG for their great support.

WWW.VIEWEGTEUBNER.DE

Gasoline Engines are the answer to the challenges of future

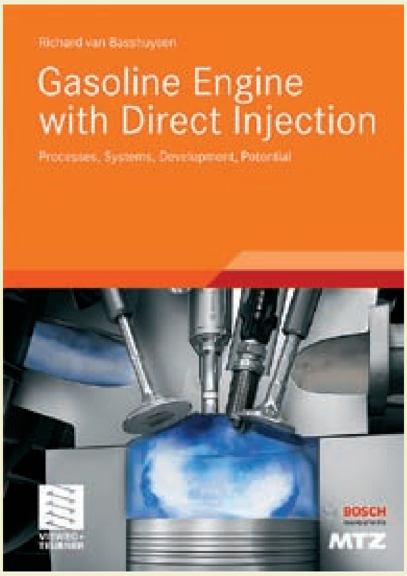

Richard van Basshuysen

Gasoline Engine with Direct Injection

Processes, Systems, Development, Potential

2009. xviii, 437 pp. With 399 Fig. Hardc. EUR 49,00
ISBN 978-3-8348-0670-3

Direct injection spark-ignition engines are becoming increasingly important, and their potential is still to be fully exploited. Increased power and torque coupled with further reductions in fuel consumption and emissions will be the clear trend for future developments. From today's perspective, the key technologies driving this development will be new fuel injection and combustion processes. The book presents the latest developments, illustrates and evaluates engine concepts such as downsizing and describes the requirements that have to be met by materials and operating fluids. The outlook at the end of the book discusses whether future spark-ignition engines will achieve the same level as diesel engines.

authors | editors

Dr.-Ing. E. h. Richard van Basshuysen was Head of Development for premium class vehicles and for engine and transmission development at Audi. Today, he is editor of the magazines ATZ and MTZ. The editor was supported by a distinguished team of authors consisting of 22 experts and scientists from industry and universities.

Please send me

____ Copies
Gasoline Engine with Direct Injection
ISBN 978-3-8348-0670-3
EUR 49,00
(+ shipping and handling)

Fax +49(0)611.7878-420

Company | Last name | First name | 321 09 001

Department

Street name | Postcode/Zip | City, Country

Date | Signature

Please supply at retail price via bookshop or directly from Vieweg+Teubner Verlag. Subject to change without notice. 1|2009.
Managing Directors: Dr. Ralf Birkelbach, Albrecht F. Schirmacher. AG Wiesbaden HRB 9754

TECHNIK BEWEGT.

VIEWEG+ TEUBNER

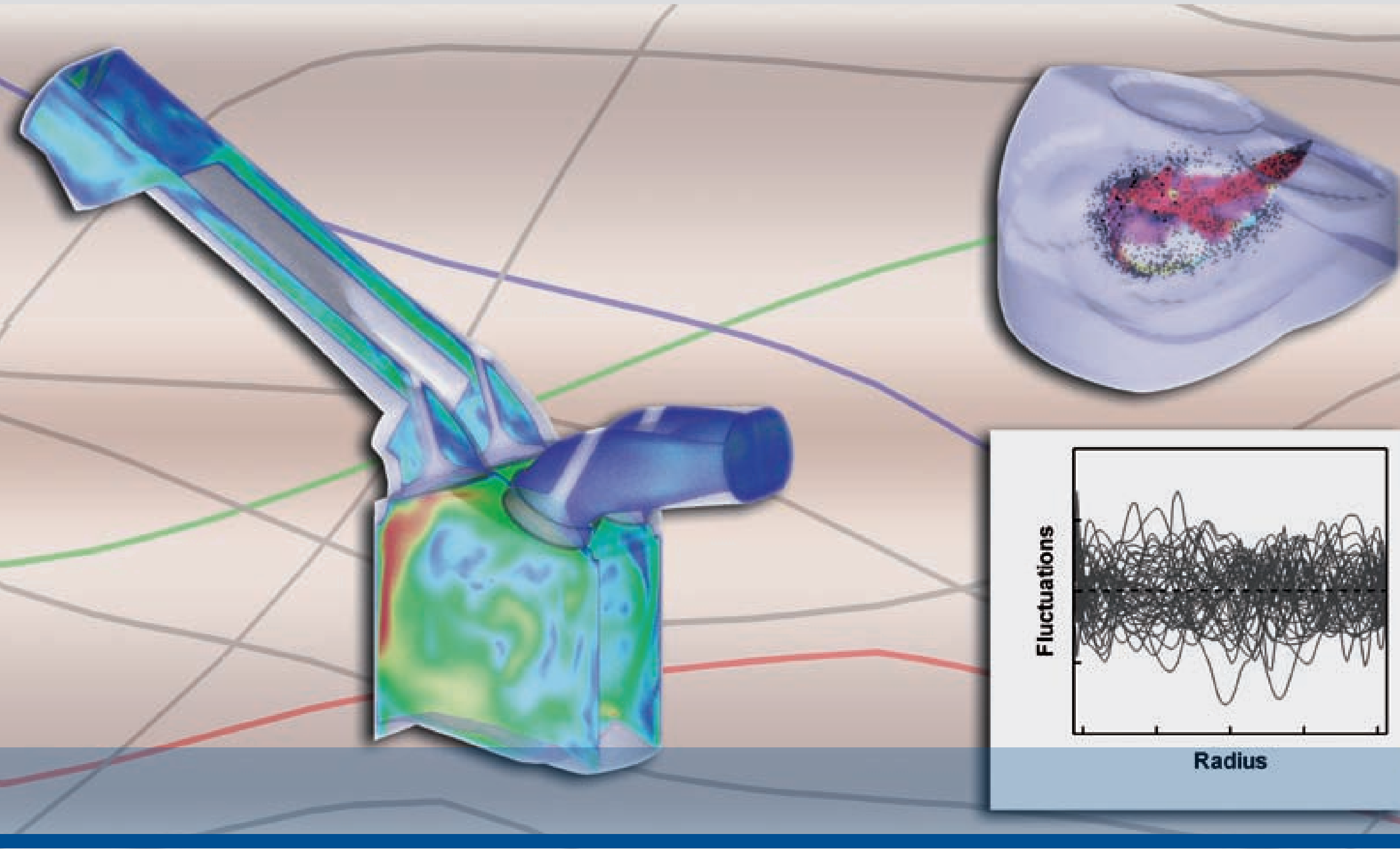

Large Eddy Simulation for a DI Gasoline Engine

Characterization of Cyclic Fluctuations of Flow and Mixing

Severe emission standards require innovative mixture formation concepts. The present work focuses on the characterization of cycle-to-cycle fluctuations of the flow field as well as the mixture preparation in a direct injection (DI) gasoline engine. For this purpose a realistic four-stroke engine with variable charge motion system has been investigated using the large eddy simulation (LES). The work was done at the Institute of Energy and Powerplant Technology (EKT), Technical University of Darmstadt (Germany), during the FVV research project No. 896.

1 Introduction

More and more severe emission standards necessitate immense efforts to develop innovative engine concepts. Direct-injection spark-ignition (DISI) engines have a large potential to reduce emissions and specific fuel consumption [1]. In part load they can be operated in stratified charge mode which combines the advantages of reduced pumping losses and lean combustion. In full load the in-cylinder charge is cooled by fuel evaporation [2]. However, especially engines operating with an air guided concept, are very sensitive to cycle-to-cycle variations of the flow and mixing field. These fluctuations result in variations of the indicated mean effective pressure and hence work output. In the worst case they can lead to combustion failures leading to a total loss of the energy stored in the cylinder and to the ejection of unburned hydrocarbons in the environment. Consequently a greater understanding of the in-cylinder flow, spray injection, fuel-air mixing and combustion is needed in order to control and optimize this crucial process.

Cyclic fluctuations have been studied extensively in the past. However the mechanisms leading to cyclic variability can not always easily be accessed experimentally [8, 15]. 3D simulations of internal combustion engines (ICE) are mostly based on statistical Reynolds-averaged-Navier-Stokes approaches (RANS) that are not able to predict cycle-to-cycle variations. For illustration **Figure 1** shows the comparison of instantaneous velocity profiles in an ICE from the large eddy simulation (LES) (a) and RANS (b). Results are shown for 50 (LES) and 10 (RANS) engine cycles, respectively. Haworth [3] argued that low to moderate Reynolds numbers make the engine an attractive candidate for investigations based on LES. Indeed it has been shown very recently that LES is a powerful tool to predict unsteady effects occurring in ICE [4–7].

The configuration, numerical method and mathematical models are briefly described in the following. The discussion of the results is firstly done for the pulled engine in Section 3 and considering injection and multi-phase flow in Section 4. The main findings are summarized in the final section of the article.

2 Configuration and Numerical Model

The configuration investigated in this work, see **Figure 2**, represents a four stroke direct spray injection engine with variable charge motion (VCM) system which has been investigated by Pischinger et al. [8]. It is a realistic IC-engine with four canted valves, an asymmetric cylinder head and an asymmetric piston bowl. The valve lift curves are shown in Figure 2 (c). Further parameters of the engine are provided in **Table 1**.

The computational geometry shown in Figure 2 (b) has been meshed with approximately 320,000 control volumes. This provides a mesh resolution of roughly 1.0 mm. No-slip velocity boundary conditions have been applied at all walls, mean atmospheric pressure has been prescribed at the intake and exhaust port. In order to gather a sufficient number of statistical samples a parallelization strategy based on the variation of initial conditions has been used. Starting from an initial perturbation ten consecutive engine cycles have been run on five

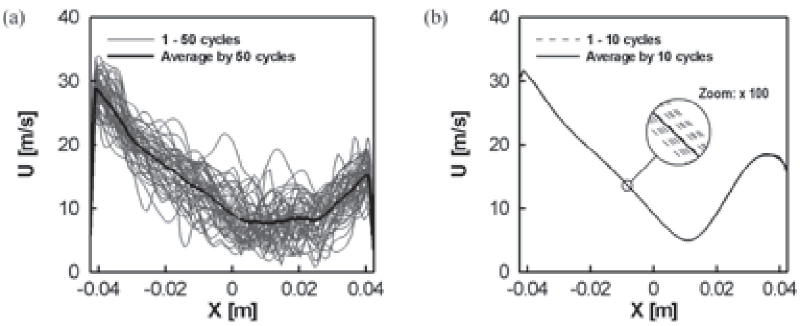

Figure 1: Comparison of calculated instantaneous velocity profiles in a combustion engine from LES (a) and RANS (b)

The Authors

Dr.-Ing.
Dmitry Goryntsev
is scientific assistant at the Institute of Energy and Powerplant Technology of TU Darmstadt (Germany).

Dr.-Ing. Markus Klein
was scientific assistant at the Institute of Energy and Powerplant Technology of TU Darmstadt (Germany) and is head „CFD and Performance" at GM Powertrain Germany in Rüsselsheim (Germany).

Prof. Dr. rer. nat.
Amsini Sadiki
is leader of Modeling and Simulation and Rheology at the Institute of Energy and Powerplant Technology of TU Darmstadt (Germany) and acts as adjunct professor at UQAT University of Québec (Canada).

Prof. Dr.-Ing.
Johannes Janicka
is the head of the Institute of Energy and Powerplant Technology of TU Darmstadt (Germany).

MTZ Peer Review
The Seal of Approval for scientific articles in MTZ.
Reviewed by experts from research and industry.

Received .... October 30, 2008
Reviewed .... November 11, 2008
Accepted .... December 12, 2008

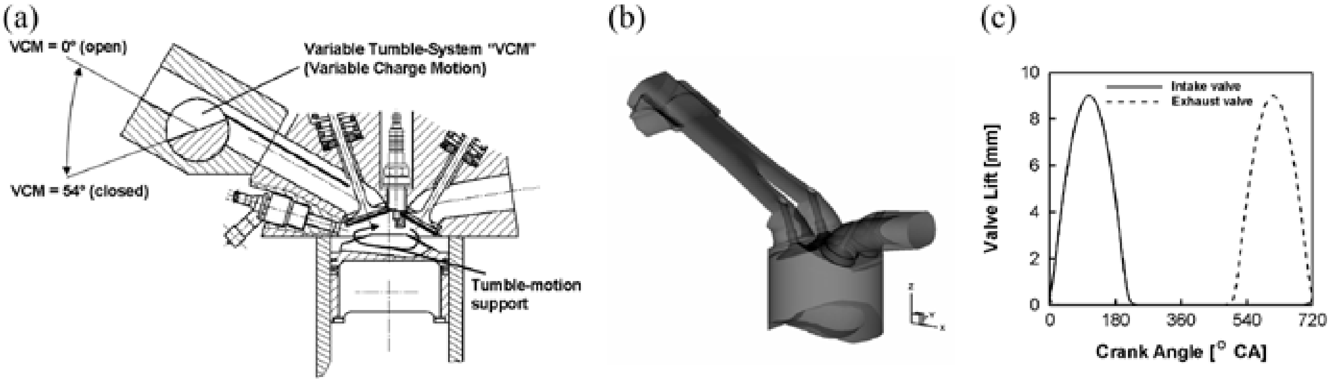

Figure 2: (a) Configuration of the test engine with variable tumble system [8]; (b) engine geometry of the test engine as it was simulated with KIVA-3V; (c) valve-lift curves

Table 1: Parameters of the test engine

Bore [mm]	Stroke [mm]	Crankshaft rotational speed [rpm]	Intake valve, opening [°]	Intake valve, closure [°]	Exhaust valve, opening [°]	Exhaust valve, closure [°]
85	85	2000	-24	240	480	744

individual processors resulting altogether in 50 individual realizations of the full motored engine cycle. This results in an estimated statistical error for mean velocity and its standard deviation of 5 % respectively 10 % [7].

The KIVA-3V software [9] used within this work has found widespread applications for the simulation of ICE flows mainly using the statistical RANS approach but more recently also in the context of LES [6, 7, 10–12]. KIVA-3V solves the unsteady equations of motion of a turbulent, chemically reactive mixture of ideal gases, coupled to the equations for a single component, vaporizing fuel spray. The code has been extended by the standard Smagorinsky model [13]. The so-called DDM (discrete droplet model) with Lagrangian, computational particles that represent parcels of spray droplets with uniform properties was applied for the spray description. The spray and fluid interactions are accounted for by means of a number of submodels, which are described in detail in the literature [9].

3 LES of the Flow Field in a Pulled Engine

In this section cycle-to-cycle fluctuations of the flow field will be analysed in an pulled engine. To this end the instantaneous velocity field is decomposed into a mean cycle averaged part and a fluctuating part and the standard deviation, denoted henceforth as root mean square (RMS), of a quantity will be considered as a measure for cyclic fluctuations. The interaction of flow and mixing will be discussed subsequently in Section 4.

The charge motion during intake stroke is governed by the negative pressure resulting from the descending piston. Once the intake valve opens a flow with local peak absolute value at the order of 200 m/s passes through the intake ports. At this operating point the variable charge motion system closes the lower part of the intake port leading to an intake jet towards the cylinder head forming a pronounced normal tumble motion, **Figure 3**.

Figure 4 (a) and (d) depict a contour plot of the in-cylinder flow field at CA = 105° shortly before maximum valve lift, together with velocity profiles for 50 consecutive engine cycles along the centre line z = 0.05 m, as well as their corresponding mean value. At the exhaust side of the combustion chamber, close to the tip of the intake jet, the velocity magnitude is 3 times higher compared to the

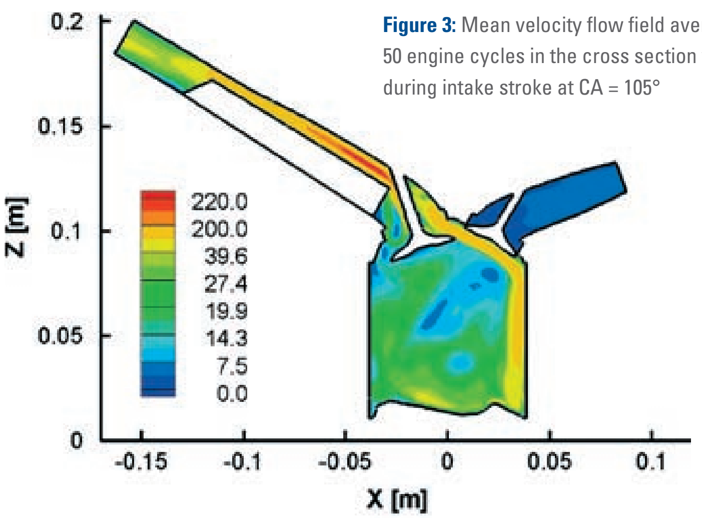

Figure 3: Mean velocity flow field averaged over 50 engine cycles in the cross section y = 0.018 m during intake stroke at CA = 105°

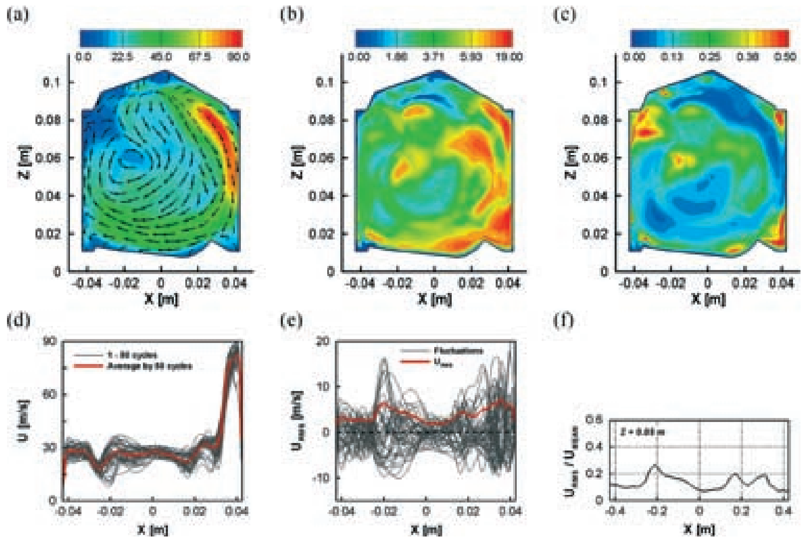

Figure 4: (a) Vector plot and velocity magnitude in the cross section of the combustion chamber at CA = 105°, averaged over 50 engine cycles; (b) standard deviation of velocity; (c) standard deviation of velocity normalised with local mean velocity; (d) instantaneous velocity profiles at z = 0.05 m for each individual cycle together with mean velocity profile; (e) instantaneous and mean standard deviation Urms profiles; (f) profile of U_{rms}/U_{mean} averaged over 50 engine cycles

intake side. These high velocities are accompanied by the highest absolute values of velocity fluctuations of up to 19 m/s as can be seen in Figure 4 (b) and (e). Another U_{rms} peak can be observed at the center of the incipient tumble flow at (x; z) = (0.0; 0.06), see Figure 4 (b). The relative strength U_{rms}/U_{mean} of velocity fluctuations is shown in the left part of Figure 4. The highest normalised values of velocity standard deviation occur in the corners of the combustion chamber where the flow is first deflected along the liner, then along the piston, again along the liner and finally along the roof of the combustion chamber. Note that cyclic variations reach values up to 50 % of the mean flow velocity.

The flow field during compression stroke (CA = 255°) shows a pronounced tumble flow, **Figure 5**, with the vortex center located at the center of the combustion chamber. CA = 15° after intake valve closure the peak velocity, that means the tip of the intake jet has moved from the exhaust to the intake side, see left part of Figure 5. Cycle-to-cycle variations are more homogeneous (see Figure 5 (b) and (e)) with maximum 6 m/s deviation from mean velocity. First and second velocity moments are roughly 3 times smaller compared to the intake stroke. However, the normalized standard velocity deviation reaches values of $U_{rms}/U_{mean} \approx 0.4$, comparable to the induction process. Local maxima occur again in the regions of flow turn and at the center of tumble motion (see Figure 5 (c) and (f)).

Expansion and exhaust stroke would look quite differently under realistic conditions including combustion and are hence not discussed further.

The control of the in-cylinder charge motion plays a key role in air-guided combustion systems. It is mostly generated during intake stroke. The cylinder head and piston bowl design assist to maintain charge motion during compression stroke. In the following (normal) tumble T_Y is defined as charge motion around an axis of rotation parallel to the crankshaft. For swirl S_Z the axis of rotation is parallel to the cylinder axis and for cross tumble T_X the axis of rotation is formed by the vector product of the former two. It is generally believed that during compression stroke conservation of angular momentum increases tumble motion, but only up to a compression ratio of roughly 3.0 [14].

Indeed a tumble spin up can be observed in **Figure 6**, before the organized motion becomes unstable and results in a production of turbulence which counteracts the decaying trend of turbulent kinetic energy (TKE) observed in Figure 6 (c). High turbulence levels increase the flame speed and improve combustion quality at part load and in local lean and rich regions. Since the intake ports are

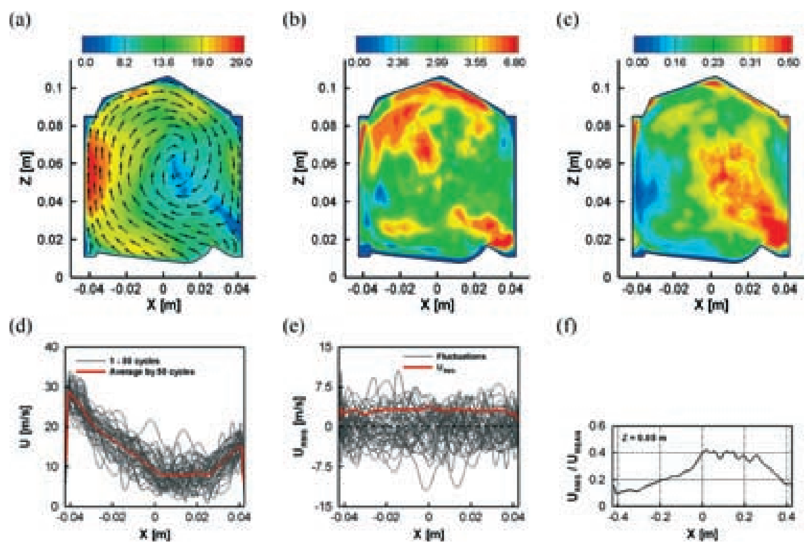

Figure 5: (a) Vector plot and velocity magnitude in the cross section of the combustion chamber at CA = 255°, averaged over 50 engine cycles; (b) standard deviation of velocity; (c) standard deviation of velocity normalised with local mean velocity; (d) instantaneous velocity profiles at z = 0.05 m for each individual cycle together with mean velocity profile; (e) instantaneous and mean standard deviation U_{rms} profiles; (f) profile of U_{rms}/U_{mean} averaged over 50 engine cycles

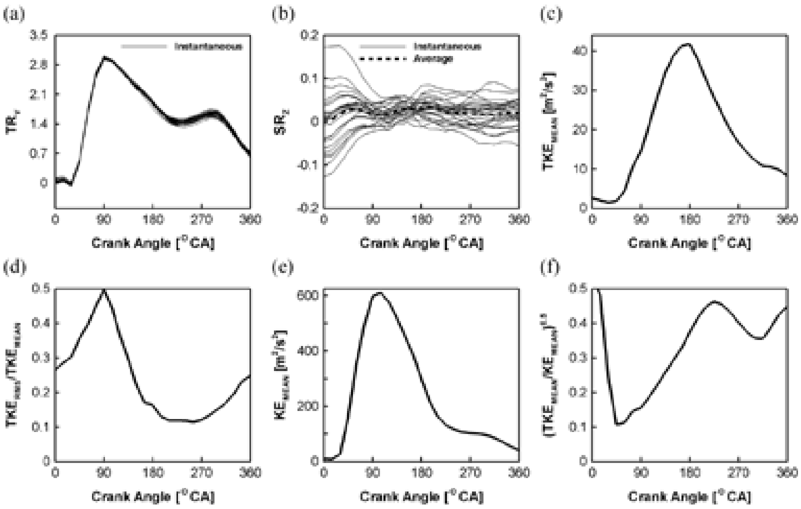

Figure 6: Profiles of globally averaged charge motion for consecutive engine cycles together with mean value; (a) normal tumble motion and (b) Swirl; (c) cycle averaged value of TKE; (d) standard deviation of TKE normalised with its mean value; (e) cycle averaged kinetic energy (KE); (f) cycle averaged value of $(TKE_{mean}/KE_{mean})^{0.5}$

symmetric, mean swirl level S_Z and mean cross tumble (which is not shown here) are nearly zero. Cyclic variations of T_X, T_Y and S_Z are at the order of 0.1 as depicted in Figure 6 (a) and (b). Another way of looking at charge motion is the cylinder averaged kinetic energy shown in Figure 6 (e). Note the phase lag between kinetic energy and turbulent kinetic energy, which are transformed from one (KE) into the other (TKE). Figure 6 (d) shows the cyclic variations of TKE expressed in terms of the standard deviation of turbulent kinetic energy normalized with its mean value. Relative cylinder averaged TKE variations are strongest around intake maximum opening point (MOP), decay close to zero at intake valve closure and then increase towards a second maximum roughly located at firing top dead center (DC).

In order to get a feeling for the magnitude of cyclic fluctuations relative to mean charge motion let us focus finally on the square root of the ratio of mean turbulent kinetic energy divided by mean kinetic energy. At gas exchange top dead centre (TDC) the value of $(TKE_{mean}/KE_{mean})^{0.5}$ is relatively high due to the very small value of kinetic energy at this instant in time. The value decreases with increasing flow velocity until turbulence production starts. Then $(TKE_{mean}/KE_{mean})^{0.5}$ increases again and reaches a constant level of roughly 0.5 during compression stroke as shown in Figure 6 (f). This result is remarkable because it shows the high intensity of cyclic fluctuations. Further this number is important for determining the required number of independent samples for an acceptable statistical analysis [6, 7].

4 LES of the Mixture Formation

It is well known that variations in global charge motion typically result in variations in turbulent kinetic energy, which in turn affect burn duration and ignition delay. Of course the mixture preparation as well as the stoichiometry influence combustion as well. In this section the effect of the cycle-to-cycle variations on the air-fuel mixing and relative air-fuel ratio close to the ignition point will be investigated. The initial field of each cycle of the single-phase flow simulations has been stored and used as a starting condition for the two-phase flow results discussed in this Section. Since there is no combustion involved each injection has been started from a fresh but different single-phase flow field realization in order to guarantee proper flow field and thermodynamical conditions at intake TDC. Injection parameters applied are provided in **Table 2**.

Figure 7 presents contour plots (a)–(c), cyclic variations (d)–(f) and standard deviation (g)–(i) of velocity for single-phase flow (left column) and two-phase flow at CA = 315° (middle column (b), (e) and (h)). The mixing field is shown in Figure 7 (c), (f) and (i). The profiles were obtained along the white line marked „A" (see Figure 7 (c)). The differences between the single-phase flow and the fuel spray injection case are well visible. At the end of the compression stroke the velocity flow field in the combustion chamber for the undisturbed case is determined by a pronounced tumble motion. The flow structure for two-phase flow in this stage is considerably different and represents a superposition of the tumble flow and the fuel spray jet. Cyclic velocity fluctuations result in the cycle-to-cycle variations of mass fraction as depicted in Figure 7 (c). It has to be mentioned that the outlier curves for the single-phase flow (Figure 7 (d)) correspond to the outlier curves for the two-phase flow (Figure 7 (e) and (f)). More general there is a high correlation between velocity and mass fraction cyclic fluctuations as can be seen in Figure 7 (h) and (i).

The normalized standard velocity deviation reaches the highest values at the center of the tumble motion (see Figure 7 (g)). In the case of two-phase flow the highest value of the standard deviation of velocity is observed at the tip of the fuel spray jet as shown in Figure 7 (h). At the time when the fuel jet reaches the center of tumble motion, there is a significant

Table 2: Parameters of injection

P_{Gas} [bar]	T_{Gas} [K]	P_{Inj} [bar]	T_{Inj} [K]	Fuel	Start of injection [°]	Duration [ms]	Cone [°]	DCone [°]
5	573	60	363	C_8H_{18}	293.4	2.01	40	12

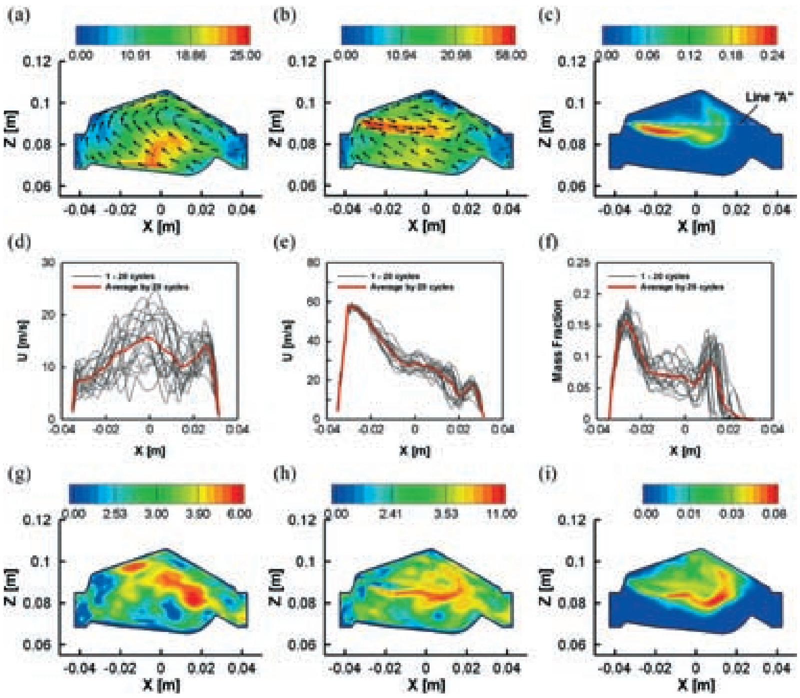

Figure 7: Contour plot of velocity (a), (b) and mass fraction (c); instantaneous profiles at z = 0.09 m for 20 consecutive engine cycles (d), (e), (f) and contour plot of standard deviation (g), (h), (i) at CA = 315° – the left column (a), (d), (g) shows velocities from single-phase flow calculation, the middle column (b), (e), (h) two-phase flow velocity results and the right column (c), (f), (i) the mass fraction

increase of cycle-to-cycle variations. Taking into account the fact that the center of in-cylinder charge motion is located near the spark plug at ignition time, the cyclic fluctuations of velocity and mass fraction achieve their maximum values exactly in this most critical region.

5 Conclusions

Using Large Eddy Simulation (LES), flow field and charge motion in a direct-injection gasoline engine have been discussed in detail by the Institute of Energy and Powerplant Technology (EKT), Technical University of Darmstadt (Germany), during the FVV research project No. 896. First and second order phase averaged velocity moments have been extracted from 50 consecutive engine cycles. The absolute value of cyclic velocity fluctuations is highest at the end of the intake stroke and then decreases during compression stroke. Peak velocity fluctuations can be found at the tip of the intake jet, at the exhaust side of the liner, and at the center of tumble motion, reaching values of nearly 50 % of the flows mean velocity.

In the case of two-phase flow the flow field in the combustion chamber is defined by a superposition of in-cylinder charge motion and injected fuel spray jet. A very high correlation has been found between velocity and mass fraction cyclic fluctuations showing that both phenomena are directly linked to each other.

References

[1] Fischer, J.; Kettner, M.; Nauwerck, A.; Pfeil, J.; Spicher, U.: Influence of an Adjustable Tumble System on In-cylinder Air Motion and Stratification in a Gasoline Direct Injection Engine. In: SAE Technical Paper Series (2002), 2002-01-1645

[2] Adomeit, P.; Lang, O.; Vogt, B.: Computational Analysis of Flow and Mixture Formation in DISI Engines. In: 12th International Multidimensional Engine Modeling User's Group Meeting, Detroit, USA, March 2002

[3] Haworth, D.: Large Eddy Simulation of In-cylinder Flows. In: Oil and Gas Science and Technology (1999), No. 54 (2), pp 175–185

[4] Vermorel, O.; Richard, S.; Colin, O.; Angelberger, C.; Benkenida, A.; Veynante, D.: Multi-cycle LES Simulations of Flow and Combustion in a PFI SI 4-valve Production Engine. In: SAE Technical Paper Series (2007), 2007-01-0151

[5] Thobois, L.; Lauvergne, R.; Poinsot, T.: Using LES to Investigate Reacting Flow Physics in Engine Design Process. In: SAE Technical Paper Series (2007), 2007-01-0166

[6] Goryntsev, D.; Klein, M.; Janicka, J.: Large Eddy Simulation of Cycle-to-cycle Variations in a Realistic Direct Injection SI Engine. In: 8th International Congress: Engine Combustion Process, Munich, Germany, 2007

[7] Goryntsev, D.; Sadiki, A.; Klein, M.; Janicka, J.: Large Eddy Simulation Based Analysis of the Effects of Cycle-to-cycle Variations on Air-fuel Mixing in Realistic DISI IC Engines. In: 32nd International Symposium on Combustion, McGill University, Montreal, Canada, August 3–8, 2008

[8] Pischinger, S.; Aymanns, R.; Graf, M.; Stapf, G.; Adomeit, P.: Analysemethoden zyklischer Schwankungen in direkteinspritzenden Ottomotoren. In: VIII. Tagung Motorische Verbrennung – Aktuelle Probleme und moderne Lösungsansätze, München, 2007

[9] Amsden, A.; O'Rourke, P.; Butler, T.: KIVA-II: A Computer Program for Chemically Reactive Flows with Sprays. Tech. Rep. LA-11560-MS, Los Alamos National Laboratory, USA, 1989

[10] Celik, I.; Yavuz, I.; Smirnov, A.: Large Eddy Simulations of In-cylinder Turbulence for IC Engines: A Review. In: Int. Journal of Engine Research (2001), Vol. 2, No. 2, pp 119–148

[11] Sone, K.; Patel, N.; Menon, S.: Large Eddy Simulation of Fuel-air Mixing in an Internal Combustion Engine. In: AIAA Paper (2001), 2001-0635, 39th AIAA Aerospace Sciences Meeting, Reno, NV, USA

[12] Hu, B.; Rutland, C.: Flamelet Modeling with LES for Diesel Engine Simulations. In: SAE Technical Paper Series (2006), 2006-01-0058

[13] Smagorinsky, J.: General Circulation Experiments with the Primitive Equations, 1. The Basic Experiment. Monthly Weather Review (1963), Vol. 91, No. 3, pp 99–164

[14] Toledo, M.; LePenven, L.; Buffat, M.; Cadiou, A.; Padilla, J.: Large Eddy Simulation of the Generation and Breakdown of a Tumbling Flow. In: Int. Journal of Heat and Fluid Flow (2007), 28, pp 113–126

[15] Goryntsev, D.: Large Eddy Simulation of the Flow and Mixing Field in an Internal Combustion Engine. Dissertation, Technical University of Darmstadt, Darmstadt, Germany, 2007

FVV

Acknowledgements

This work is the result of studies performed at the Institute of Energy and Powerplant Technology (EKT), Technical University of Darmstadt (Germany), during the FVV research project No. 896 "Large Eddy". The authors would like to thank the German Research Association for Combustion Engines (FVV), Frankfurt/Main (Germany), and also the working group including its chairman for their support.